HMGA2-mediated epigenetic regulation of *Gata6* controls epithelial canonical WNT signaling during lung development and homeostasis

INAUGURALDISSERTATION

zur Erlangung des Doktorgrades der Naturwissenschaften

- *Doctor rerum naturalium* -

(Dr. rer. nat.)

eingereicht am Fachbereich Biologie und Chemie der

Justus-Liebig-Universität Giessen

vorgelegt von

Indrabahadur Singh

Bad Nauheim, 2014

Die vorliegende Arbeit wurde am Max-Planck-Institut für Herz- und Lungenforschung in der Abteilung **"Epigenetik des Lungenkrebs"** unter der Leitung von Herrn **Dr. Guillermo Barreto** angefertigt.

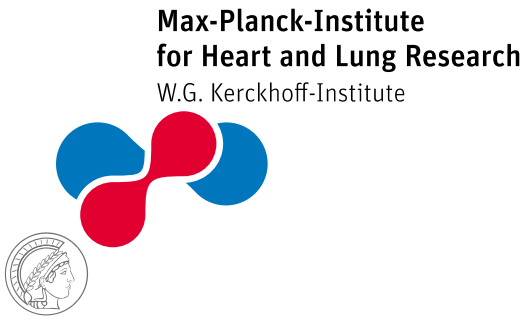

Erstgutachter:
Prof. Dr. Dr. Thomas Braun
Abteilung Entwicklung und Umbau des Herzens
Max-Planck-Institut für Herz- und Lungenforschung
Ludwigstraße 43, 61231 Bad Nauheim

Zweitgutachter:
Prof. Dr. Rainer Renkawitz
Institut für Genetik
Justus-Liebig-Universität Giessen
Heinrich-Buff-Ring 58, 35392 Giessen

Disputation am 24-09-2014

DEDICATED TO MY

PARENTS & GRANDPARENTS

Whose perpetual affection and blessing always

Inspired me for higher ambition in life

Table of Contents

List of Figures and Tables

ZUSAMMENFASSUNG

Die Regeneration von Organen bedarf einer physiologischen Balance zwischen Selbsterneuerung und Ausdifferenzierung von gewebespezifischen Vorläuferzellen, wobei die Expansion und Ausdifferenzierung dieser Vorläuferzellen zahlreiche Regulationsmechanismen der Embryonalentwicklung verlangt.

*High mobility group (*HMG*)*-Proteine sind die häufigsten Vertreter innerhalb der Gruppe des Nicht-Histon-Chromatins assoziierten Proteine und treten verstärkt in verschiedenen, undifferenzierten Geweben während der Embryonalentwicklung auf. Im entsprechenden adulten Gewebe sind diese nur noch geringfügig vorhanden und für die Aufrechterhaltung und Aktivierung von Stamm- oder Vorläuferzellen verantwortlich. In der vorliegenden Studie wurde die Rolle des *high mobility group AT-hook* Proteins *2* (HMGA2) als Schlüsselmolekül während der Morphogenese, sowie während der Ausdifferenzierung des Epithels in der embryonalen als auch in der adulten Lunge beschrieben. Durch detaillierte Analyse der Lunge von Hmga2$^{-/-}$ Mäusen in Kombination mit Experimenten ohne funktionierendes *Hmga2* konnte eine verstärkte Signaltransduktion des kanonischen WNT-Signalwegs festgestellt werden, die nicht nur zur fehlerhaften Ausdifferenzierung des Epithels, sondern auch zu einem erhöhten Vorkommen von Bronchoalveolaren Stammzellen (BASCs) in der adulten Lunge führte. Durch die erhöhte Anzahl von Vorläuferzellen in den Lungen von *Hmga2*$^{-/-}$ Mäusen veränderte sich das Gleichgewicht zwischen Selbsterneuerung und Ausdifferenzierung, was in einer verminderten Anzahl von Typ2 Pneumozyten (ATII) resultierte und eine veränderte Lungenmorphologie, sowie Funktionalität zur Folge hat. Weiterhin zeigte, dass HMGA2 ein direkter Regulator von *Gata6* ist, der eine entscheidende Transkcriptionsfaktor in der WNT-Signaltransduktion ist. Insgesamt konnte eine direkte transkriptionale Aktivierung von *Gata6* durch HMGA2 beobachtet werden, wobei diese Aktivierung abhängig von der Phosphorylierung von S65 (H1S65ph) an Histon H1 sowie von S139 (H2AXS139ph) an Histon H2AX durch die Kinase *Ataxia telangiectasia mutated* (ATM) ist. Hierbei folgt H2AXS139ph auf H1S65ph und erst im Anschluss finden der Abbau von Promoter-assoziierten Nukleosomen und die transkriptionale Aktivierung statt. Diese Interaktionen von HMGA2, ATM, H1 und H2AX zeigen einen neuen Mechanismus für die Initiation der Transkription.

Zusammengefasst, demonstriert die vorliegende Studie, dass HMGA2-vermittelte Veränderungen in der Chromatinstruktur die kanonische WNT-Signaltransduktion regulieren, wodurch das physiologische Gleichgewicht zwischen Expansion oder Differenzierung von Vorläuferzellen in Balance gehalten wird, was entscheidend für die Lungenentwicklung als auch für die Homöostase ist.

ABSTRACT

Organ regeneration requires a proper balance between self-renewal and differentiation of tissue-specific progenitor cells. Progenitor cell expansion and differentiation recapitulate many of the mechanisms regulating embryonic development. The high-mobility-group (HMG) proteins are the most abundant non-histone chromatin-associated proteins. They are present at high levels in various undifferentiated tissues during embryonic development and their levels are strongly reduced in the corresponding adult tissues, where they have been implicated in maintaining and activating stem/progenitor cells. Here, this study uncovered the role of the high mobility group AT-hook protein 2 (HMGA2) as a key regulator of branching morphogenesis and epithelial differentiation during embryonic lung development as well as in adult lung. Detailed analysis of the *Hmga2* knockout (*Hmga2*$^{-/-}$, KO) mice together with *in vitro Hmga2* loss-of-function (LOF) experiments revealed enhanced canonical WNT signaling resulting not only in defective lung epithelial differentiation but also in increased numbers of bronchioalveolar stem cells (BASCs). Increased numbers of progenitor cells in the lung of *Hmga2*$^{-/-}$ mice generated an imbalance in cell differentiation that is reflected in a reduction of alveolar type II (ATII) cells, thereby affecting both lung morphology as well as lung functionality. It also showed that HMGA2 directly regulates *Gata6* which is crucial for fine-tuning canonical WNT signaling in airway epithelium.

In addition, this study deciphered the molecular mechanism of transcriptional activation mediated by HMGA2. It showed that *Hmga2*-induced transcriptional activation of *Gata6* requires phosphorylation of the linker histone H1 at S65 (H1S65ph) and the core histone variant H2AX at S139 (H2AXS139ph), both mediated by the kinase, ataxia telangiectasia mutated (ATM). It also demonstrated the sequential order of events in which H1S65ph precedes H2AXS139ph and both are a prerequisite for the subsequent disassembly of promoter-associated nucleosomes and transcriptional activation. The functional interplay between HMGA2, ATM, H1 and H2AX is a novel mechanism of transcription initiation.

Together, this data demonstrate that HMGA2-mediated changes in chromatin structure regulate canonical WNT signaling and control the balance between progenitor cells expansion and differentiation required for both lung development and homeostasis.

Chapter 1: INTRODUCTION

In air-breathing vertebrates, lung is the essential respiratory organ where gas exchange occurs to bring in oxygen and to expel carbon dioxide. Therefore, it is constantly exposed to particulate matters, microorganisms and toxins from the environment. Thus, the alveolar epithelium, which represents 99% of the surface area of the lung, must execute simultaneously programs of oxygen provision for the entire body and of self-protection and repair. This implicates coordinated cellular and molecular processes allowing the maintenance of alveolar stability during breathing, through an organ regeneration process.

1.1 Lung Homeostasis

Organ regeneration requires a proper balance between differentiation and self-renewal of tissue-specific progenitor cells during both homeostatic turnover and repair after injury (Figure 1). The lung shows slow homeostatic turnover but rapid repair after injury. Tissue-resident lung-endogenous progenitor cell niches are thought to be responsible for both processes [1-3].

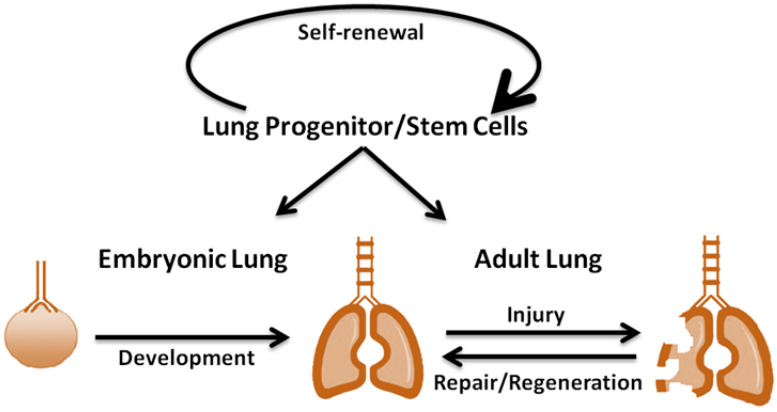

Figure 1. Schematic representation of Lung progenitor/stem cells function. Adapted and modified [4].

The adult lung is a complex, integrated system of numerous types of specialized cells that originate from epithelial and mesenchymal cell lineages and are organized in a proximal-distal manner to make gas exchange possible. There are different progenitor cell niches in the lung located in specific regions along the proximal–distal axis of the airways (Figure 2) [1]. BASCs represent one of these regional progenitor cell populations and are located at the terminal ends of distal bronchioles in the bronchioalveolar duct junctions (BADJ) [5]. BASCs are responsible for

regeneration of bronchiolar and alveolar epithelium during homeostatic turnover and in response to injury [6]. Characterization of the regulatory mechanisms controlling the proper balance between expansion and differentiation of BASCs would make a profound impact on our understanding and treatment of lung diseases. Many of the mechanisms involved in regulating embryonic development are recapitulated in progenitor expansion and tissue regeneration. Therefore, new experimental approaches, especially those based on embryonic development studies, are needed to elucidate the transcriptional mechanisms and signaling pathways required to direct proper balance between differentiation and self-renewal of progenitor cells.

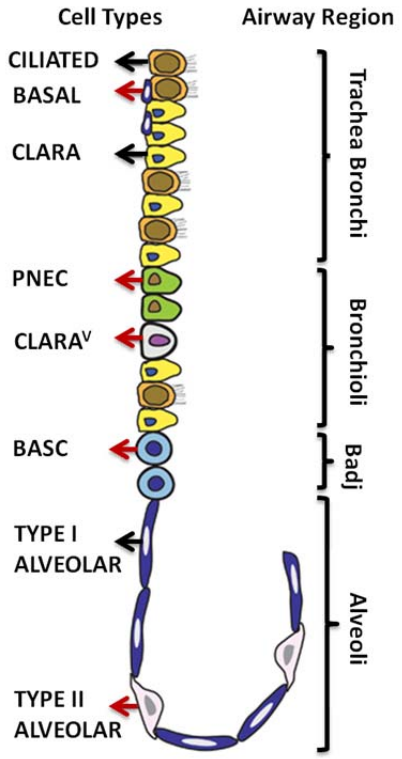

Figure 2. Schematic representation of adult lung airways and the different cell types present in each region. Cells with stem cell potential are shown with red arrow. Adapted and modified [1, 7, 8].

1.2 Lung Development

The mouse lung arises from the anterior endoderm and forms during five overlapping phases of lung development: embryonic (E9.5-E12.5), pseudoglandular (E12.5-E16.5), canalicular (E16.5-E17.5), saccular (E17.5-P5) and alveolar (P5-P28) (Figure 3) [9-11].

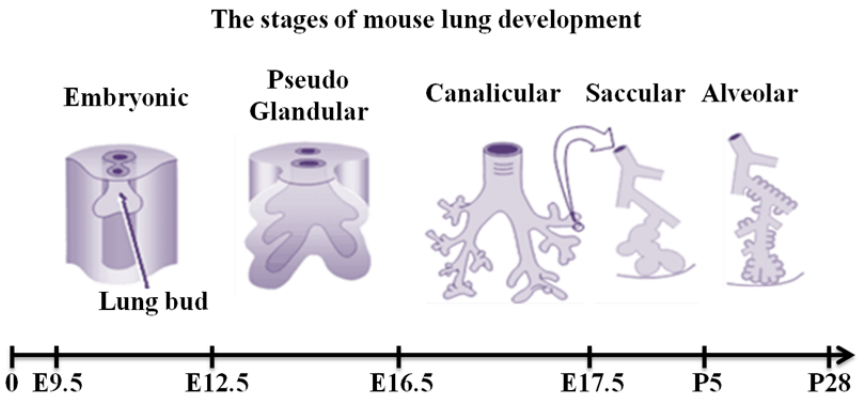

Figure 3. The stages of mouse lung development. E, embryonic day; P, postnatal day. Adapted and modified [12].

At the end of the embryonic phase, primary and secondary lung buds have formed and the establishment of proximal-distal axis has occurred from a morphologically uniform progenitor cell population. Later, the proximal embryonic progenitors give rise to proximal adult epithelium with the emergence of neuroendocrine, basal, ciliated and secretory cells while the distal tips of embryonic progenitors give rise to distal adult epithelium comprising of Alveolar Type I and Type II cells (Figure 4).

Several evolutionarily conserved signaling pathways have been implicated in different phases of embryonic lung development. In particular, members of the fibroblast growth factor (FGF), bone morphogenetic protein (BMP), hedgehog/Gli, epidermal growth factor (EGF) and wingless secreted glycoproteins (WNT) families have been implicated in lung morphogenesis and epithelial differentiation [9, 13-16]. In addition, a well-organized and balanced interplay between these signaling pathways and key transcription factors of lung development, including NK2 homeobox 1 (NKX2-1), Forkhead box protein A2 (FOXA2) and GATA binding protein 6 (GATA6) is required for proper lung formation [9, 11, 16].

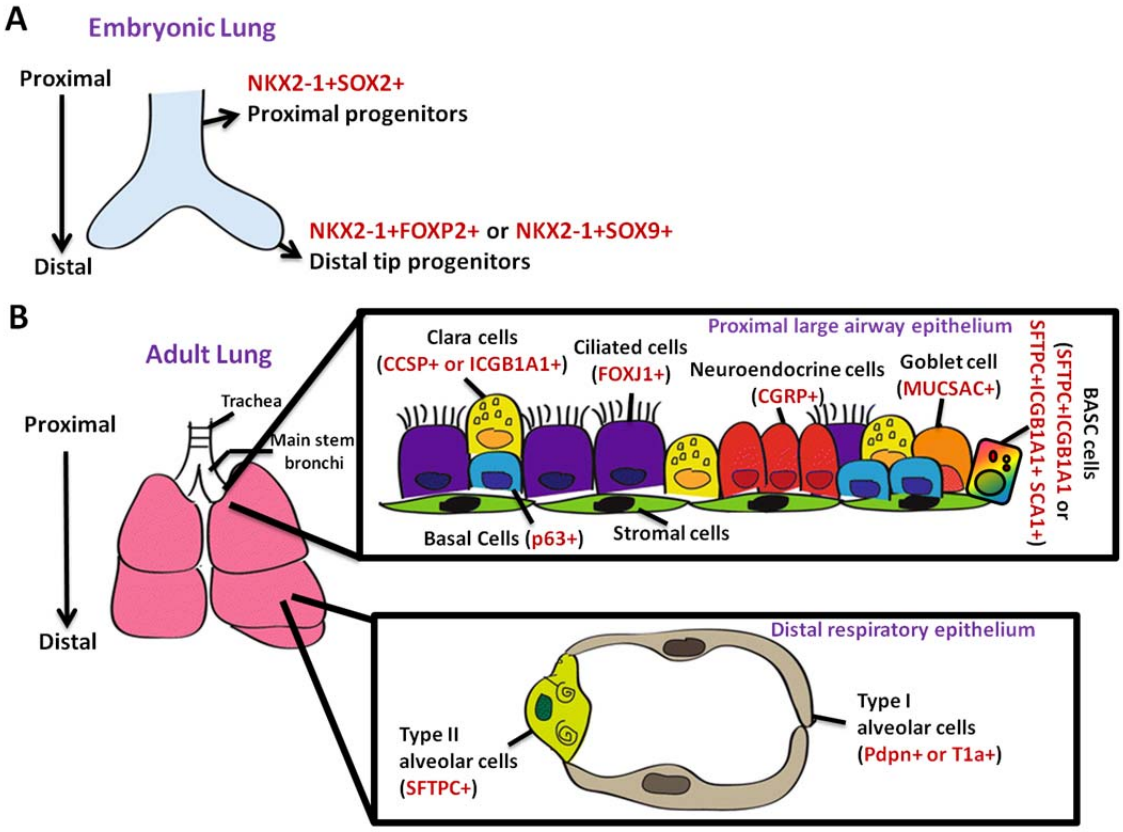

Figure 4. Lung at embryonic (A) and adult (B) stages. In the developing lung proximal progenitors (A) give rise to proximal cells lineages observed in the adult lung (B) and the distal tip progenitors (A) contribute to the stereotypical branching morphogenesis and eventually the distal respiratory epithelial cells (B). Adapted and modified [17, 18].

1.2.1 WNT signaling during lung development

The WNT signaling pathways are the evolutionary conserved pathways that regulate cell fate determination, cell polarity, cell migration and organogenesis during embryonic development. They are subdivided into canonical WNT pathway (Figure 5), non-canonical planar cell polarity pathway and non-canonical WNT/calcium pathway [19].

Canonical WNT signaling pathway is β-catenin (CTNNB1)-dependent WNT signaling pathway. In the absence of WNT ligands (Figure 5, left), the destruction complex (CKIα, GSK3β, APC, AXIN) hyperphosphorylates β-catenin. Hyperphosphorylated β-catenin is later ubiqitinated and

degraded by the proteosome. However, WNT ligands binding to a Frizzled/LRP (low-density lipoprotein receptor related protein)-5/6 receptor complex (Figure 5, right) leads to stabilization of hypo phosphorylated β-catenin, which translocate from cytosol to nucleus and interacts with T-cell factors (TCF) / Lymphoid enhancing factor (LEF) proteins to activate transcription of target genes.

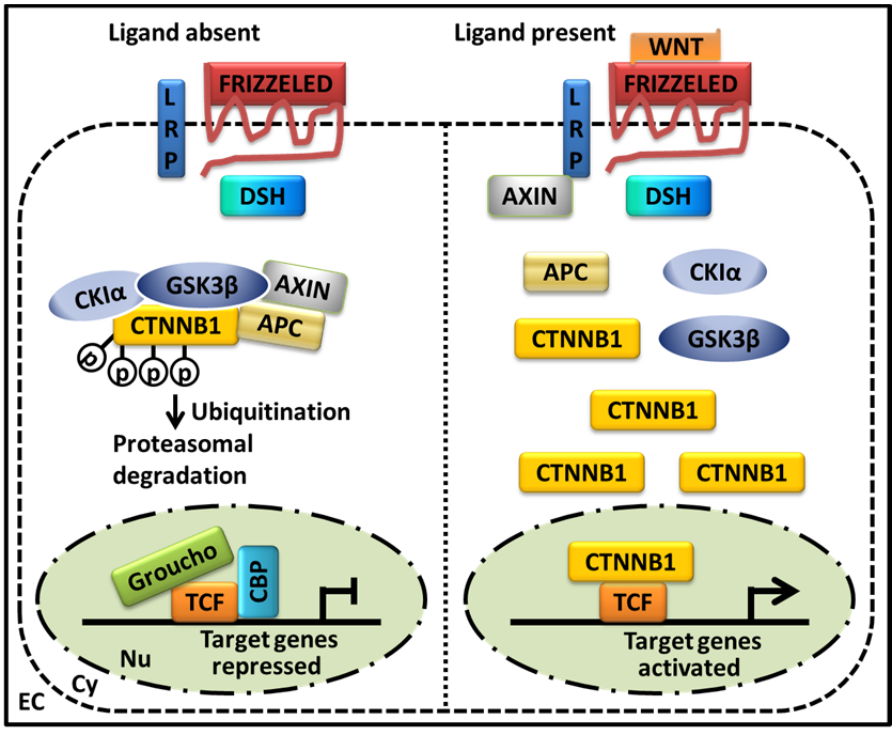

Figure 5. Overview of a canonical WNT signaling pathway. Adapted and modified [20].

WNT signaling molecules such as Frizzled receptors (Fz-1, -2, -7), TCF (-1,-3,-4), LEF-1, WNT -2/2b, -11, -7b, -5a, and secreted Fz related proteins (sFrp-1, -2 and -4) are expressed during lung development in specific spatiotemporal patterns [21-24]. WNT signaling pathways are essential for proximal-distal patterning and for the specification of the proximal-distal cell fate during lung morphogenesis [25-27].

1.2.2 GATA6 function during lung development

GATA6 is the only zinc finger transcription factor member of GATA family that is expressed in the distal epithelium of the developing lung [28, 29]. GATA6 is essential for branching morphogenesis and regulating differentiation of distal lung epithelium [29, 30]. Moreover, GATA6 positively regulates *Fzd2* expression which results in blocking canonical WNT signaling

in lung epithelial cells to control the balance between BASCs expansion and lung epithelial differentiation [31].

1.3 HMG proteins

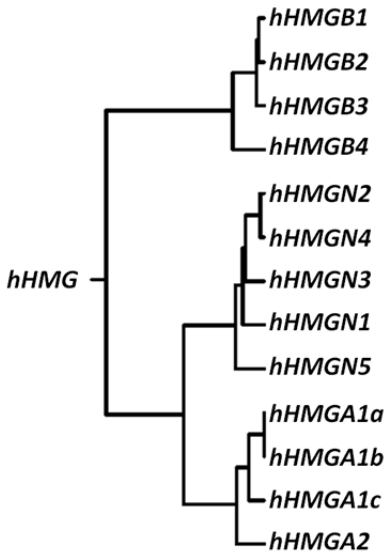

Figure 6. Genealogical Tree of human HMG proteins. HMG proteins are divided into three families depending on their DNA binding domains: HMGA, HMGB and HMGN. CLUSTALW software used to build rooted phylogenetic tree with branch length (UPGMA) of human HMG group family members. Adapted [32].

The genome of eukaryotic cells is highly organized and packed into chromatin. The nucleosome is the structural and functional unit of chromatin and consists of a nucleosome core particle, a linker histone of the H1 family and 20-30 base pair (bp) of linker DNA. The nucleosome core particle is built of 147 bp of DNA wrapped around a histone octamer, which is composed of two copies of each of the four core histones (H2A, H2B, H3 and H4). Histone H1 binds the linker DNA asymmetrically at the nucleosomal entry and exit sites, limiting the mobility of the nucleosome core particle and increasing the compactness of higher order chromatin [33]. In addition to nucleosomes, chromatin consists of non-histone chromatin-associated proteins, of which the HMG proteins are the most abundant. Based on their DNA binding domains, the HMG proteins are subdivided into three families (Figure 6): HMGA (containing AT-hooks), HMGB (containing HMG-boxes) and HMGN (containing nucleosomal binding domains) [33, 34]. HMG proteins can recognize structure rather than a particular nucleotide sequence and are able to bind to specific structures in DNA or chromatin in a sequence-independent manner via their respective functional motifs [35, 36]. Interestingly, HMG proteins are called architectural

transcription factors because, although they do not possess intrinsic transcriptional activity, they modulate transcription of their target genes by altering the chromatin structure at the promoter and/or enhancers [35, 37]. Here we deciphered the mechanism of transcriptional regulation mediated by the HMGA2, a HMGA family member and its implication during lung development and homeostasis.

1.3.1 HMGA

HMGA family comprises HMGA1a, HMGA1b, HMGA1c and HMGA2 (Figure 7). They are encoded by two distinct genes. The *HMGA1* gene gives rise to three proteins (HMGA1a, HMGA1b and HMGA1c) by alternative splicing of a common transcript. With the exception of HMGA1c, the HMGA proteins contain three short basic repeats called AT-hook motif and a C-terminal acidic tail (Figure 7) [38-41].

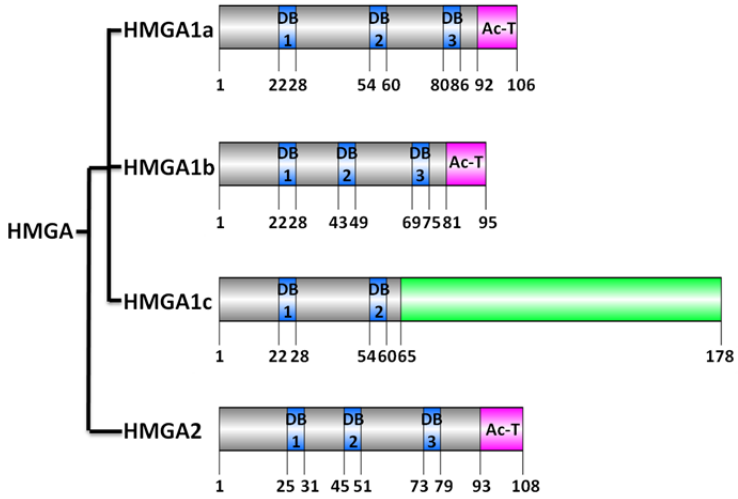

Figure 7. Schematic representations of human HMGA proteins. HMGA1a, HMGA1b, HMGA1c and HMGA2 proteins contain unique AT-hook motif (DNA binding domain (DB), blue boxes) and a C terminal acidic domain (Ac-T, pink boxes). The amino acid sequence of HMGA1c differs from the one from HGMA1a and 1b starting from amino acid 65 (green box). Adapted [32].

The amino acid sequence of the AT-hook motif is K/RXRGRP (X = glycine or proline) and is flanked on each side by positively charged residues. These characteristics determine the binding preference of HMGA proteins to both the minor groove of AT-rich DNA stretches [42, 43] and to nucleosomes in a cooperative manner [44]. The function of the C-terminal acidic region is poorly understood. However, there are speculations that C-terminal acidic tail is involved in protein-protein interaction and recruitment of factors during regulation of gene transcription [45].

1.3.2 HMGA2

HMGA2 is a nuclear non-histone chromatin associated protein. Its second AT-hook domain is required for nuclear localization [46]. This protein is conserved across the species (Figure 8). It is present at high level in various undifferentiated tissues during embryonic development and its level is strongly reduced or almost absent in the corresponding adult tissues [47-49]. In addition, HMGA2 is highly expressed in transformed cells in a variety of malignant and benign tumors of different origins [41, 50-55] suggesting its role during embryonic development and disease.

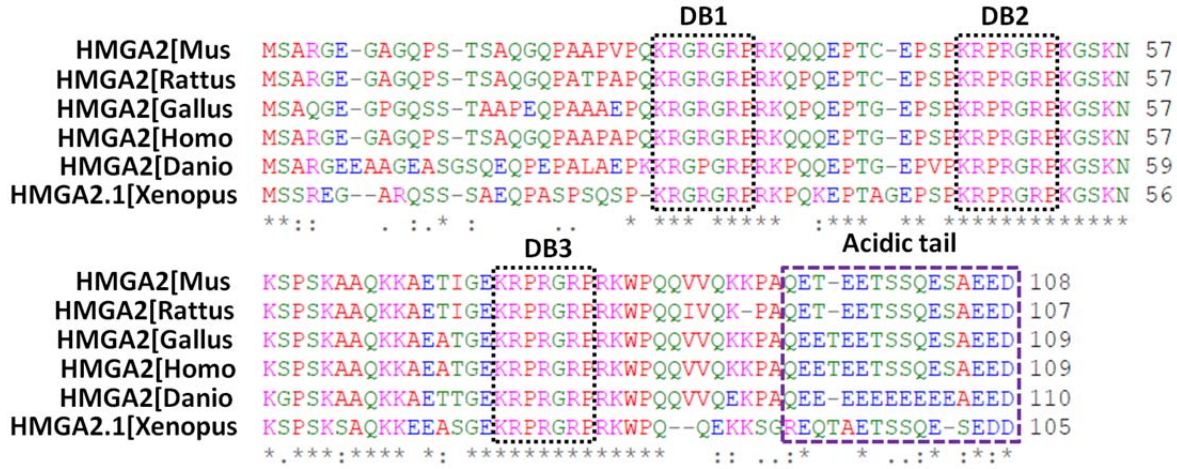

Figure 8. Clustal 2.1 multiple sequence alignment for HMGA2 across the species. AT-hook domain is shown in black dotted box and acidic tail is shown in blue dotted box. gi|6754210|ref|NP_034571.1| HMGA2 [Mus musculus]; gi|166157846|ref|NP_001107346.1| HMGA2.1 [Xenopus tropicalis]; gi|14091756|ref|NP_114459.1| HMGA2 [Rattus norvegicus]; gi|47086681|ref|NP_997845.1| HMGA2 [Danio rerio]; gi|45384530|ref|NP_990332.1| HMGA2 [Gallus gallus]; gi|4504431|ref|NP_003474.1| HMGA2a [Homo sapiens].

Hmga2 expression is regulated at transcriptional and post-trasncriptional level, for example transforming growth factor beta (TGF-β) and RAS-MAPK signaling pathways positively regulate *Hmga2* expression at transcriptional level [56-58]. However, miRNAs such as let-7, miR-21, and miR-33a negatively regulate *Hmga2* expression at post-transcriptional level [59-62].

Hmga2$^{-/-}$ mice show a pygmy phenotype due to reduced expression of the insulin-like growth factor 2 mRNA binding protein 2 (*Igf2bp2*) gene [63-66]. They also show reduced fat tissue which is linked to a function of *Hmga2* in pre-adipocyte precursor cell proliferation [49]. In addition, *Hmga2*$^{-/-}$ embryonic fibroblasts have a proliferative defect. A recent study had showed the *Hmga2* importance for the self-renewal potential of hematopoietic stem cells [67]. On other hand, transgenic mice overexpressing a carboxyl-terminally truncated version of *Hmga2* show a giant phenotype, are obese and develop lymphomas [68, 69]. It was shown that HMGA2 is necessary for the commitment of mouse embryonic stem cells to the skeletal muscle [48, 65] and cardiac muscle lineages [70]. HMGA2 proteins are also important for the proliferation of early stage neural precursor cells (NPCs) and for their neurogenic potential and overexpression of these genes can reprogram late stage NPCs into cells with early stage-specific capacities suppressing astrogenesis [71]. There is also report that *Hmga2*$^{-/-}$ mice show an impaired spermatogenesis and are sterile [47], thus HMGA2 protein is required for normal sperm development (Figure 9).

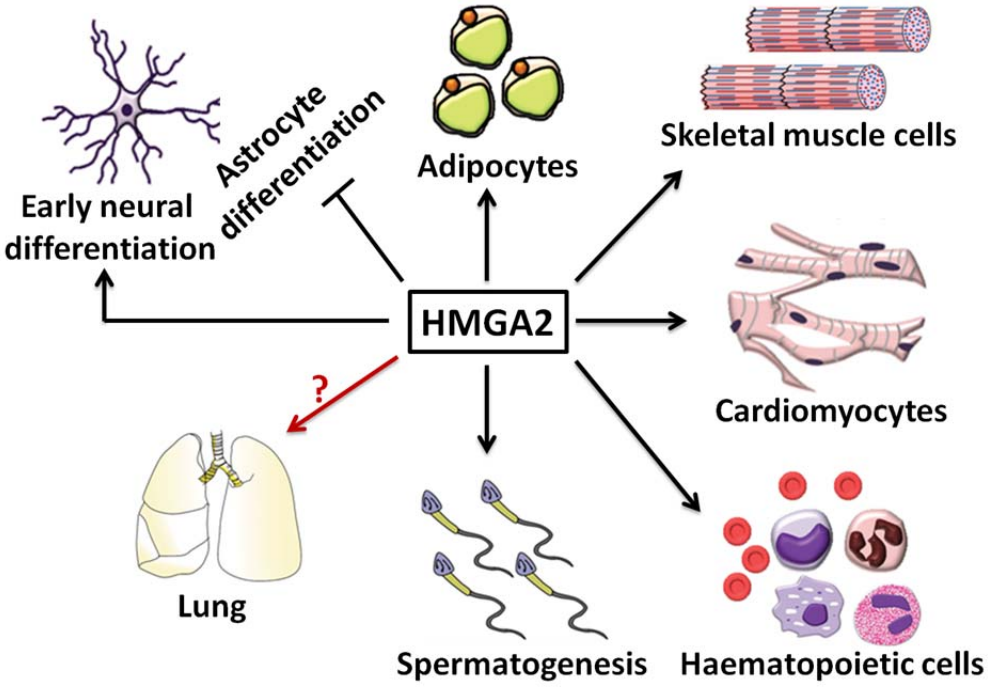

Figure 9. Schematic representation of HMGA2 role during cell differentiation. HMGA2 protein is required for proper development and progenitor cell differentiation to adipocyte, skeletal muscle, cardiac muscle, neurons, spermatozoids and hematopoietic cells. Adapted [32].

1.3.3 HMGA and Transcription

In eukaryotes, two types of core promoters are used for gene transcription initiation: promoters that are enriched with the di-nucleotide sequence CpG and promoters that are CpG poor [72-74].

CpG poor core promoters usually contain a TATA box, initiator sequences (INR), a transcription factor IIB recognition element (BRE) and downstream promoter elements (DPE) [75-77]. These promoters have specific single transcription start sites (TSS). In addition, a strong stimulation of RNA polymerase II (Pol II) dependent transcription initiation has been reported for these promoters by the synergistic interplay of the TATA box and INR core promoter elements. Recently, HMGA1 was identified as one of the factors required for the synergy between the TATA box and INR elements [45]. However, there is still need for further investigation to test the relevance of this finding as a general mechanism of transcription initiation. Gene transcription can also be regulated by the interplay of core promoter elements along with regulatory DNA elements, such as enhancers and silencers, which might be located several kilo base pairs (kbp) upstream or downstream of the promoter. In response to defined signals, specific proteins bind to the enhancer and form a complex called enhanceosome [78-81]. Looping of the DNA brings the enhaceosome and the core promoter in close proximity resulting in enhanced gene transcription. HMGA proteins are involved in enhanceosome formation [82, 83]. In addition, it has been reported that HMGA proteins have the ability to bend DNA [84]. Thus, a model can be suggested in which HMGA proteins participate not only in the formation of the enhanceosome but also in DNA looping and chromatin rearrangements that occur to bring enhanceosomes and core promoter in close proximity so that a coordinated assembly of the transcription initiation complex at core promoter can take place. It has been reported that the C-terminal domain of HMGA proteins is required for the interaction of HMGA1 with TFIID [45]. This interaction seems to mediate core promoter specific functions since a C-terminal deletion mutant of HMGA1 fails to initiate transcription. This domain contains several conserved phosphorylation sites, for example SQ (Serine-Glutamine amino acid residues) sites, which are substrates for the kinases DNA-dependent protein kinase (DNA-PK), ATM and ataxia telangiectasia & Rad3-related protein (ATR). It has already been reported that ATM and ATR interact with and phosphorylate HMGA group proteins [85-87]. Hence they might be involved in fine-tuning the HMGA mediated cell specific gene transcription.

The second type of promoters, which contain CpG islands, lack TATA boxes and display multiple heterogeneous TSS. These promoters tend to be enriched with binding elements for SP1, NRF-1, E2F and ETS transcription factors [74, 88]. It was shown that HMGA1 interacts with SP1 and facilitates its binding to both the human insulin receptor gene promoter and the herpes simplex virus latency-active promoter 2 [89, 90]. This suggests that HMGA family members may also be involved in the transcriptional activation of CpG rich promoters.

1.3.4 HMGA and Chromatin

Chromatin constitutes the physiological template for all kinds of DNA-dependent processes as replication, recombination, repair and transcription. However, chromatin represents a strong barrier to sequence specific recognition sites on the DNA thereby increasing the complexity of DNA-dependent regulation processes. To overcome this barrier, it is a prerequisite to open the higher order chromatin structure so that regulators of the above mentioned processes can access their recognition sites on DNA and execute their function.

There are several reports that HMGA proteins compete with H1 for binding to linker DNA thereby inducing a loosening of the chromatin structure (Figure 10B) [71, 91, 92]; However, the molecular mechanism underlying the replacement of histone H1 by HMGA proteins which results in chromatin opening is not well understood. Several post-translational modifications have been reported for Histone H1, such as phosphorylation, methylation, acetylation and poly-ADP-ribosylation (PARylation) [93]. Similar to the core histones, these post-translational modifications of the linker histone H1 play a role chromatin structure regulation. PARP-1 mediated PARylation of histone H1 leads to nucleosome-specific exchange of histone H1 by HMGB proteins inducing local changes of chromatin structure [94]. In a similar manner, histone H1 post-translational modifications could facilitate replacement of histone H1 by HMGA proteins thereby inducing chromatin decompaction. It is well known that the globular domain of histone H1 interacts and binds with linker DNA. Several motifs for kinases are located inside the globular domain or flank it. Phosphorylation of these sites might modulate the binding affinity of histone H1 to linker DNA [95] and might play a role during replacement of histone H1 by HMGA proteins.

Histone H1 eviction from chromatin is not enough to facilitate the access of regulatory elements on target genes because the DNA is still wrapped around the core histones hindering the accessibility of transcription factors to their binding elements. Hence, it further requires either eviction or mobilization of core histones. Several chromatin remodelers might be involved in these processes. For example, the facilitates chromatin transcription (FACT) complex has been reported to participate in H2A/H2B histone eviction/deposition [96], whereas anti-silencing factor 1 (ASF1) is involved in H3/H4 histone eviction/deposition [97]. HMGA proteins bind to both nucleosomes [44] and chromatin remodelers [98] suggesting co-ordination of these proteins in eviction and/or mobilization of core histones during transcriptional regulation (Figure 10).

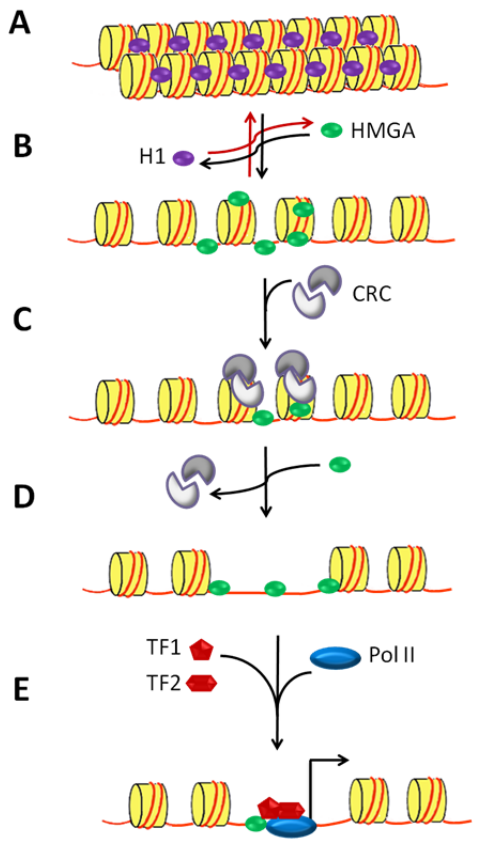

Figure 10. A model for the putative mechanism of HMGA proteins as factors promoting nucleosome mobility and accessibility to specific DNA sites for transcription activation. (A) The nucleosome is built of 146bp DNA (red line) surrounding the histone octamer (yellow cylinder), which consist of two H2A-H2B dimers and one $(H3\text{-}H4)_2$ tetramer. The linker histone H1 (purple oval) binds to linker DNA outside the histone octamer at the position where the DNA enters and exits the nucleosome core particle. (B) HMGA proteins (green oval) can compete and displace histone H1 from the chromatin. HMGA binding to linker DNA in the chromatin and the subsequent displacement of histone H1 leads to decompactness of the chromatin. (C) The relaxed chromatin structure acts as an anchoring site for the recruitment of chromatin remodeling complexes (CRC, grey). Binding of this complex is enhanced by HMGA proteins and induces eviction of core histones and/or mobilization of complete histone octamers. (E) The chromatin remodeling events make sequence-specific sites on the DNA accessible for transcription factor (TF, red pentagon and hexagon) binding. HMGA proteins might facilitate the formation of transcription factor complexes binding to these sequence-specific sites. Later, Pol II (blue oval) is recruited for transcription initiation (black arrow). Adapted [32].

1.4 ATM and H2AXS139ph

ATM belongs to the superfamily of phosphatidylinositol 3-kinase-related kinases and phosphorylates SQ motifs. Mutations in the ATM gene cause a rare autosomal recessive neurodegenerative disorder named ataxia telangiectasia which involves a marked defect in responding to DNA double strand breaks (DSB) [99]. Histone variant H2AX, which represents about 2-25% of the cellular H2A pool in mammals, is well-known substrate of ATM. ATM phosphorylates H2AX on the serine 139 residue (also known as γ-H2AX). The H2AXS139ph is often used as a biomarker for DNA-DSB [100, 101]. However, there are accumulating evidences for additional functions related to this histone modification, such as neovascularization, Igk allelic exclusion, and ES cells self-renewal [102-104]. In addition, McManus et. al. analyzed the dynamics of H2AXS139ph in normally growing mammalian cells and found ATM-dependent H2AX phosphorylation in all phases of cell cycle with a peaking during M phase [105] thereby suggesting that H2AXS139ph may contribute to the fidelity of the mitotic process, even in the absence of DNA damage, thereby ensuring the correct transmission of genetic information from one generation to the next.

Chapter 2: AIMS

In order to identify novel regulators of lung epithelial cell lineage during lung development, Dr. Guillermo Barreto screened a *short interfering RNA* (*siRNA*) library for pools that were able to reduce the basal transcription of a *luciferase* (*Luc*) reporter gene under the control of the *surfactant protein C* (*Sftpc*) promoter. *Sftpc* is the most specific marker of lung epithelial cell lineage [11]. *Hmga2* was identified in this screening. Its role during lung development and homeostasis was unknown. Thus, the aim of this thesis was to characterize the role of HMGA2 as a novel regulator of lung development and further to elucidate its molecular mechanism.

The specific aims of this study were:

Aim 1: To determine spatiotemporal expression pattern of *Hmga2* during mouse lung development.

Aim 2: To assess the function of HMGA2 during mouse lung development by utilizing *Hmga2*$^{-/-}$ mice and *siRNA* based knock down of *Hmga2* in mouse embryonic lung explant culture.

Aim 3: To elucidate the molecular mechanism of HMGA2 mediated transcriptional gene regulation.

Chapter 3: MATERIALS & METHODS

3.1 Molecular Biology Methods

3.1.1 RNA isolation and reverse transcription

For gene expression analysis, total RNA was isolated with RNeasy® plus mini kit (Qiagen) and quantified using NANODROP 2000 spectrophotometer (Thermo Scientific). The mouse tissue samples were collected; washed in ice-cold PBS (137 mM NaCl, 2.7 mM KCl, 4.3 mM Na_2HPO_4-$2H_2O$, 1.4 mM KH_2PO_4) and snap frozen in liquid nitrogen. The homogenization of a tissue was conducted using Homogenizer (PEQLAB) in the presence of RLT buffer (Qiagen). After purification of RNA, purified RNA were reverse transcribed using the High Capacity cDNA Reverse Transcription kit (Applied Biosystem) to synthesise the DNA complementary to mRNA (cDNA) according to the manufacturer's protocol. In brief, 2 µg RNA were mixed with 0.8 µl 100 mM dNTP, 2 µl 10X random primers, 2 µl 10X reverse transcription buffer, 1 µl RNase inhibitor, 1 µl MultiScribe™ Reverse Transcriptase and upto 20 µl Nuclease free H_2O. And then, following thermal cycle condition was used for cDNA synthesis.

Step	**Temperature (^{0}C)**	**Time (minute)**
1	25	10
2	37	120
3	85	5
4	4	infinite

3.1.2 Quantitative PCR

Quantitative polymerase chain reactions (qPCR) were performed using SYBR® Green on the Step One plus Real-time PCR system (Applied Biosystem).

For quantitative reverse transcription PCR (RT-PCR), the qPCR results were normalized with respect to the housekeeping gene Glyceraldehyde 3-phosphate dehydrogenase (*Gapdh*) and/or Alpha-tubulin (*Tub1a1*).

qPCR reactions were carried out in 20 µl volume including:

2x SYBR® Green buffer	5 µl
10µM primer mix	0.5 µl
Template (DNA/cDNA)	1 µl
H2O	up to 20 µl

For the qPCR, following thermal cycle condition was used:

Step	**Temperature (°C)**	**Time (second)**	
Initial denaturation	95	120	
Denaturation	94	30	} 40 cycles
Extension	60	15	
Pause	4	infinite	

Primers used for PCR are listed in the Appendix Table1.

The DNA sequences for all used genes are accessible via Ensembl database (http:// ensembl.org). For the designing and testing specificities of primers, Primer-BLAST (http://www.ncbi.nlm.nih.gov/tools/primer-blast/) was utilized.

Primer pairs were designed for gene expression analysis in a way that they are separated by at least one intron on the corresponding genomic DNA.

3.1.3 Primer efficiency determination

To determine efficiency of primers for qPCR, different dilutions (1:1, 1:2, 1:4, 1:8 & 1:16) of template (DNA or cDNA) were used. And following formula used to calculate primer efficiency from graph of CT values for each primer.

Efficiency = $\mathbf{10^{((-1/slope)-1)} X\ 100}$

3.1.4 Affymetrix Microarrays

For gene expression analysis, Affymetrix microarray-based transcriptome analysis of *Hmga2*$^{-/-}$ and Wild type (WT, *Hmga2*$^{+/+}$) embryonic lung (E18.5) was performed and analyzed as described [106]. Kyoto Encyclopedia of Genes and Genomes (KEGG) pathway enrichment based analysis of deregulated pathways in *Hmga2*$^{-/-}$ *vs.* *Hmga2*$^{+/+}$ was done using DAVID software [107] and generation of fold change and Heat map were performed using DNAStar Arraystar 11.0. The data discussed in this thesis have been deposited in NCBI's Gene Expression Omnibus [108] and are accessible through GEO Series accession number GSE55340 (http://www.ncbi.nlm.nih.gov/geo/query/acc.cgi?acc=GSE55340).

3.1.5 Semiquantitative PCR

For genotyping the transgenic mice, cloning and Chromatin immunoprecipitation (ChIP) experiments semiquantitative PCR was used. For semiquantitative PCR, DNA templates were diluted to 1:10 and all reactions were carried out in 25 µl volume including:

10X Taq Pol buffer	2.5 µl
100 mM dNTP	0.5 µl
10 µM primer mix	1 µl
DNA template	1 µl
Taq polymerase (Sigma)	1-2 units
H2O	up to 25 µl

For the semiquantitative PCR, following thermal cycle condition was used:

Step	**Temperature (°C)**	**Time (second)**	
Initial denaturing	95	120	
Denaturing	94	30	X cycles
Annealing	56-60	30	
Extension	72	60	
Final extension	72	300	
Pause	4	infinite	

The amplified PCR products were mixed with gel loading dye (Fermentas) and then loaded on 1% to 2% agarose gel for DNA band separation. 1X Tris/Borate/EDTA (TBE) electrophoresis buffer (1 l of 20X TBE: 1g NaOH, 216 g Tris Base, 110 g Boric acid, 14.8 g EDTA) was used to run agarose gel and ethidiumbromide (EtBr) was used to visualize DNA bands under UV light. The band size of the products was controlled by standard marker (100 bp or 1 kb GeneRuler™ DNA Ladder Mix, Fermentas).

3.1.6 DNA elution from agarose gel

Resolved DNA bands on agarose gel were purified using the QIAquick gel extraction kit (QIAGEN) according to the manufacturer's instruction and eluted with 30 µl nuclease free H_2O.

3.1.7 Nucleic acids concentration determination

The DNA and RNA concentrations in solution were estimated using NANODROP 2000 spectrophotometer (Thermo Scientific). The absorbance of the solution was measured at 260 nm and the concentration of nucleic acids was calculated by the manufacturer's software based on Beer-Lambert Law ($A\lambda = \varepsilon bc$).

Where,

$A\lambda$ is the absorbance ($A\lambda = log_{10} P_0 / P$);

ε is the molar absorbtivity (molar extinction coefficient);

b is the path length of the sample;

c is the concentration of the compound in solution.

The molar absorbtivity for double stranded DNA is $\varepsilon = 50\ cm^{-1}\ M^{-1}$.

The molar absorbtivity for single stranded DNA is $\varepsilon = 33\ cm^{-1}\ M^{-1}$.

The molar absorbtivity for RNA is $\varepsilon = 40\ cm^{-1}\ M^{-1}$.

3.1.8 Cloning

The proximal 631bp *Gata6* promoter was amplified and cloned into TOPO TA cloning vector (Invitrogen) and further subcloned into the pGL4 basic vector to generate *pGL4-Gata6* promoter luciferase vector.

Hmga2 cDNA fragment was subcloned from pcDNA3.1 *Hmga2* WT (Addgene plasmid 14789) vector to pcDNA3.1(A)-myc\His (Invitrogen) to generate C-terminal myc\His tagged *Hmga2* mammalian overexpression vector.

To generate point mutation in constructs of H2AX-flag (S139 to D) and H1-flag/myc (S65 to A and D), QuickChange™ Site-Directed Mutagenesis Kit (Stratagene) was used.

Primers used for PCR were listed in the Appendix Table1.

For cloning, ligation reaction was used as follows:

Reagent	**Reaction volume (µl)**
2X Rapid ligation buffer	5
Vector	1
Insert	X
T4 DNA ligase (3 Wiess U/µl)	1
ddH_2O	up to 10

The ligation reaction mixture was mixed by pipetting, centrifuged briefly and incubated for 1 h at room temperature. Later, T4 DNA ligase in the ligation mix was heat inactivated for 20 minute at 65°C, and used for bacterial transformation.

A 1:3 (vector: insert) ratio was used for the ligation reaction.

The Insert to Vector molar ratio was optimized using the following formula:

X ng of Insert = [(ng of Vector x kb size of Insert) / kb size of Vector] x Insert: Vector molar ratio.

3.1.9 Preparation of competent E.coli cells

A single colony of *E. coli* strain (Top10 or XL1Blue) was inoculated in 5-6 ml Luria-Bertani (LB) medium and cultured overnight at 37°C on shaker with 200 RPM. 5 ml of grown culture was added into fresh 250 ml LB medium and grown to early logarithmic phase (OD 600 = 0.3 - 0.6) at 37°C on shaker with 200 rpm. The culture was centrifuged for 10 min at 3000 rpm at 4°C in a table top centrifuge. The bacterial pellet was resuspended in 1/10th volume of cold TSB buffer [100 ml LB, 10 g PEG (MW = 3,350), 5 ml DMSO, 0.1 ml 1 M $MgSO_4$, 0.1 ml 1M $MgCl_2$] and incubated on ice for 10 min. Competent cell suspension was aliquoted into cold

eppendorf tubes (50 µl and 100 µl) and snap frozen in liquid nitrogen. Aliquoted snap frozen competent bacterial cells were stored at -80 °C.

3.1.10 Transformation of E. coli competent cells

Ligation reaction mixture (4-8 µl) or plasmid DNA (1-20 ng) was added to the thawed competent cells and mixed by flicking. The reaction mixture was incubated on ice for 30 min followed by incubation at 42°C for 1.5 min and then kept on ice for 10 min. Later, 500 µl of LB medium (without any antibiotic) was added to the mixture and incubated for 1 hr at 37°C on shaker with 200 rpm. And then, cells were spread plated on LB Agar plates containing appropriate antibiotic. Plates were incubated at 37°C overnight and next day colonies were observed.

3.1.11 Plasmid DNA isolation

The "mini-prep" method is useful for positive colonies screening i.e. to prepare plasmid DNA in small quantities from a number of transformants. A single colony was selected from LB agar plate and inoculated in 5 ml of LB medium containing the appropriate antibiotic with a sterile pipette tip. Bacterial cells were cultured overnight at 37°C on shaker with 200 rpm. The cells were harvested by centrifugation for 15 min at 4500 rpm in a table top centrifuge (Eppendorf 5415C). Plasmid DNA was isolated using the Plasmid Miniprep kit (Sigma) following the manufacturer's instructions. Large amount of plasmid DNA was prepared for downstream experiment using the Plasmid Midiprep Kit (Sigma) according to the manufacturer's instructions.

3.1.12 In situ hybridization of whole mount mouse embryonic lungs

In situ hybridization is a method to visualize spatiotemporal presence of a specific RNA sequence in the entire tissue by labeled complementary RNA strands (probes). For this study, it was used to analyze the expression pattern of *Hmga2* in murine embryonic tissues. For sample preparation, timed-pregnant C57BL6 wild type mice were sacrificed at indicated time points and embryos and embryonic lungs were isolated according to standard methods and whole mount mouse embryo and embryonic lung *in situ* hybridization was performed as described [109] with minor modifications. Briefly, to synthesize digoxigenin- labeled RNA probes, pcDNA3-*mHmga2* plasmid (a kind gift from Prof. Peter Grouse; [110]) template was linearized, and UTP-digoxigenin (Roche) substituted antisense RNA probes were transcribed with T7 and sense RNA

probes were transcribed with SP6 RNA polymerase (as negative control). After *in situ* hybridization, embryonic lungs were post-fixed in 4 % PFA and imaged using Leica M205 FA.

3.1.13 Chromatin immunoprecipitation

Chromatin immunoprecipitation (ChIP) analysis of the mouse *Gata6* promoter was performed as described [111] with slight modifications. Briefly, MLE-12 cells were crosslinked by 1% formaldehyde for 10 minutes, neutralized with glycine for 5 min on ice, lysed and sonicated with Diagenode Biorupter to an average DNA length of 500-600 bp. After isolation, the soluble chromatin was immunoprecipitated with antibodies listed in the Appendix Table 2. ChIP-reChIP experiment was performed as previously described [112]. Reverse cross-linked immunoprecipitated chromatin was subjected to qPCR using the primers listed in the Appendix Table1.

3.1.14 Luciferase Reporter Assay

Dual-Luciferase reporter assays (Promega) were performed as described [113] following transient transfection of MLE-12 cells in 96-well plates with a total of 100 ng DNA per well, containing 15 ng effector plasmid, 15 ng pGL4-*Sftpc* promoter or *SV40* promoter luciferase reporter plasmid, 1 ng *Renilla* luciferase reporter plasmid and 69 ng pBlueScript (pBS). Each sample was performed in triplicate and error bars indicate standard error of the mean. Each experiment was repeated at least three times.

3.2 Cell biological methods

3.2.1 Cell culture

MLE-12 and HEK293T cells were obtained from American Type Culture Collection (Manassas, VA). MLE-12 cells were cultured at 37°C in 5% CO_2 in DMEM F12 with 5% fetal calf serum (FCS), 100 U\ml penicillin and 100 U\ml streptomycin. HEK293T cells were cultured at 37 ^{0}C in 5% CO_2 in DMEM with high glucose (4.5 g/l), 10% FCS, 2 mM L-Glutamine, 1 mM Pyruvate, 100 U\ml penicillin and 100 U\ml streptomycin. Cellular growth and viability were assessed by phase contrast microscopy. The culture medium was replaced every other day. After attaining confluence, medium was aspirated from the cells, the cells were washed with 1X PBS and trypsinized with 1x trypsin-EDTA solution,diluted in 1x PBS. The trypsin-EDTA solution was neutralized with complete DMEM medium containing FCS. For experiment purposes, cells were

seeded at density $2x10^5$/ml, which gave 70% confluence in 24 h. All the solutions added to cell cultures were prewarmed in a 37°C water bath. All manipulations were performed aseptically in a cell culture hood using sterile equipment.

For the generation of FLAG-H2AX stable cell lines, HEK293T cells were co-transfected with a vector encoding for FLAG-H2AX wild type or S139A mutant (both gift of Dr. Kwon, [114]) and an empty pBABE vector, which provides the puromycin resistance. Cells at 80-90% confluence were transfected with Lipofectamine 2000 (Invitrogen) according to the manufacturer instructions. 48h after transfection the cells were split 1:4 and the next day 2.5 μg/ml of puromycin were added to the media. Single positive clones were isolated and stably maintained in 1 μg/ml of puromycin. Stable transfected HEK293T cells were cultured at 37 ^{0}C in 5% CO_2 in DMEM with high glucose (4.5 g/l), 10% FCS, 2 mM L-Glutamine, 1 mM Pyruvate, 100 U\ml penicillin, 100 U\ml streptomycin and 1 μg/ml puromycin.

3.2.2 Cryopreservation and thawing of cells

Cultured cells were cryopreserved by resuspending the harvested pellet in freeze medium which contains 10% DMSO. The cells were transferred to a cryogenic vial and immediately placed in a -80°C freezer overnight before transfer to -195°C liquid nitrogen for long term storage. To thaw, cell vials removed from liquid nitrogen and were thawed rapidly in a 37°C water bath and cells were immediately rinsed once in growth medium to remove the freeze medium and then cultured.

3.2.3 Transient transfection

Cells were transiently transfected using lipofectamine 2000 reagent (Invitrogen), a 1:1 (w/w) liposome formulation of the cationic lipid N-[1-(2,3-dioleyloxy)propyl] n,n,ntrimethylammonium chloride (DOTMA) and dioleoyl phosphotidylethanolamine (DOPE) in membrane filtered water.

Cells were maintained as described (Section 3.2.1). 70-80% confluent cells were used for the transfection experiments. On the day of transfection, plasmid DNA or siRNA was diluted in Opti MEM medium (Gibco). Separately, Lipofectamine 2000 reagent (Invitrogen) was diluted in Opti MEM medium. DNA: Lipofectamine was used in the ratio of 1:2.The diluted plasmid DNA/ siRNA and the diluted lipofectamine 2000 reagent were pre-incubated at room temperature for 5 min before being mixed to make complexes. Complexes were allowed to form for a further 15

min at room temperature and then, added onto the cells. After 6 hrs, this medium was replaced with complete DMEM medium. Cells were analyzed after a given time point. Transfection volumes were scaled up or down according to the surface area of the tissue culture vessel in use (Lipofectamine 2000 reagent, Invitrogen, data sheet).

3.2.4 Transient transfection efficiency assessment

For overexpression studies, transfection efficiency was monitored after transiently transfecting cells with GFP (Green fluorescence protein) over expressing construct and later after 48 hrs assessing the percentage of GFP positive cells under fluorescent microscope (Leica). For siRNA-mediated inhibitory studies, transfection efficiency was monitored after transiently transfecting the cells with Cy3 labeled siRNA (AM4621, Applied biosystem) and later after 48 hrs assessing the percentage of Cy3 positive cells under fluorescent microscope (Leica).

siRNA used in the study are 40 nM *siCtrl* (Negative control, AM4611; Ambion), 40 nM *siGata6* (L-065585-00; Dharmacon), 20 nM *siFzd2* (s81164; Applied Biosystem), 20 nM si*Hmga2* (s67600, Applied Biosystems), 20 nM *siRNA* control (*siCtrl;* D-001210-01-05; Dharmacon), 20 nM *siATM* (SIHK0133; Sigma) and 20 nM *siHMGA2* (M-013495-02; Dharmacon).

3.2.5 Cell treatment

HEK293T cells were treated with 10 µM ATM kinase inhibitor KU-55933 (Merk Chemicals Ltd.; Cat. No.: 118500). DMSO used as solvent for ATM kinase inhibitor KU-55933. Cells were harvested after 48 h for further analysis.

3.2.6 Lung explants culture methods

Timed-pregnant [C57BL6 wild type or beta-catenin/TCF/LEF reporter transgenic (BAT-GAL)] mice were sacrificed on *post coitum* day 12.5 (E12.5, day of plug = E0.5) according to standard methods. BAT-GAL transgenic mice were genotyped by ß-galactosidase staining and PCR (a gift of Stefan Liebner [115]). Lungs were dissected from the embryos and cultured for 72 hours equivalent to E15.5 (E15.5*) as previously described [116]. The lungs were treated with 3 µM *siRNAs* against *Hmga2* (Applied Biosystems, Silencer Select siRNAs, Assay ID s67600), *Gata6* (L-065585-00; Dharmacon) and *Scrambled siRNA* (negative control, *Ctrl*) (Sigma, MISSION *siRNA* Universal Negative Control, SIC001) or 200 nM of mouse recombinant Dickkopf-1 (DKK1, R&D Systems, 5897-DK-010). The *siRNA* and protein treatments were renewed every

24 h. After 72 h, the lungs were checked for morphological changes by standard microscopy techniques and harvested for *RNA* (QIAGEN Rneasy Micro Kit) and protein isolation. Transfection efficiency was monitored after transiently transfecting the lung explants at E12.5 with Cy3 labeled siRNA (AM4621, Applied Biosystem) and later, after 72 hrs assessing the percentage of Cy3 positive cells under fluorescent microscope (Leica). The images were used to determine the total number of terminal bud branches and for quantification of total branch length as described [117].

3.3 Animal experiments

3.3.1 Mice

C57BL/6 and *Hmga2*$^{+/-}$ mice (stock # 002644, Jackson Laboratories;[118]) were obtained from Charles River Laboratories, Germany at 5 to 6 week of age. *Hmga2* overexpression mice were kind gift from Prof. Monica Bessler [119]. Animals were housed and bred under controlled temperature and lighting [12/12-hour light/dark cycle], fed with commercial animal feed and water *ad libitum*. All experiments were performed with 6-8 week old mice according to the institutional guidelines that comply with national and international regulations.

Wild type, beta-catenin$^{+/-}$ (*CMV-Cre-,Ctnnb1*^{tm2Kem,} [120]) and Doxycycline-inducible Dkk1 (*Rosa26rtTA, Tet (0) Dkk1;* [121]) mice were administered orotracheally *control* [*PLKO.shControl*] or *Hmga2* [*PLKO.sh Hmga2*] plasmids. *Hmga2*$^{-/-}$ mice were administered orotracheally *control [empty vector]* or *Gata6* expression vector [*pCMV6-entry-Gata6-flag/myc* (origene)]. The plasmids were prepared in PEI transfection reagent (Sigma-Aldrich) at 50 µg/Kg dose, and administered three times (days -10; -7 and -3). Doxycycline-inducible Dkk1 mice were treated with doxycycline (0.4 mg/ml in water) starting at -7 day. The lungs were harvested (day 0) and used for RNA isolation, FACS analysis and immunohistochemistry. The *pLKO.1-puro shDNA* constructs were obtained from the Sigma MISSION shRNA library/TRC [122].

3.3.2 Compliance Measurement

Anesthetized and relaxed Wild type and *Hmga2 -/-* mice were tracheotomized, placed in a small animal whole-body plethysmographic chamber (Buxco), and ventilated in volume-driven mode (with a positive end-expiratory pressure [PEEP] of 300 mmHg) as described [123]. Before measurement of lung compliance, chambers were calibrated with a rapid injection of 300 µl

room air. Respiration rate was set to 20/min, and ventilation pressure was recorded while inflating the lung at a tidal volume of 200 µl. Ventilator compliances are given in kPa/ml and corrected for mouse whole-body weight.

After compliance measurement, thorax was opened and lung was then perfused with 1X PBS. The lung was either frozen for protein and mRNA isolation or perfusion-fixed with 4% paraformaldehyde for 15 min with a pressure of 20 cm H_2O for histology.

3.4 Histology and Immunohistochemistry

3.4.1 H&E staining

Hematoxylin & Eosin (H&E) staining was done for morphometric analyses. Mouse embryonic lung and adult lung were fixed in 4% PFA/PBS at 4°C overnight. Fixed embryos were dehydrated by incubating them in series of ethanol:water mixtures (50:50, 70:30, 80:20, 90:10, 96:04) and twice with 100% ethanol for mouse 2 h each step at room temperature. Dehydrated lungs were washed with butanol overnight at RT and then twice with paraffin (at least 2-3 h each step at 65°C). Washed lungs were embedded in parraffin and sectioned with a microtome (4 µm thick) and mounted on glass slides after stretching them by putting them in a 42°C water bath. After mounting, glass slides were incubated at 42°C overnight and stored at RT for further experiments. Mounted sections were deparaffinised by washing thrice with xylol (10 min each step), twice with 100% ethanol (5 min each step) and then series of ethanol: water mixtures (96:4, 90:10, 70:30, 50:50) for 5 min each step. At last sections were washed with tap water at least for 5 min. For staining rehydrated mounted sections were incubated in Hemalum for 10 min and washed with warm running tap water until sections became blue. Sections were rinsed with distilled water for 1-2 min. After Hemalum staining sections were incubated with eosin solution for 6 min and shortly washed once with 95% ethanol and once with 100% ethanol. At last sections were put into xylol and mounted with xylol-based mounting medium (Entellan, Merck). Mounted samples were analyzed by bright field microscopy.

3.4.2 Immunostaining

For cryosections of mouse lung tissue, lungs were harvested and embedded in polyfreeze tissue freezing medium (Polysciences, Inc.). Sections of 10 µm were cut on a cryostat (Leica Germany). Sections were post-fixed in 4% PFA for 10 min. Antibody staining was performed

following standard procedures. All incubations and washes were done with histobuffer containing 3% BSA and 0.2% Triton X-100 in 1× PBS, pH 7.4. Unspecific binding sites were blocked over 45-60 minutes with donkey serum and histobuffer (1:1 (v/v) ratio). The sections were then incubated with primary and secondary antibodies for 60 min followed by nuclear staining. The sections were examined with a Zeiss confocal microscope (Zeiss, Germany).

For Paraffin embedded mouse lung tissue, Lungs were post-fixed overnight in 1% PFA at 4°C, dehydrated over a graded series of alcohol, and paraffin embedded. Sections of 4 µm were cut on a microtome (Leica Germany). Antigen retrieval was performed by microwave heating for 8 min using 1mM EDTA. Antibody staining was performed following standard procedures. All incubations and washes were done with histobuffer containing 3 % BSA and 0.2 % Triton X-100 in 1× PBS, pH 7.4. Unspecific binding sites were blocked over 45-60 minutes with donkey serum and histobuffer (1:1 (v/v) ratio). The sections were then incubated with primary and secondary antibodies for 60 min followed by nuclear staining. The sections were examined with a Zeiss confocal microscope (Zeiss, Germany).

Primary and secondary antibodies used were listed in Appendix Table 2. DAPI (Invitrogen) or DRAQ5 (eBioscience) was used as nuclear dye.

Paraformaldehyde fixed and paraffin embedded lung tissue sections were further used for H & E staining using standard method for the lung morphology and morphometric analysis. Leica DM6000B microscope with an automated stage and Leica QWIN V3 digital image processing and analysis software were used for the lung morphometric analysis.

3.4.4 β-Gal staining

BAT-GAL transgenic mice embryonic lung explants were fixed at room temperature for 15 min in solution A (0.4 ml 25% Gluteraldehyde, 0.5 ml 0.5M EDTA, 0.2 ml 0.5M $MgCl_2$ to 50 ml with 1X PBS). After fixation washed three times for 10 min in solution B (0.8 ml 0.5 M $MgCl_2$, 2 ml 2% NP-40, 2 ml 10% Na-deoxycholate to 200 ml with 1X PBS). After washing lung explants were stained at 37 ^{0}C in solution C (100 ul K-hexacyanoferrate (II) [Ferroso], 100 ul K-hexacyanoferrate (III) [Ferrico], 200 ul 50 ug/ml X-gal and 9.6 ml solution B). Once color is developed then washed 3 times for 10 min each in solution B and once in PBS and image were taken using inverted light microscope.

3.4.5 Flow Cytometry

Flow cytometry analysis was performed as described [31] using mouse adult lungs. Single cell suspension from lung was obtained as described earlier [6]. Cells were analysed for SFTPC- and SCGB1A1-staining using BD LSRII flow cytometry. Data were analysed with Weasel software.

3.5 Biochemical methods

3.5.1 *In vitro* chromatin reconstitution and Histone eviction assays

An 806 bp 5'-biotin labeled PCR amplicon carrying the mouse *Gata6* promoter was immobilized on streptavidin-coated magnetic Dynabeads following supplier's instruction (Invitrogen). Immobilized *Gata6* promoter and recombinant histones (NEB; H3.3, M2507S; H2B, M2505S; H2A, M2502S; H4, M2504) and/or H4-his tag (KeraFAST, FS0004) or H2A-his tag (BPS BioScience, 52025) were used for *in vitro* chromatin reconstitution by salt dialysis method [124] using a molar ratio of 1:0.6 (w:w) of DNA : histone octamer. The optimal molar ratio of histone octamer: DNA was titrated in a series of reactions, in which different molar input ratios were tested and analyzed. Quality of reconstituted chromatin was analyzed using 0.1 unit Micrococcal nuclease as previously described [125]. Proximal 631 bp mice *Gata6* promoter was cloned into TOPO TA cloning vector (Invitrogen) and used as template. T7 primer along with 5'-biotin labeled SP6 primer was used for 806 bp long 5'-biotin labeled amplicon synthesis by PCR.

In vitro reconstituted chromatin was incubated with 40 µg HEK293T nuclear protein lysates for 15 min at room temperature. After incubation with nuclear protein lysates, supernatant was removed and the immobilized chromatin was washed once followed by Hind III (NEB) digestion to separate the *in vitro* reconstituted chromatin from magnetic beads. Later, the supernatant and separated chromatin from beads was used for western blot analysis.

3.5.2 Affinity-precipitation and Immunoprecipitation

Total of 5 x 10^7 of each MLE-12 cells and *Hmga2* over expressed MLE-12 cells were collected and washed three times in cold PBS, spun down at 1100 rpm for 10 min at 4 ^{0}C. Cells were incubated in 2 ml of hypotonic cell lysis buffer (10 mM (pH7.4) Tris-HCl, 1.5 mM $MgCl_2$, 10 mM KCl, 1 mM DTT, 25 mM NaF, 0.5 mM Na_3VO_4, 40 µg/ml phenylmethylsulfonyl fluoride (PMSF) and protease inhibitor (Calbiochem)) on ice for 10 min and then spun down at 3500 rpm for 10 min at 4^0C. Nuclear cell pellets were resuspended in 300 µl Nuclear lysis buffer (50 mM

(pH 7.4) Tris-HCl, 170 mM NaCl, 20% glycerol, 15 mM EDTA, 0.1% (v/v) Triton X-100, 0.2 mM DTT, 20 mM NaF, 0.5 mM Na_3VO_4, 40 µg/ml PMSF and protease inhibitor). Nuclear protein lysates were incubated overnight rolling at 4^0C with 60 µl Ni+ sepharose beads (GE Healthcare) which were preincubated with lysis buffer containing 1% BSA. An amount of 5% nuclear lysate was kept as Input control. Beads were collected at 2500 rpm for 3 min at room temperature and washed with 500 µl washing buffer (50 mM (pH 7.4) Tris-HCl, 170 mM NaCl, 15 mM EDTA, 0.4% (v/v) Triton X-100, 20 mM Imidazole, 20 mM NaF, 0.5 mM Na_3VO_4, 40 µg/ml PMSF and protease inhibitor) 5 times. Elution was performed in 60 ul of elution buffer (50 mM (pH 7.4) Tris-HCl, 500 mM NaCl, 15 mM EDTA, 0.4% (v/v) Triton X-100, 500 mM Imidazole, 20 mM NaF, 0.5 mM Na_3VO_4, 40 µg/ml PMSF and protease inhibitor). The eluates were subjected to mass spectrometry analysis.

Co-IPs were performed as described [86] with minor adaptations. Briefly, nuclear protein lysates were prepared as described above. Precleared 500 µg nuclear protein lysates were incubated with the 0.5 to 1 µg antibodies on ice for 2 h and then 30 µl protein-G-sepharose beads (GE Healthcare; equilibrated once in 10 ml water and three times in washing buffer) were added and incubated overnight at 4 ^{0} C rolling. Beads were collected and washed 5 times with 500 µl ice cold washing buffer. 30µl 2x SDS sample loading buffer was added to beads, boiled at 95 ^{0}C for 5min, spun down and loaded on SDS-PAGE.

Immunoprecipitation to analyze ATM kinase activity was performed as previously described [85, 86] using an antibody specific against phospho-(Ser/Thr) ATM substrate (Cell Signaling).

3.5.3 Mass spectrometry: sample preparation, methods and data analysis

Mass spectrometry identifies proteins by ionization of chemical compounds to charge peptides and measurement of their mass to charge ratio. This technique was utilized for proteomic based HMGA2 interactome analysis. Therefore, cell nuclear lysates from control and Hmga2-myc/his over-expressed MLE-12 cells were used for affinity-precipitation (Histidine-pulldown) and later were run on NuPAGE 4-12% BIS-TRIS gel (Invitrogen, Carlsbad, USA). Gels were stained with colloidal blue (Invitrogen), and evenly sized gel pieces were excised and processed for mass spectrometry. The gel pieces were subjected to in-gel reduction and alkylation, followed by trypsin digestion as described previously [126].

Reverse phase nano-LC-MS/MS was done by using an Agilent 1200 nanoflow LC system (Agilent Technologies, Santa Clara, CA) with a cooled thermostated 96-well autosampler. The LC system was coupled to LTQ-Orbitrap instrument (Thermo Fisher Scientific) equipped with a nanoeletrospray source (Proxeon, Denmark). Chromatographic separation of peptides was performed in a 10 cm long and 75 µm inner diameter capillary needle. The column was custom-made with methanol slurry of reverse-phase ReproSil-Pur C18-AQ 3 µm resin (Dr. Maisch GmbH). The tryptic peptide mixtures were autosampled at a flow rate of 0.5 µl/min and then eluted with a linear gradient at a flow rate 0.25 µl/min. The mass spectrometers were operated in the data-dependent mode to automatically measure MS and MS/MS spectra. LTQ-FT full scan MS spectra (from m/z 350 to 1750) were acquired with a resolution of r = 60,000 at m/z 400. The five most intense ions were sequentially isolated and fragmented in the linear ion trap by using collision-induced dissociation with collision energy of 35%. Further mass spectrometric parameters: spray voltage of 2.4 kV, no sheath gas flow, and the temperature of the heated capillary was 200 °C.

For data analysis we used the MaxQuant software tool (Version 1.2.0.8). The measured raw data were processed and quantitated as described [127].

3.5.6 Western blot

Western blotting used standard methods. Antibodies used were listed in Appendix Table 2. Immunoreactive proteins were visualized with the corresponding HRP-conjugated secondary antibodies using the Super Signal West Femto detection solutions (Thermo Scientific). Signals were detected and analyzed with Luminescent Image Analyzer (Las 4000, Fujifilm). Protein concentrations were determined using BCA kit (Sigma).

3.6 Statistical analysis

Statistical analyses were performed using Excel Solver. All data are represented as mean ± Standard Error (mean ± s.e.m). One-way analyses of variance (ANOVA) were used to determine the levels of difference between the groups and *P* values for significance. *P* values after one-way ANOVA,* $P \leq 0.05$; ** $P < 0.01$ and *** $P < 0.001$ Only in Figures 17C-D unpaired t-test was used to calculate *P* values, *** $P<0.001$; ** $P<0.01$; * $P<0.05$.

Chapter 4: RESULTS

4.1 *Hmga2* is required for proper distal epithelial cell differentiation during lung development and homeostasis

4.1.1 *Hmga2* is expressed in the mouse embryonic lung at the distal airways

To verify that *Hmga2* is expressed during lung development, qRT-PCR based gene expression analysis was performed (Figure 11A). *Hmga2* transcript was detected at E11.5, when the primary lung buds have evaginated from the foregut and secondary buds are forming as outgrowths from the primary lung buds. During the pseudoglandular stage of lung development (E12.5 – E16.5), *Hmga2* expression progressively decreased. Between canalicular (E16.5 – E17.5) and initial saccular stages (E17.5 – E18.5), the levels of *Hmga2* transcript increased again. Later in gestation (saccular stages, E18.5 – P5), *Hmga2* expression was further reduced and reached a basal level of expression that was maintained through alveolar phase (P5 – P28). Thus, *Hmga2* mRNA levels were high during early stages of lung development, in which cells are undifferentiated, and decreased as lung development progressed, coincident with cell differentiation.

In situ hybridization expression pattern analysis in the embryonic lung at E12.5 (Figure 11B), revealed that *Hmga2* is ubiquitously expressed with higher levels of expression at the tips of the growing lung buds. Interestingly, *Hmga2* expression became restricted to the distal lung endoderm at E14.5. Consistently, immunostaining on sections of the embryonic lung at E14.5 (Figure 11C) supported the presence of HMGA2 in cells of the distal lung endoderm. Co-staining with an antibody specific for the nuclear envelope protein LMNB1 demonstrated the nuclear localization of HMGA2 (Figure 11C). The observed expression patterns in embryonic lung suggest a role for HMGA2 in epithelial differentiation.

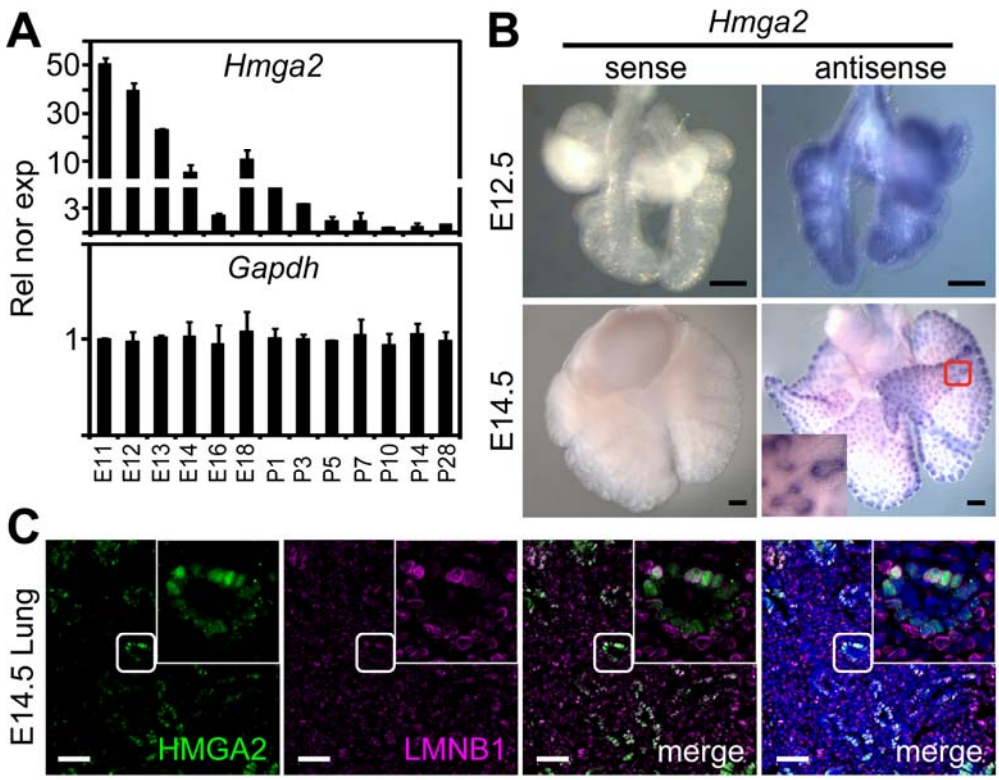

Figure 11. *Hmga2* is expressed in the mouse embryonic lung at the distal airways. (A) *Hmga2* and *Gapdh* expression was analyzed by qRT-PCR in mouse embryonic lung at different days *post coitum* (E11.5-E18.5) and in mouse lung at different days after birth (P1-P28). Rel nor exp, relative expression normalized to *Tuba1a*. Error bars, s.e.m. (n=4). (B) *Hmga2* mRNA was detected in mouse embryonic lung at E12.5 and E14.5 by in situ hybridization using an *Hmga2*-specific antisense RNA probe. Sense probe, negative control. Scale bars, 200 μm. Square shows details at higher magnification. (C) Fluorescence microscopy of embryonic lung sections (E14.5) after double immunostaining using HMGA2- and LMNB1-specific antibodies. Nuclear staining with DAPI (blue). Squares as in B. LMNB1, LAMIN B1. Scale bars, 40 μm.

4.1.2 Hmga2 is required for proper differentiation of the distal epithelium during lung development

To determine the role of *Hmga2* during lung development, embryonic lung of *Hmga2*$^{-/-}$ mice [118] was analyzed at E18.5. *Hmga2*$^{-/-}$ mice embryos showed reduced body weight (Figure 12A) and lung-to-body-wet-weight ratio (Figure 12B). *Hmga1*, another member of HMGA group protein family member expression was analyzed in *Hmga2*$^{-/-}$ mice embryos by qRT-PCR (Figure 12C). *Hmga2*$^{-/-}$ mice embryos showed no change in *Hmga1* expression when compared to the wild type mice.

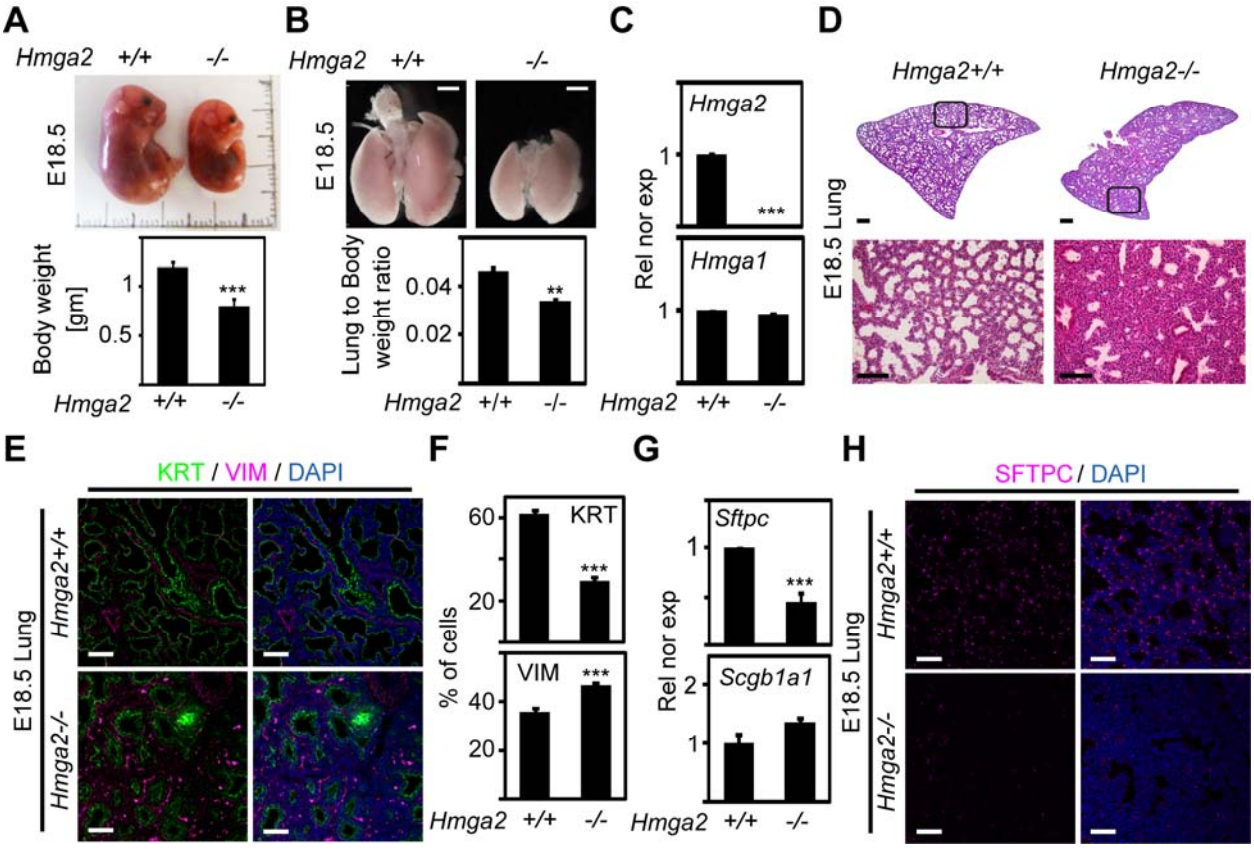

Figure 12. *Hmga2*$^{-/-}$ mice showed embryonic lung defect. (A) Top, *Hmga2*$^{-/-}$ mouse embryos at E18.5 were smaller than WT embryos. Main interval of the scale is equivalent to 1 cm. Bottom, *Hmga2*$^{-/-}$ embryo showed 40% body wet weight reduction when compared to WT embryos. Data are represented as mean ± s.e.m. (n=3). Asterisks, *P* values after one-way ANOVA, *** $P < 0.001$; ** $P < 0.01$; * $P < 0.05$. (B) Lungs of *Hmga2*$^{-/-}$ embryo were smaller (top) and showed a reduced lung-to-body-wet-weight ratio (bottom) when compared to WT embryos at E18.5. Scale bars, 1 mm. Error bars, s.e.m. (*n*=6). Asterisks as in A. (C) Expression analysis of the indicated genes by qRT-PCR in embryonic lung (E18.5) of WT and *Hmga2*$^{-/-}$ mice. Error bars, s.e.m. (n=4). Asterisks as in A. (D) Representative of histological analysis using H&E staining on sections of WT and *Hmga2*$^{-/-}$ embryonic lung at E18.5. Squares as in Fig. 11B. Scale bars, 100 μm. (E) Sections of embryonic lung (E18.5) of WT and *Hmga2*$^{-/-}$ mice were analyzed by confocal microscopy after double immunostaining using KRT- and VIM-specific antibodies. KRT, Pan Cytokeratin and VIM, Vimentin. Scale bars, 40 μm. (F) Quantification of epithelial (KRT) and mesenchymal (VIM) cells of *Hmga2*$^{-/-}$ and WT embryonic lung immunostained as in E. Error bars, s.e.m. (*n*=3). Asterisks as in A. (G) Expression analysis of the indicated genes by qRT-PCR at E18.5 of WT and *Hmga2*$^{-/-}$ mice lung. *Scgb1a1*, Secretoglobin 1A1. Error bars, s.e.m. (n=4). Asterisks as in A. (H) Sections of embryonic lung (E18.5) of WT and *Hmga2*$^{-/-}$ mice were analyzed by confocal microscopy after immunostaining using SFTPC- specific antibody. Scale bars, 40 μm.

Histological analysis of the embryonic lung at this stage (Figure 12D) revealed a marked increase of cell density in the *Hmga2*$^{-/-}$ mice when compared to the WT mice suggesting increased cell proliferation. Furthermore, immunostaining on sections of embryonic lung (Figure 12E) using antibodies specific for the epithelial marker KRT (pan-cytokeratin) and the mesenchymal marker VIM (vimentin) showed an increase in the mesenchymal cells and an irregularly shaped epithelium in *Hmga2*$^{-/-}$ mouse lungs when compared to the WT lung, suggesting an expansion of the mesenchyme at the expense of the epithelium. Consistent with this observation, quantification of KRT-positive cells (Figure 12F, top) showed a decrease from 61.7% to 29.5% ($P < 0.001$; $n = 3$), whereas the number of VIM-positive cells (Figure 12F, bottom) increased from 35.7% to 46.3% (($P < 0.001$; $n = 3$) in *Hmga2*$^{-/-}$ mice when compared to the WT mice. Thus, to examine lung epithelium differentiation, expression of proximal, *Scgb1a1*, and distal, *Sftpc*, epithelial markers was analyzed in the embryonic lung of WT and *Hmga2*$^{-/-}$ mice (Figure 12G). Whereas *Scgb1a1* expression did not change significantly, *Sftpc* expression was reduced after *Hmga2*$^{-/-}$, suggesting defects in distal epithelium differentiation. These defects were confirmed by immunostaning on sections of embryonic lung (Figure 12H) that showed reduced levels of SFTPC after *Hmga2*$^{-/-}$ when compared to the WT mice. Furthermore, co-localization of HMGA2 and SFTPC in the same cells of the embryonic lung at E14.5 (Figure 13A) supported *Hmga2* direct involvement in distal lung epithelial differentiation.

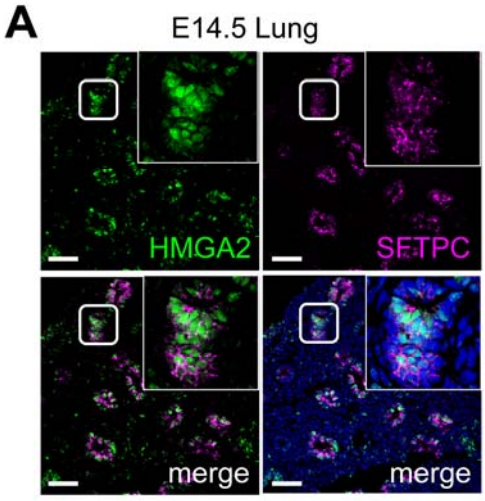

Figure 13. HMGA2 and SFTPC co-localized in the same cells of the embryonic lung. Fluorescence microscopy of embryonic lung section (E14.5) after double immunostaining using HMGA2- and SFTPC-specific antibodies. Squares as in Fig. 11B.

To further investigate the effect of *Hmga2*$^{-/-}$ on cell proliferation in embryonic lung, immunostaining on sections of embryonic lung was performed using cell proliferation markers PCNA (proliferating cell nuclear antigen) and MKI67 (antigen identified by monoclonal antibody Ki 67) (Figure 14A, B) which showed increased levels of proliferation markers in both the epithelium and the mensenchyme of the *Hmga2*$^{-/-}$ mice as shown by co-staining with antibodies specific for CDH1 or KRT or VIM supporting interpretation of the histological analysis. However, quantification of these results (Figure 14C) showed more prominent cell proliferation in the mesenchyme (right), from 3.9% to 43.3% ($P < 0.001$; $n = 3$), when compared to the epithelium (left), from 8% to 23.6% ($P < 0.001$; $n = 3$). To confirm increased cell proliferation in the embryonic lung after *Hmga2*$^{-/-}$, expression of cell cycle progression markers *Ccne1*, *Ccne2* and Ccnd2 (Cyclin E1, E2 and D2; Figure 14D) was analyzed. Enhanced expression of these genes in *Hmga2*$^{-/-}$ embryonic lung when compared to WT lung supported the observation of the elevated cell proliferation.

Further, co-staining with distal epithelial cell marker SFTPC and cell proliferation marker PCNA on sections of embryonic lung (Figure 15A, left) was performed which showed that reduced numbers of SFTPC-positive cells from 10.8% to 2.7% ($P < 0.001$; $n = 3$) in *Hmga2*$^{-/-}$ when compared to the WT mice, while no change was observed in the proliferation of the SFTPC positive cells (Figure 15B, left). Thus, to check distal epithelial progenitor cell population, immunostaining on sections of embryonic lung was performed using antibodies specific for the distal epithelial progenitor cell marker SOX9 (sex determining region Y-box 9) and PCNA (Figure 15A, right). The number of SOX9-positive cells increased from 3.8% to 35.3% ($P < 0.001$; $n = 3$) in *Hmga2*$^{-/-}$ when compared to WT mice (Figure 15B, right). Interestingly, most of the SOX9-positive cells in the *Hmga2*$^{-/-}$ lung were proliferating as shown by PCNA co-staining supporting the distal epithelial progenitor cell differentiation defect in *Hmga2*$^{-/-}$ embryonic lung when compared to WT lung.

In addition to cell proliferation, programmed cell death is an important process involved in lung development [128]. Thus, co-staining on sections of embryonic lung (Figure 16A,B) was performed using antibodies specific for the active form of the apoptosis-related cysteine peptidase, cleaved caspase 3 (clCASP3) and the epithelial marker KRT (Figure 16A, left) or the mesenchymal marker ACTA2 (smooth muscle actin alpha 2, Figure 16A, right). Quantification

of clCASP3-positive cells showed that while the level of apoptosis in the mesenchyme (Figure 16B, right) was not significantly affected in *Hmga2*$^{-/-}$ (0.2% in the WT versus 0.3% in the KO), it increased in the lung epithelium (Figure 16B, left) of *Hmga2*$^{-/-}$ mice from 2.7% to 7.5% ($P < 0.01$; $n = 3$) supporting the reduction of epithelium when compared to WT mice.

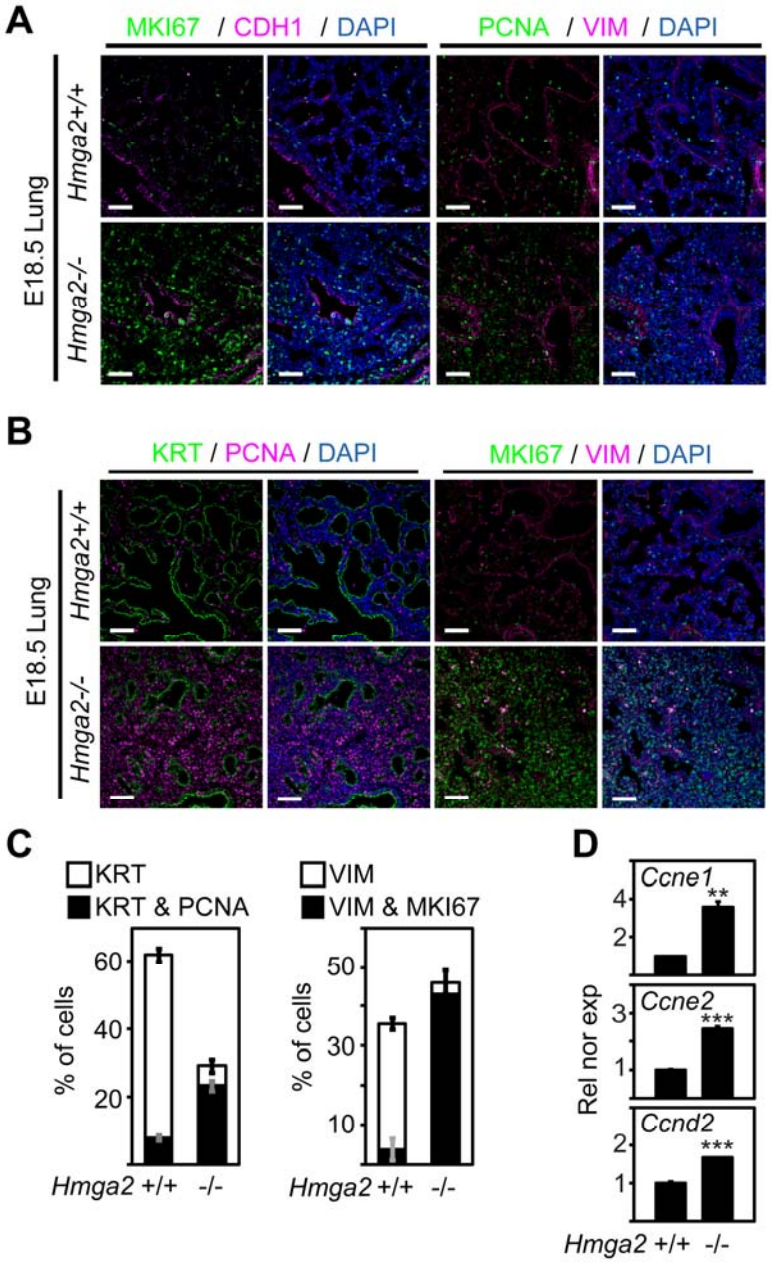

Figure 14. *Hmga2*$^{-/-}$ mice embryonic lung showed increased cell proliferation. (A) Sections of embryonic lung (E18.5) of *Hmga2*$^{-/-}$ mice were analyzed by confocal microscopy after double immunostaining using (left) MKI67- and CDH1-specific antibodies or (right) PCNA- and VIM-specific antibodies. CDH1, E-cadherin. Scale bars, 40 μm. (B) Sections of embryonic lung (E18.5) of *Hmga2*$^{-/-}$ mice were analyzed as in A using (left) KRT- and PCNA-specific antibodies or (right) VIM- and MKI67-specific antibodies. Scale bars, 40 μm. (C) Quantification of proliferating (PCNA or MKI67 positive) epithelial (KRT) and mesenchymal (VIM) cells at E18.5 of WT and *Hmga2*$^{-/-}$ mice lung immunostained as in B. Error bars, s.e.m. (n=3). (D) Expression analysis of the indicated cell proliferation marker genes by qRT-PCR in E18.5 lung of WT and *Hmga2*$^{-/-}$ mice. Error bars, s.e.m. (n=3). Asterisks as in Fig. 12A.

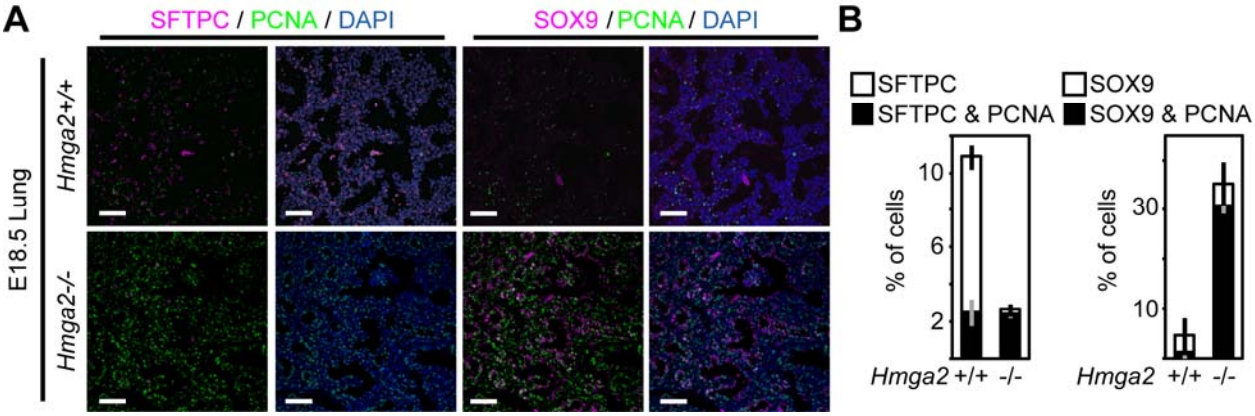

Figure 15. *Hmga2*$^{-/-}$ mice embryonic lung showed increased cell proliferation in the distal lung epithelial progenitor cells. (A) Sections of embryonic lung (E18.5) of *Hmga2*$^{-/-}$ mice were analyzed by confocal microscopy after double immunostaining using SFTPC- and PCNA-specific antibodies (Left) and using SOX9- and PCNA-specific antibodies (Right). Scale bars, 40 μm. (B) Sections of embryonic lung (E18.5) of *Hmga2*$^{-/-}$ mice were analyzed by confocal microscopy after double immunostaining as in A and quantified. Error bars, s.e.m. (*n*=3).

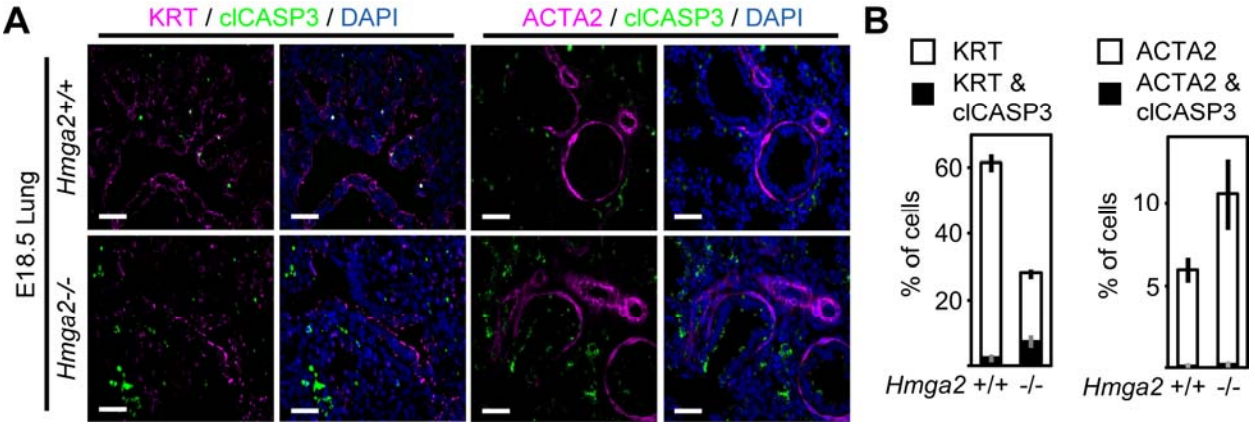

Figure 16. *Hmga2*$^{-/-}$ mice embryonic lung showed increased cell apoptosis in the distal lung epithelial cells. (A) Sections of embryonic lung (E18.5) of *Hmga2*$^{-/-}$ mice were analyzed by confocal microscopy after double immunostaining using KRT- and clCASP3-specific antibodies (Left) and using ACTA2- and clCASP3-specific antibodies (Right). Scale bars, 40 μm. (B) Sections of embryonic lung at E18.5 of *Hmga2*$^{-/-}$ mice were analyzed by confocal microscopy after double immunostaining as in A and quantified. Error bars, s.e.m. (*n*=3).

4.1.3 *Hmga2* knockout compromised adult lung function due to epithelial cell differentiation defect

Adult lung of *Hmga2*$^{-/-}$ mice was analyzed to confirm the phenotype of embryonic lung. *Hmga2*$^{-/-}$ adult lung also showed a reduced lung-to-body-wet-weight ratio (Figure 17A). H&E staining of *Hmga2*$^{-/-}$ adult lung section showed marked impairment in cellular structure (Figure

17B). Consequently, *Hmga2*$^{-/-}$ affected both lung morphology, as shown by increased septal wall thickness and reduced air space (Figure 17C), as well as lung function, as shown by increased airway resistance and reduced compliance (Figure 17D).

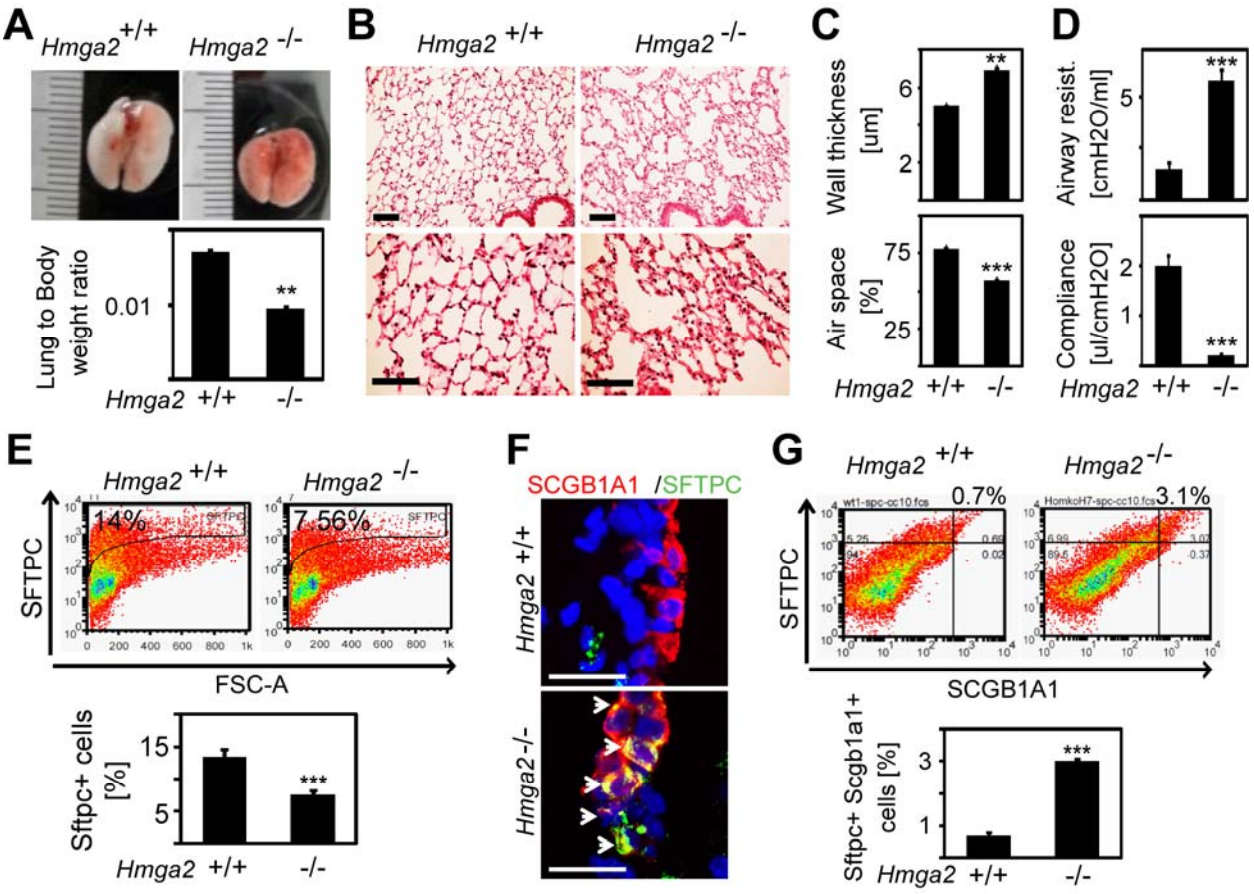

Figure 17. *Hmga2*$^{-/-}$ showed compromised adult lung function due to epithelial cell differentiation defect. (A) Lungs of *Hmga2*$^{-/-}$ mice were smaller (top) and showed a reduced lung-to-body-wet-weight ratio (bottom) when compared to WT. Main interval of the scale is equivalent to 1 cm. Error bars, s.e.m. (n=3). Asterisks as in Fig. 12A. (B) Histological analysis using H&E staining on sections of WT and *Hmga2*$^{-/-}$ adult lung. Scale bars, 100 μm. (C) *Hmga2*$^{-/-}$ increased septal wall thickness and reduced air space in adult lung. Sections of adult lung of WT and *Hmga2*$^{-/-}$ mice were performed as in B and analyzed by stereology. Error bars, s.e.m. (n=2 for WT and n=4 for *Hmga2*$^{-/-}$). Asterisks as in Fig. 12A. (D) Top, Airway resistance [cmH_2O/ml]. Bottom, Compliance [μl/cm H_2O]. Error bars, s.e.m. (n=4 in each group). Asterisks as in Fig. 12A. (E) Cell suspensions of adult lung of WT and *Hmga2*$^{-/-}$ mice were analyzed by flow cytometry after immunostaining using SFTPC-specific antibody. Error bars, s.e.m. (n=4). Asterisks as in Fig. 12A. (F) Sections of adult lung of WT and *Hmga2*$^{-/-}$ mice were analyzed by confocal microscopy after double immunostaining using SFTPC- and SCGB1A1-specific antibodies. Arrowheads, BASCs. Scale bars, 40 μm. (G) Cell suspensions of adult lung of WT and *Hmga2*$^{-/-}$ mice were analyzed by flow cytometry after double immunostaining using SCGB1A1- and SFTPC-specific antibodies. Error bars, s.e.m. (n=4). Asterisks as in Fig. 12A.

Hmga2$^{-/-}$ mice showed a reduction of ATII cells by flow cytometry analysis of single cell suspension of adult lung after SFTPC immunostaining (Figure 17E). ATII cells were reduced from 14 % (WT) to 7.56 % (P<0.01; n=4) in *Hmga2*$^{-/-}$ mice. Next, the effect of *Hmga2*$^{-/-}$ on one of the adult lung progenitor cell population BASCs was investigated (Figure 17F, G). BASCs express both *Scgb1a1* and *Sftpc*, a trait not shared by other epithelial cells in the adult lung [6]. Therefore, immunostaining in sections of adult lung using SCGB1A1- and SFTPC-specific antibodies was performed for the assessment of BASCs (Figure 17F). *Hmga2*$^{-/-}$ resulted in an expansion of BASCs when compared to the lung of WT mice. Moreover, flow cytometry analysis in cell suspension of adult lung (Figure 17G) revealed that the percentage of SFTPC- and SCGB1A1-positive cells increased from 0.7 % (WT) to 3.1 % (P<0.01; n=4) in *Hmga2*$^{-/-}$ mice. Thus, increased numbers of progenitor cells in the lung of *Hmga2*$^{-/-}$ mice generated an imbalance in cell differentiation that is reflected in a reduction of ATII cells, thereby affecting both lung morphology as well as lung functionality.

4.2 *Hmga2* modulates canonical WNT signaling during lung development and homeostasis

4.2.1 *Hmga2* knockout led to enhanced canonical WNT signaling during lung development

To identify the cause of the *Hmga2*$^{-/-}$ mice lung phenotype, Affymetrix microarray-based expression analysis of embryonic lung of *Hmga2*$^{-/-}$ mice was performed (Figure 18A). It revealed an increased expression of cell cycle related genes in *Hmga2*$^{-/-}$ when compared to the WT mice confirming immunohistological results. In addition, it also revealed increased canonical WNT signaling target genes or positive regulators and reduced negative regulators in the embryonic lung of *Hmga2*$^{-/-}$ mice. These results indicate enhancement of canonical WNT signaling in *Hmga2*$^{-/-}$ that was further validated by increased activity of the CTNNB1/TCF/LEF WNT-reporter (BAT-GAL) in embryonic lung of the BAT-GAL: *Hmga2*$^{-/-}$ double transgenic mice when compared to BAT-GAL: *Hmga2*$^{+/+}$ (Figure 18B). WB analysis of embryonic lung protein extracts (Figure 18C) showed increased levels of activated-beta-catenin (ABC) and phosphorylation of the WNT co-receptor LRP6 [129-131] after *Hmga2*$^{-/-}$ confirming enhancement of canonical WNT signaling. However, CTNNB1 has a dual role in both WNT signaling and cell adhesion processes.

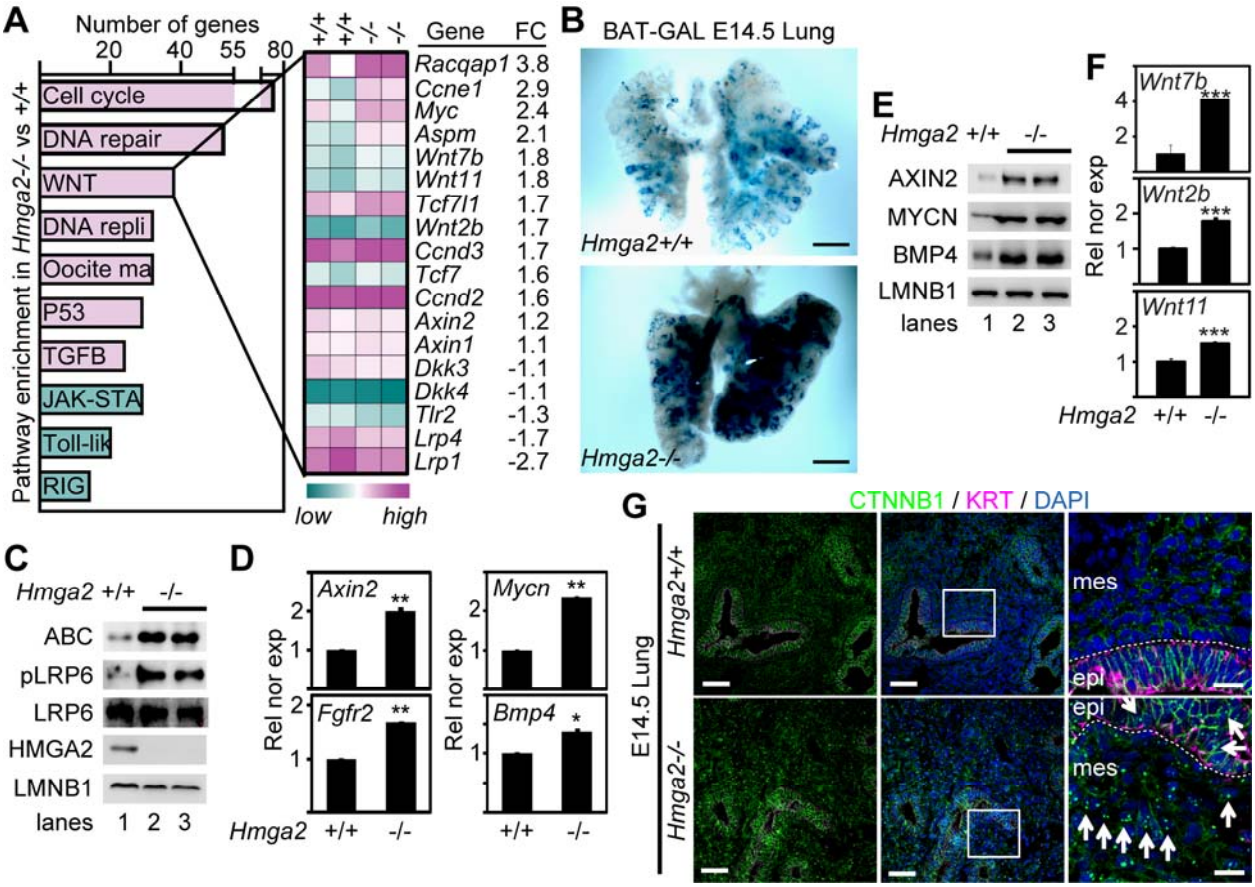

Figure 18. *Hmga2*$^{-/-}$ mice embryonic lung showed enhanced canonical WNT signaling. (A) Graph represent top enriched cellular pathways (P<0.05) in transcriptome analysis of *Hmga2*$^{-/-}$ E18.5 lung when compared to WT. Kyoto Encyclopedia of Genes and Genomes (KEGG) based analysis using DAVID bioinformatics tool (left). Magenta columns, pathways with increased expression (fold change≥1.2); Green columns, pathway with reduced expression (fold change<1.2); repli, replication; ma, maturation; JAK-STA, JAK-STAT signaling; Toll-lik, Toll-like-receptor signaling; RIG, RIG-like-receptor signaling. Heat map (right) analysis was done using DNAStar Arraystar 11.0. Green, low expression; Magenta, high expression; FC, fold change. (B) *Hmga2*$^{-/-}$ enhanced the activity of the beta-catenin/TCF/LEF reporter in embryonic lung of the BAT-GAL transgenic mice. Beta-galactosidase staining was performed in E14.5 lung (blue color). Representative BAT-GAL staining is shown (*n*=5). Scale bars, 2mm. (C) Protein extracts from WT or *Hmga2*$^{-/-}$ E18.5 lungs were analyzed by western blot using the indicated antibodies. Two biological duplicates were analyzed (lanes 2-3). (D) Expression analysis of the indicated genes by qRT-PCR in E18.5 lung of WT and *Hmga2*$^{-/-}$ mice. *Mycn*, v-myc myelocytomatosis viral related oncogene; *Fgfr2,* fibroblast growth factor receptor 2. Error bars, s.e.m. (*n*=4). Asterisks as in Fig. 12A. (E) Protein extracts from WT or *Hmga2*$^{-/-}$ E18.5 lungs were analyzed as in C using the indicated antibodies. (F) Expression analysis as in D of the indicated genes. (G) Sections of E14.5 lung of WT and *Hmga2*$^{-/-}$ mice were analyzed by confocal microscopy using KRT- and CTNNB1-specific antibodies. Square shows details at higher magnification on the right. Arrows indicate nuclear CTNNB1. Scale bars, 40 μm and 10 μm (right).

To confirm an enhanced WNT signaling after *Hmga2*$^{-/-}$, expression of canonical WNT targets, *Axin2, Mycn*, *Fgfr2* and *Bmp4* in the embryonic lung was analyzed (Figure 18D). Expression of canonical WNT targets increased after *Hmga2*$^{-/-}$ when compared to WT mice, demonstrating elevated canonical WNT signaling. WB analysis of protein extracts from embryonic lung (Figure 18E) showed increased levels of canonical WNT targets in *Hmga2*$^{-/-}$ confirming gene expression analysis.

Affymetrix microarray-based expression analysis (Figure 18A) also showed elevated expression of *Wnt11*, *Wnt7b* and *Wnt2b* in embryonic lung of *Hmga2*$^{-/-}$ mice when compared to WT. These results were confirmed by qRT-PCR based expression analysis (Figure 18F). Furthermore, immunostaining on sections of embryonic lung using CTNNB1-specific antibody (Figure 18G) showed increased nuclear localization of CTNNB1 in both the epithelium and the mesenchyme cells in *Hmga2*$^{-/-}$ when compared to WT.

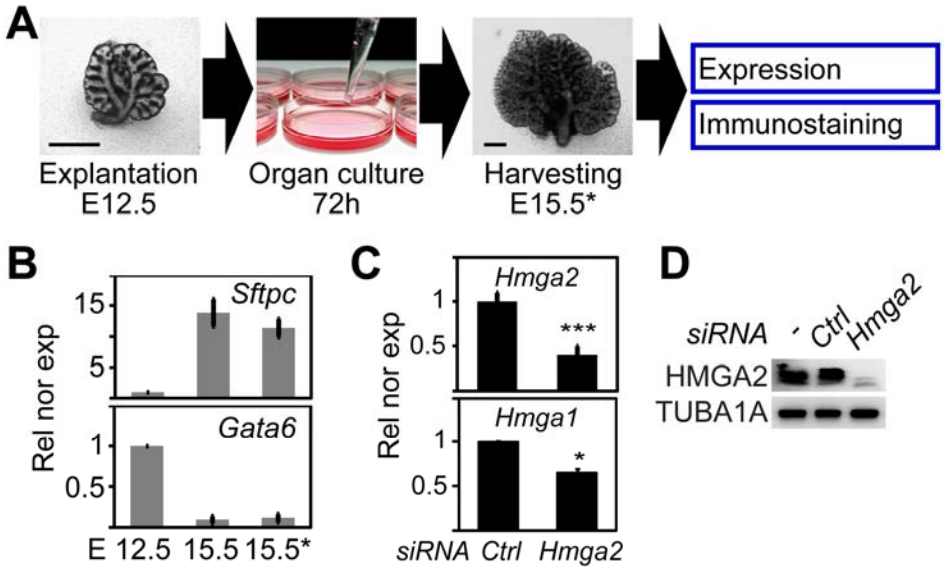

Figure 19. *Hmga2* loss-of-function (LOF) in embryonic lung explants. (A) Schemata of embryonic lung explant culture experiment. Mice embryonic lungs were explanted at E12.5 and cultured for 72 h (E15.5*). Scale bars, 500 µm. (B) Expression analysis of the indicated genes by qRT-PCR in embryonic lungs (E12.5, E15.5) and in explanted lungs (E15.5*) as in A. Error bars, s.e.m. (*n*=4). (C) Lung explants were treated with *Hmga2*- specific *siRNA*. Expression of the indicated genes was analyzed by qRT-PCR. Error bars, s.e.m. (n=4). Asterisks as in Fig. 12A. (D) Protein extracts of *siHmga2* treated lung explants were analyzed by WB using indicated antibodies.

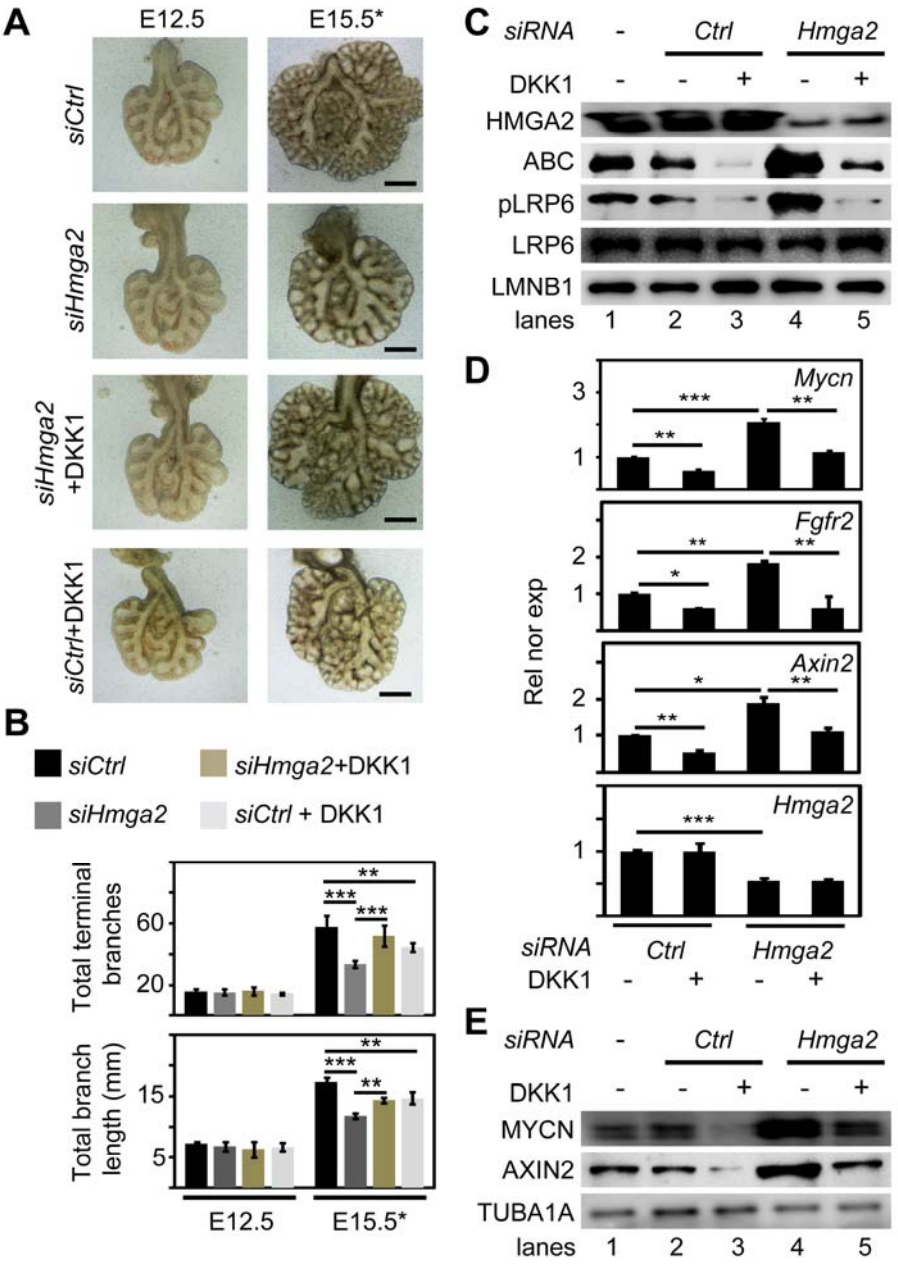

Figure 20. Inhibition of canonical WNT signaling partially rescued the *Hmga2* LOF phenotype. (A) Embryonic lung explants were cultured as in Fig. 19A. Explants were treated with indicated *siRNAs* together with the canonical WNT inhibitor dickkopf homolog 1 (DKK1). Scale bars, 500 μm. (B) Terminal branches and total branch length were quantified at E12.5 and E15.5*. Embryonic lung explants were treated as in A. Error bars, s.e.m. (n=6). Asterisks as in Fig. 12A. (C) Protein extracts from the lung explants treated as in A were analyzed by WB using indicated antibodies. (D) Expression analysis of the indicated genes by qRT-PCR in embryonic lung explants that were treated as in A. Error bars, s.e.m. (n=3). Asterisks as in Fig. 12A. (E) Protein extracts from the lung explants treated as in A were analyzed by WB using indicated antibodies.

To confirm the causal involvement of canonical WNT signaling in mediating the effect of *Hmga2*-LOF, an organ explant culture system that mimics the normal embryonic lung development was used (Figure 19A-B) [24]. Depletion of *Hmga2* in these organ explants using *siRNA* led to a marked impairment in branching morphogenesis when compared to control explants (Figure 20A). These defects during formation of bronchial and respiratory tree after *Hmga2*-LOF were validated by quantification of the total number of terminal branches and

branch length (Figure 20B). When E12.5 lungs were cultured for 72 hours in the presence of a *Hmga2*-specific siRNA (*siHmga2*), the total number of terminal branches (top) as well as the branch length (bottom) were reduced from 58 (*siCtrl*) to 34 ($P < 0.001$; $n = 6$) and from 17 mm (*siCtrl*) to 12 mm ($P < 0.001$; $n = 6$) respectively. However, treatment of the explants with the secreted canonical WNT inhibitor DKK1 [132] antagonized the defects caused by *siHmga2* (Figure 20A-B) reconstituting the total number of terminal branches to 51 ($P < 0.01$; $n = 6$) and the branch length to 14 mm ($P < 0.01$; $n = 6$). DKK1 treatment alone had also been shown to affect branching morphogenesis by blocking WNT signaling as previously described in embryonic lung explants [133]. WB analysis of protein extracts from embryonic lung explants (Figure 20C) showed increased levels of ABC and phosphorylated LRP6 (pLRP6) after *Hmga2*-KD (Figure 20C, lane 4) demonstrating enhancement of canonical WNT signaling that was antagonized after DKK1 treatment (Figure 20C, lane 5). Furthermore, the partial rescue of the *Hmga2*-LOF phenotype achieved by DKK1-mediated block of WNT signaling was validated by expression analysis of canonical WNT targets (Figure 20D) and by WB analysis of protein extracts from embryonic lung explants (Figure 20E).

4.2.2 *Hmga2* knockout showed enhanced canonical WNT signaling in adult lung

Adult mouse lung was analyzed to verify the enhanced canonical WNT signaling data that was obtained in the embryonic lung of *Hmga2*$^{-/-}$ mice. Immunostaining in sections of adult lung of *Hmga2*$^{-/-}$ mice showed increased levels of nuclear ABC (Figure 21A) and qRT-PCR showed elevated expression of canonical WNT signaling markers (Figure 21B) suggesting an enhancement of canonical WNT signaling in adult lung consistent with previous results in the embryonic lung presented in this study.

To verify the involvement of canonical WNT signaling in mediating the effect of *Hmga2*$^{-/-}$ in adult lung, *shDNA* mediated *in vivo Hmga2*-LOF experimental system was used in which *Hmga2* depletion was induced by Polyethylenimine (PEI) mediated transfection of a specific *shDNA* construct into cells of the lung epithelium after orotracheal administration of the transfection mix (Figure 22A) in transgenic mice in which WNT signaling is attenuated (*Ctnnb1*$^{+/-}$ mice; *CMV-Cre-,Ctnnb1*^{tm2Ke}) [120] or blocked by Doxycycline-inducible expression *Dkk1* (Dox-ind *Dkk1* mice; *Rosa26rtTA, Tet (O) Dkk1*) [121]. Immunostaining in sections of adult lung using

SCGB1A1- and SFTPC-specific antibodies was performed (Figure 22B) for the assessment of BASCs after *shDNA* mediated *Hmga2* depletion. *ShDNA* mediated *Hmga2* knockdown resulted in an expansion of BASCs when compared to the lung of *ShCtrl* treated mice. Moreover, flow cytometry analysis in cell suspensions of WT mice adult lung revealed that the percentage of SFTPC- and SCGB1A1-positive cells increased from 0.6 % (*Ctrl*) to 3.2 % ($P<0.001$; $n=5$) after *shDNA* mediated *Hmga2* depletion supporting previous results in *Hmga2*$^{-/-}$ mice (Figure 22C) presented in this study. However, *Hmga2*-LOF in *Ctnnb1*$^{+/-}$ mice or Dox-ind *Dkk1* mice increased the percentage of SFTPC- and SCGB1A1-positive cells to only 1.5 % ($P<0.05$; $n=5$) or 1.2 % ($P<0.05$; $n=5$) respectively confirming the requirement of canonical WNT signaling in mediating the effect of *Hmga2*-LOF in adult lung.

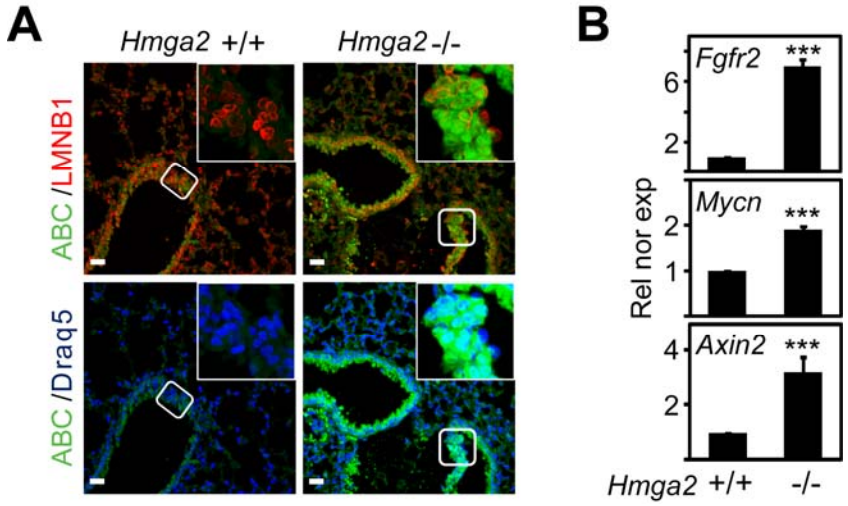

Figure 21. *Hmga2*$^{-/-}$ enhanced canonical WNT signaling in the adult lung. (A) Sections of adult lung of *Hmga2*$^{-/-}$ mice were analyzed by confocal microscopy after double immunostaining using ABC- and LMNB1-specific antibodies. Nuclear staining with Draq5. Scale bars, 40 μm. Squares as in Fig.11B. (B) Expression analysis of the indicated genes by qRT-PCR in adult lung of WT and *Hmga2*$^{-/-}$ mice. Error bars, s.e.m. (n=5). Asterisks as in Fig. 12A.

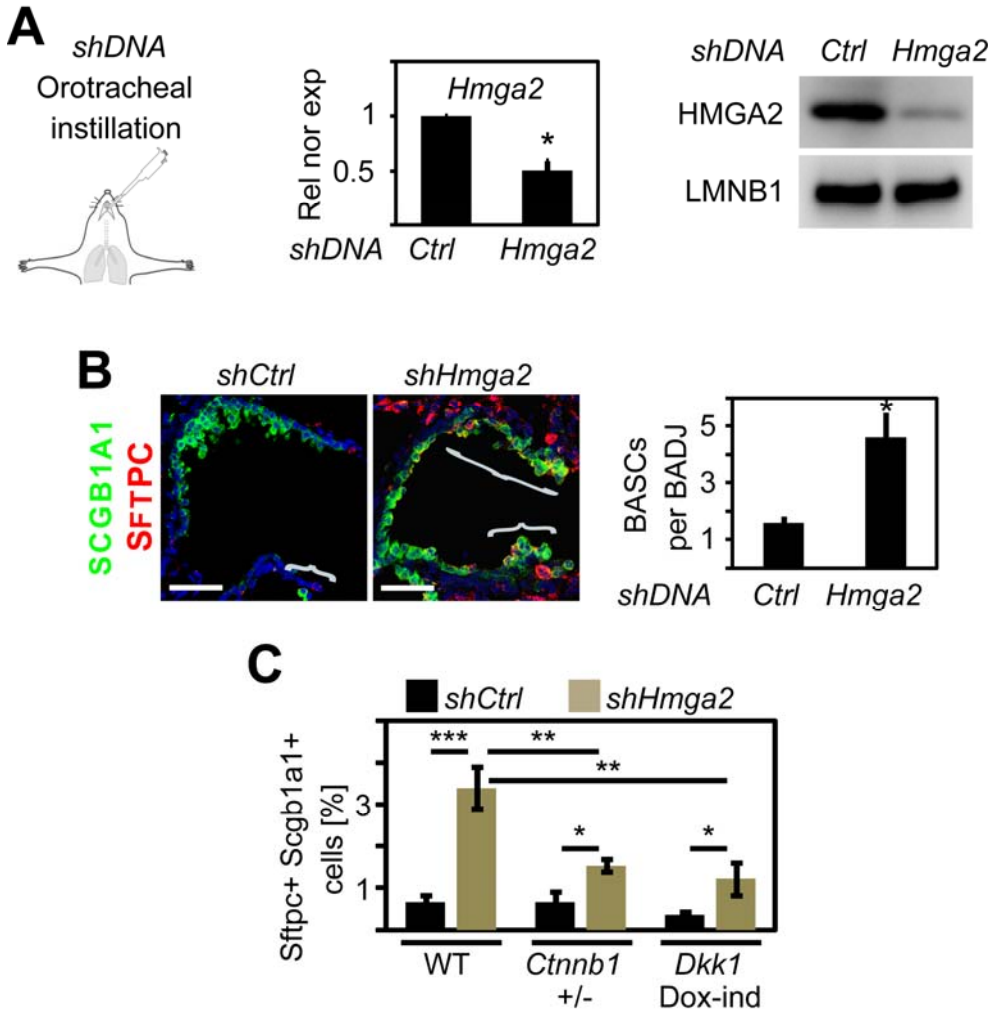

Figure 22. Transgenic inhibition of canonical Wnt signaling partially rescued the effect of *in vivo Hmga2*-LOF. (A) *In vivo shDNA* mediated *Hmga2*-LOF was efficient. Left, schemata of *in vivo Hmga2*-LOF. *Hmga2* depletion was induced by orotracheal application of a transfection mix containing PEI (transfection reagent) and either control (*shCtrl*) or *Hmga2*-specific (*shHmga2*) DNA plasmid for the production of short hairpin RNA (shDNA). PEI mediated transfection was performed three times (at days 0, 3 and 6) before lung harvesting (at day 10) for monitoring LOF efficiency. *In vivo shDNA* mediated *Hmga2*-LOF was monitored by qRT-PCR (Middle) and WB (Right) using HMGA2-specific antibodies. Error bars, s.e.m. (n=10). Asterisks as in Fig. 12A. (B) Depletion of *Hmga2* in adult lung led to expansion of BASCs in the BADJ region. Mice were treated as in A. At day 10, confocal microscopy of adult lung sections was performed after immunostaining (Left) using SFTPC- and SCGB1A1-specific antibodies to monitor BASCs (brackets) and quantified (Right) per BADJ. Scale bars, 40 µm. Error bars, s.e.m. (n=9). Asterisks as in Fig. 12A. (C) *Hmga2* depletion was induced as in A in adult lung of WT mice, *Ctnnb1* heterozygous mice (*Ctnnb1* +/-) and Doxycyclin-inducible Dkk1-expressing mice (*Dkk1* Dox-ind). Cell suspensions of the lung of treated mice were analyzed by flow cytometry using SFTPC- and SCGB1A1-specific antibodies. Error bars, s.e.m. (n=5). Asterisks as in Fig. 12A.

4.2.3 HMGA2 directly activates *Gata6* expression and thereby modulates canonical WNT signaling

GATA6 is a transcription factor that is essential for branching morphogenesis and inhibits canonical WNT signaling in the distal epithelium of the lung by transcriptional activation of its downstream target, the canonical WNT/CTNNB1 pathway antagonist *Fzd2* [31, 134]. The defects observed after *Hmga2*-LOF (Figure 23A-B) were similar to the *Gata6*-LOF phenotype [29]. Therefore, whether *Hmga2* directly regulates *Gata6* was further investigated. Immunostaining on sections of embryonic lung (E14.5) using HMGA2- and GATA6-specific antibodies (Figure 24A) showed the presence of both proteins in the same cells of the distal lung endoderm. Interestingly, qRT-PCR based expression analysis in embryonic lung showed that *Gata6* and its downstream target gene *Fzd2* decreased in *Hmga2*$^{-/-}$ when compared to WT mice (Figure 24B). WB analysis of protein extracts from embryonic lung (Figure 24C) showed reduced levels of GATA6 and FZD2 after *Hmga2*$^{-/-}$ supporting gene expression analysis.

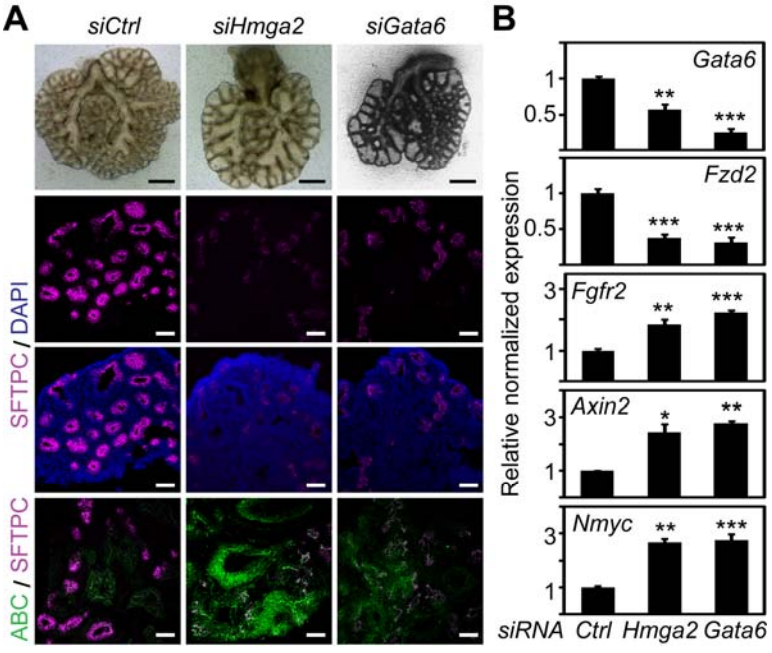

Figure 23. *Hmga2*- and *Gata6*-LOF in embryonic lung explants led to a marked impairment of airway epithelial differentiation due to enhanced canonical WNT activity. (A) Phenotype of *Gata6*-LOF in lung explants was similar to the *Hmga2*-LOF. Top, embryonic lungs were explanted and cultured as in Fig. 19A. Explants were treated with indicated *siRNAs*. Scale bars, 500 μm. Bottom, sections of treated explants were analyzed by confocal microscopy after immunostaining using indicated antibodies. Scale bars, 40 μm. (B) Expression analysis of the indicated genes by qRT-PCR in lung explants treated as in A. Error bars, s.e.m. (*n*=4). Asterisks as in Fig. 12A.

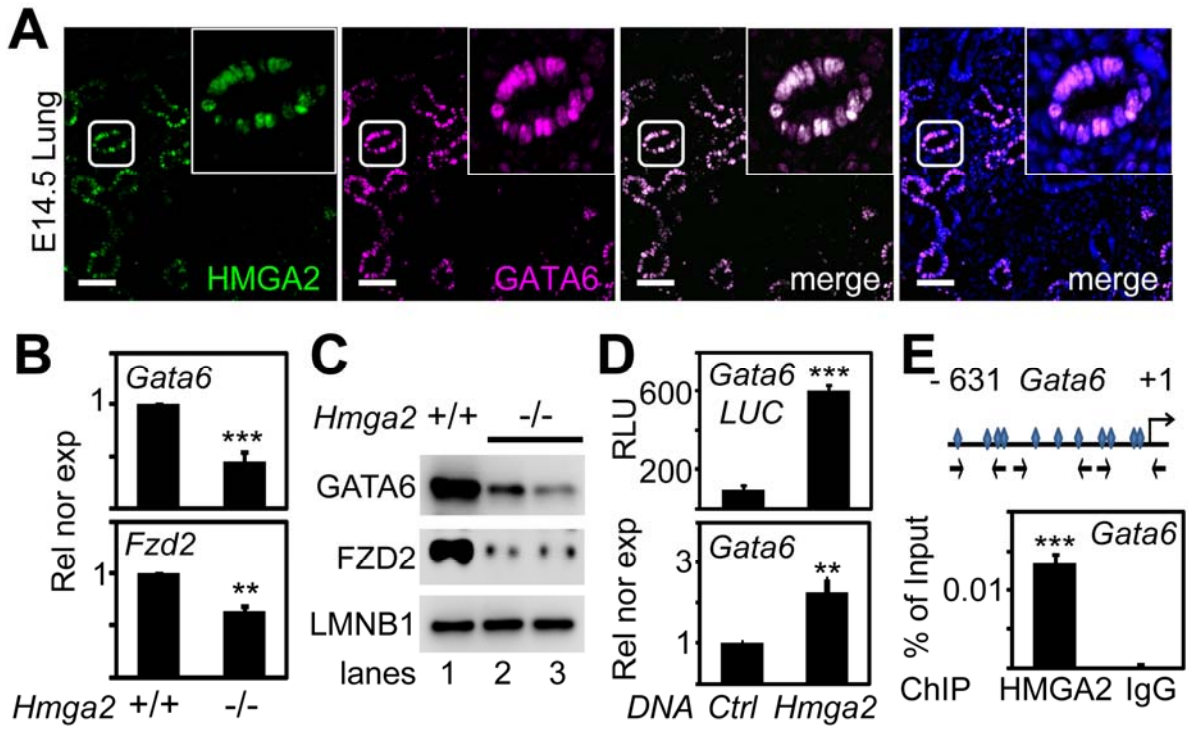

Figure 24. HMGA2 directly regulates *Gata6* and thereby modulates *Fzd2* expression. (A) Fluorescence microscopy of embryonic lung sections (E14.5) after double immunostaining using HMGA2- and GATA6-specific antibodies. Nuclear staining with DAPI (blue). Square shows details at higher magnification. Scale bars, 40 μm. (B) Expression analysis of the indicated genes by qRT-PCR in Hmga2 $^{-/-}$ and WT mice. Error bars, s.e.m. (*n*=4) and asterisks as in Fig. 12A. (C) Protein extracts from WT or *Hmga2*$^{-/-}$ embryonic lung (E18.5) were analyzed by WB using the indicated antibodies. (D) *Hmga2* over expression increased *Gata6* transcription. Top, Luciferase reporter assays of MLE-12 cells transiently transfected with a *Gata6*-luciferase (*Gata6-Luc*) reporter plasmid and control (empty vector) or *Hmga2* expression construct. RLU, Relative light units. Bottom, *Gata6* expression was monitored by qRT-PCR in MLE-12 cells treated as above. Error bars, s.e.m. (n=4) and asterisks as in Fig. 12A. (D) Endogenous HMGA2 binds to the endogenous *Gata6* promoter. Top, *in silico* analysis of the *Gata6* gene (-631 - +1 bp relative to transcription initiation site) revealed several HMGA2 binding elements (squares). Arrows, position of the primers used for ChIP. Bottom, ChIP of the *Gata6* promoter using HMGA2-specific antibody or Immunoglobulin G (IgG, negative control). %, percentage. Error bars, s.e.m. (n=4) and asterisks as in Fig. 12A.

To investigate the effect of *Hmga2* gain-of-function (GOF) on *Gata6* expression, MLE-12 cells were transiently transfected with *Hmga2* and a plasmid containing the luciferase (*Luc*) reporter gene under the control of the *Gata6* promoter (Figure 24D, top). Forced expression of *Hmga2* increased more than fivefold the basal transcription of the *Gata6-Luc* reporter. In addition, expression of endogenous *Gata6* increased more than twofold after *Hmga2* transfection (Figure 24D, bottom). Consistently, *in silico* analysis of the murine *Gata6* gene (Figure 24E, top)

revealed several HMGA2 binding elements near the transcription initiation site. Moreover, ChIP in MLE-12 cells (Figure 24E, bottom) showed a direct association of endogenous HMGA2 to the endogenous *Gata6* promoter. Thus, it was concluded that HMGA2 directly activates *Gata6* gene expression and the enhanced WNT signaling caused by *Hmga2*-LOF could also be mediated by a reduction of the WNT signaling antagonizing proteins GATA6 and FZD2.

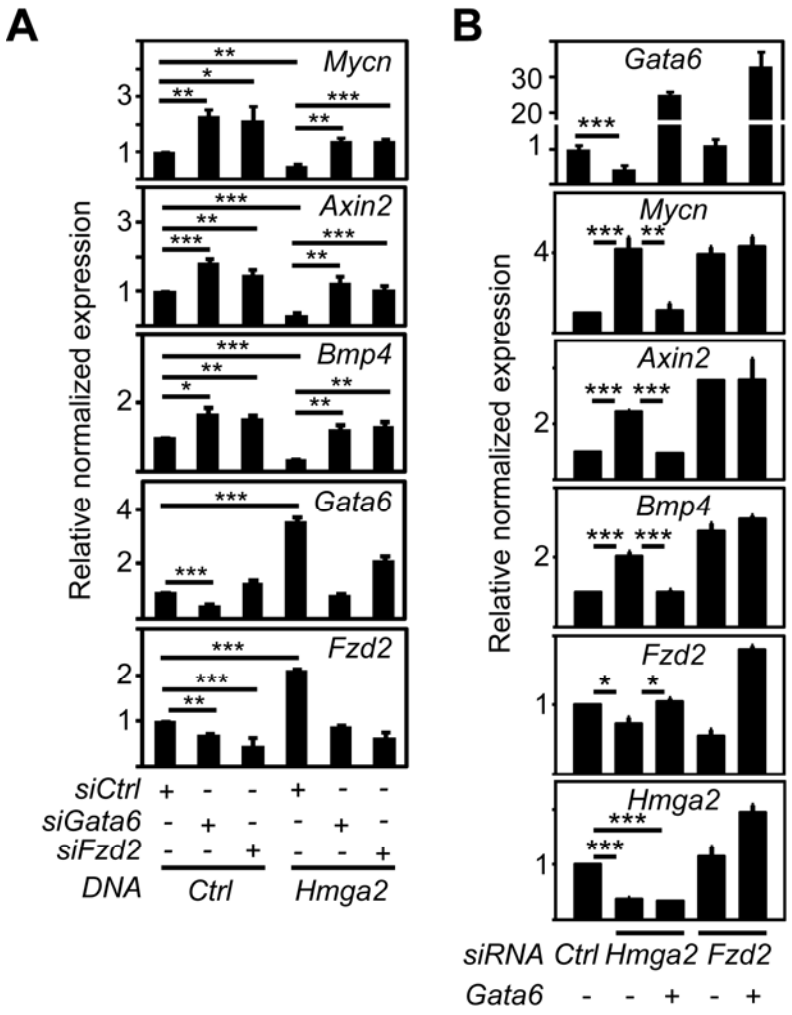

Figure 25. *Hmga2* acts upstream of *Gata6* during WNT signaling regulation. (A) *Gata6* and *Fzd2* are required for the effect of *Hmga2*-GOF on expression of WNT targets. Expression analysis of the indicated genes by qRT-PCR in MLE-12 cells that were transfected with either *Ctrl* or *Gata6*- or *Fzd2*-specific siRNA and *Hmga2* expression plasmid as indicated. Error bars, s.e.m. (n=4). Asterisks as in Fig. 12A. (B) *Gata6*-GOF rescued the effect of *Hmga2*-LOF on expression of WNT targets. Expression analysis of the indicated genes by qRT-PCR in MLE-12 cells that were transfected with either *Ctrl* or *Hmga2*- or *Fzd2*-specific siRNA and *Gata6* expression plasmid as indicated. Error bars, s.e.m. (n=4). Asterisks as in Fig. 12A.

To show the requirement of *Gata6* in *Hmga2*-mediated regulation of WNT signaling, MLE-12 cells were transfected with *Hmga2* after *siRNA*-mediated *Gata6*- or *Fzd2*-depletion (Figure 25A). Expression analysis showed that *Hmga2*-GOF increased the levels of *Gata6* and *Fzd2* whereas it reduced the levels of canonical WNT targets *Mycn*, *Axin2* and *Bmp4*, confirming a role of *Hmga2* in inhibition of canonical WNT signaling. Interestingly, *Gata6*- or *Fzd2*-depletion antagonized the effect of *Hmga2*-GOF on both groups of markers analyzed, indicating the

requirement of *Gata6* and *Fzd2* for the negative regulation of WNT signaling mediated by *Hmga2*.

To determine the causal involvement of *Gata6* in *Hmga2*-mediated regulation of WNT signaling, MLE-12 cells were transfected with *Gata6* after *siRNA*-mediated *Hmga2*- or *Fzd2*-depletion (Figure 25B). Expression analysis showed that *Hmga2*- and *Fzd2*-LOF enhanced the expression of canonical WNT targets, supporting previous expression analysis in the embryonic lung of *Hmga2*-KO mice and as expected from WNT signaling antagonizing genes. Interestingly, *Gata6* transfection compensated the effect of *Hmga2*-LOF, but not of *Fzd2*-LOF.

To rescue *Hmga2*$^{-/-}$ adult lung phenotype, a variation of the *in vivo* transfection method (Figure 22A) was used to overexpress *Flag-Gata6* in the lungs of WT and *Hmga2*$^{-/-}$ mice (Figure 26A). Using this system, transfection of a major part of the bronchiolar as well as alveolar epithelium was achieved. Forced expression *of Flag-Gata6* in lungs of WT mice (Figure 26B) reduced the percentage of SFTPC- and SCGB1A1-positive cells from 0.7 % (Ctrl) to 0.4 % (P<0.01; n=3) as expected for a reduced WNT signaling. Importantly, *Flag-Gata6* overexpression antagonized the effect of *Hmga2*$^{-/-}$ reducing the percentage of SFTPC- and SCGB1A1-positive cells from 3.0 % (Ctrl) to 1.2 % (P<0.01; n=3) showing thereby a partial rescue of the *Hmga2*$^{-/-}$ phenotype that was further validated by expression analysis of *Fzd2* (Figure 26C) and canonical WNT targets (Figure 26D).

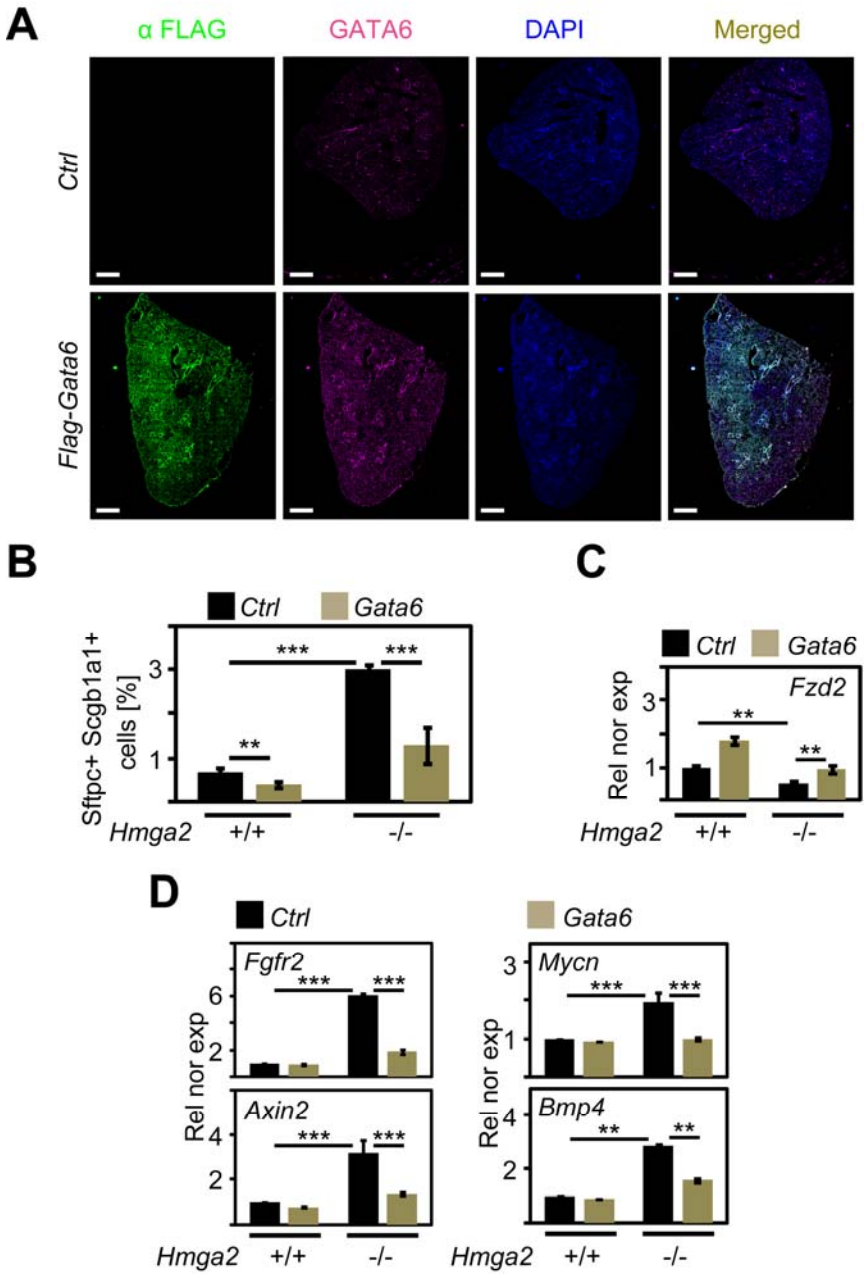

Figure 26. *Gata6* over expression in adult lung partially rescued the effect of *Hmga2*$^{-/-}$. (A) Transfection of bronchiolar and alveolar epithelium in adult mouse lung was induced by orotracheal instillation of a transfection mix containing PEI and either an empty plasmid (*pBS*, negative control) or an expression plasmid for *flag* tagged *Gata6* (*flag-Gata6*) as in Fig. 22A. PEI mediated transfection was performed three times (days 0; 3 and 6) before lung harvesting (day 10) for monitoring transfection efficiency by confocal microscopy by immunostaining using flag- and GATA6- specific antibodies. DAPI, nuclear staining. Scale bars, 500 μm. (B) *Gata6* overexpression was induced in *Hmga2*$^{-/-}$ mice adult lung as in A. Cell suspensions of the lung of treated mice were analyzed by flow cytometry using SFTPC-and SCGB1A1-specific antibodies. Error bars, s.e.m. (n=3). Asterisks as in Fig. 12A. (C and D) *Gata6* overexpression was induced in *Hmga2*$^{-/-}$ mice adult lung as in A. Expression analysis of the indicated genes by qRT-PCR. Error bars, s.e.m. (n=3). Asterisks as in Fig. 12A.

4.3 HMGA2 mediated *Gata6* transcriptional activation requires ATM-mediated histones phosphorylation and nucleosome eviction

4.3.1 ATM is required for HMGA2-mediated transcriptional activation of *Gata6*

A proteomic approach to identify HMGA2 interacting proteins (Figure 27A) and subsequent confirmation by Co-IP of endogenous proteins (Figure 27B) revealed the interaction between HMGA2 and, among others, the kinase ATM, the core histone variant H2AX and the linker histone H1. Thus, we decided to focus our attention on a potential role of ATM-mediated protein phosphorylation on transcriptional activation regulated by HMGA2.

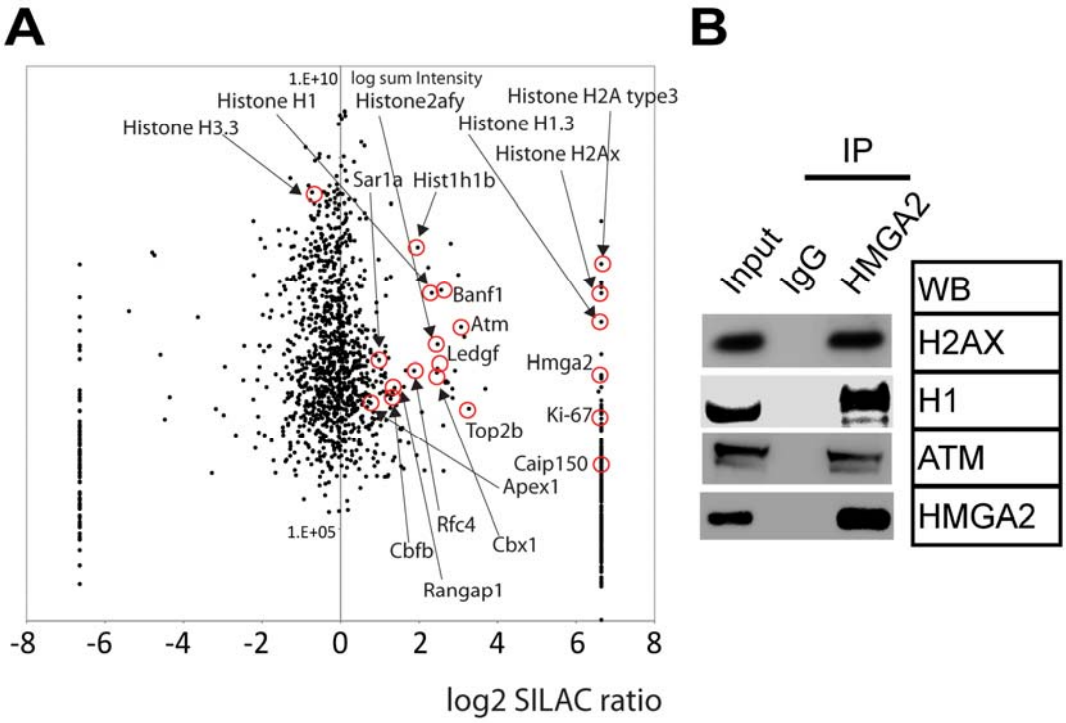

Figure 27. HMGA2 interacts with ATM, Histone H1 and H2AX. (A) HMGA2 interacting proteins identified by mass spectrometry analysis. Label free quantitation between control and HMGA2 co-affinity precipitations. Scatter plot of peak intensities and label free protein quantitation. Detected proteins in Experiment 1 and Experiment 2 with a fold change > 2 were labeled with a red circle. (B) Endogenous HMGA2 was immunoprecipitated (IP) from nuclear protein extracts of HEK293T cells using either immunoglobulin G (IgG, as control) or HMGA2-specific antibody. Co-immunoprecipitated proteins were analyzed by WB using the indicated antibodies. Input, 5% of material used for the IP.

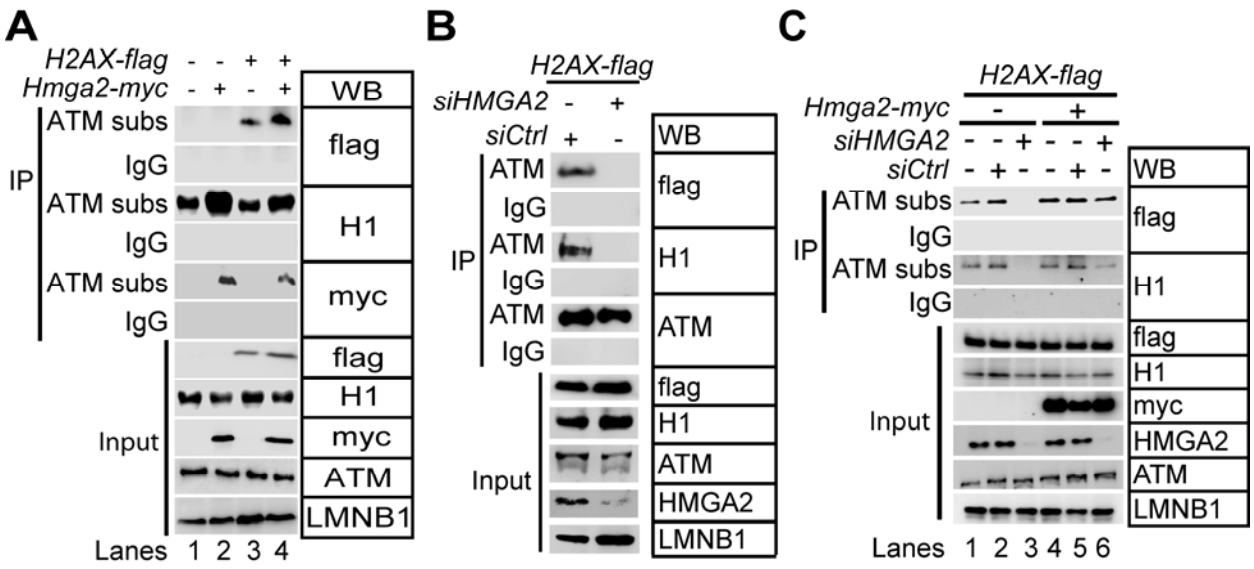

Figure 28. HMGA2 is required for ATM-mediated phosphorylation of H2AX and H1. (A) HEK293T cells stably expressing flag-tagged H2AX (*H2AX-flag*) were transiently transfected with either an *Hmga2-myc* expression plasmid or an empty vector. Nuclear protein extracts from transfected cells were analyzed by protein IP using an antibody specific for phosphorylated ATM substrates (ATM subs) or IgG control. Immunoprecipitated proteins were analyzed by WB using the indicated antibodies. (B) HEK293T cells stably expressing *H2AX-flag* were transfected with either *Ctrl* or *HMGA2*-specific *siRNA*. Nuclear protein extracts of transfected cells were analyzed by IP using ATM-specific antibody or IgG control. Immunoprecipitated proteins were analyzed by WB using the indicated antibodies. (C) HEK293T cells stably expressing *H2AX-flag* were transiently transfected with empty vector or an *Hmga2-myc* expression plasmid and *Ctrl* or *HMGA2*-specific *siRNA*. Nuclear protein extracts of transfected cells were analyzed by IP using an antibody specific for ATM subs or IgG control. Immunoprecipitated proteins were analyzed by WB using the indicated antibodies.

Immunoprecipitation using an antibody specific for phosphorylated ATM substrates revealed that HMGA2, H2AX and H1 are phosphorylated by ATM (Figure 28A, lanes 1-3) and HMGA2 overexpression enhanced H2AX and H1 phosphorylation (Figure 28A, lanes 2-4). Hence to check the effect of HMGA2 depletion on interaction of ATM with H1 and H2AX, siRNA-mediated *HMGA2*-LOF (Figure 28B) was performed. *HMGA2*-LOF compromised the interactions between ATM and the histones H2AX and H1 showing the requirement of HMGA2 for these interactions and suggesting a role of HMGA2 as an adaptor between these proteins. Confirming previous reports, Co-IP using an antibody specific for phosphorylated ATM substrates showed that H2AX and H1 are phosphorylated by ATM (Figure 28C, lanes 1-2). Interestingly, *HMGA2*-LOF abolished ATM-mediated phosphorylation of H2AX and H1 (Figure 28C, lane 3) demonstrating the requirement of *HMGA2* for these post-translational

modifications. The specificity of this finding was confirmed by a partial rescue of ATM-mediated phosphorylation of H2AX and H1 in *HMGA2* depleted HEK293T cells after expression of the mouse *Hmga2* ortholog (lane 6).

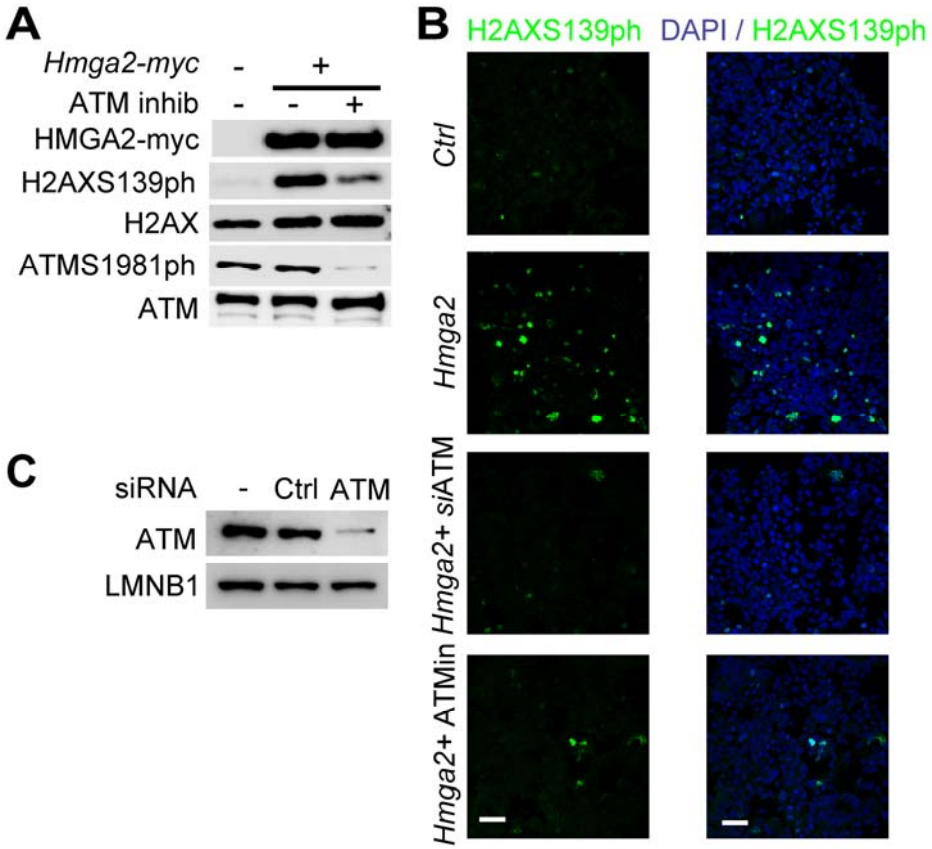

Figure 29. ATM kinase activity inhibition reduced *Hmga2*-induced H2AX phosphorylation. (A) HEK293T cells were transiently transfected with either an *Hmga2-myc* expression plasmid or an empty vector. Transfected cells were either untreated or treated with the ATM inhibitor KU-55933 (ATMin). Nuclear protein extracts from treated cells were analyzed by WB using the indicated antibodies. ATMS1981ph, phosphorylated ATM at serine 1981. (B) HEK293T cells were transiently transfected with an empty vector or an *Hmga2* expression plasmid and *Ctrl* or *ATM*-specific *siRNA*. Transfected cells were either untreated or treated with the ATMin as indicated. Confocal microscopy of HEK293T cells after immunostaining using H2AXS139ph-specific antibody. Scale bars, 40 μm. (C) Protein extracts from HEK293T cells transfected with *Ctrl* or *ATM*-specific *siRNA* were analyzed by WB using the indicated antibodies.

Transfection of *Hmga2-myc* in HEK293T cells (Figure 29A, B) increased the levels of H2AXS139ph (lane 2) in an ATM dependent manner, since treatment of the cells with the ATM inhibitor (ATMin) KU-55933 counteracted the effect of *Hmga2* (lane 3). The inhibiting effect of KU-55933 on ATM was monitored by the reduction of phosphorylated ATM [135, 136]. In addition, neither *Hmga2* transfection nor ATM inhibition altered the total level of H2AX and

ATM, supporting that the observed effects are related to post-translational modifications of H2AX and ATM.

To investigate whether transcriptional regulation of *GATA6* by HMGA2 involves ATM-mediated phosphorylation of H2AX and H1, the *GATA6* promoter of HEK293T cells was analyzed by ChIP after transfection of empty vector or *Hmga2* (Figure 30A). *Hmga2* overexpression led to an enrichment of ATM, H2AXS139ph and Pol II on the *GATA6* promoter. Interestingly, ATM-LOF either by co-transfection with *siATM* (Figure 29C) or by KU-55933 treatment antagonized the effects caused by *Hmga2* transfection thereby showing the requirement of ATM for these effects.

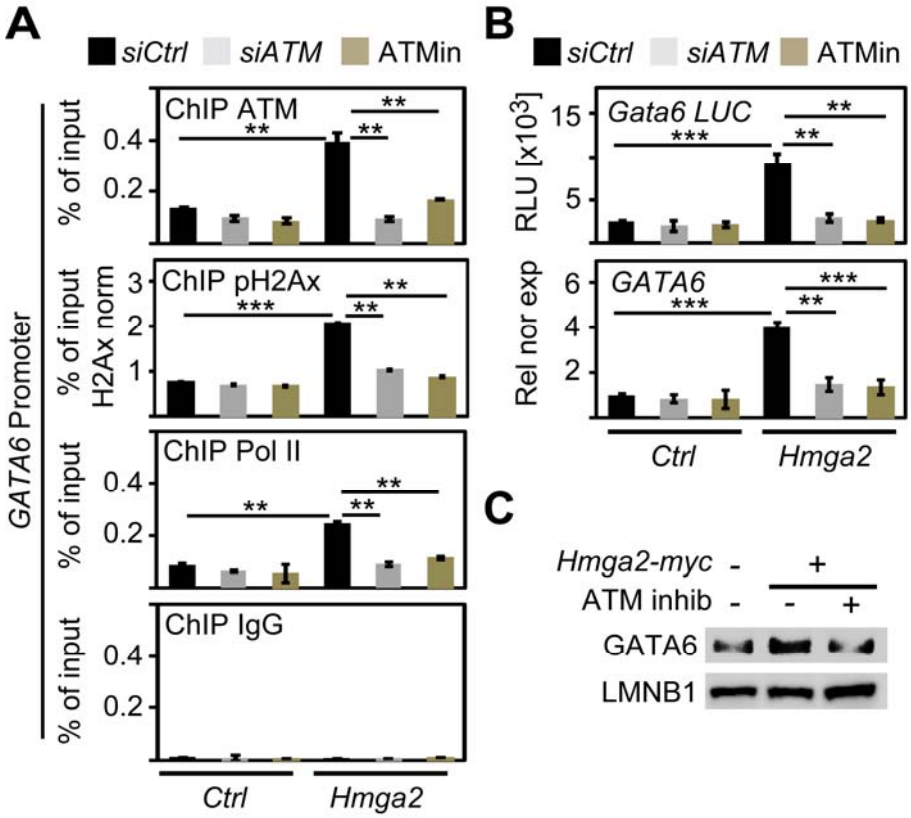

Figure 30. ATM is required for HMGA2-mediated transcriptional activation of *GATA6*. (A) ChIP analysis was performed using the indicated antibodies in HEK293T cells that were transiently transfected with a *Ctrl* or an *Hmga2* expression plasmid and *Ctrl* or *ATM*-specific *siRNA*. Transfected cells were either untreated or treated with the ATMin as indicated. Enrichment of the indicated proteins on the *GATA6* promoter after ChIP was monitored by qPCR. % of input H2AX norm, percentage of input normalized with H2AX; Pol II, polymerase II. Error bars, s.e.m. (n=4). Asterisks as in Fig. 12A. (B) Top, Luciferase reporter assays of HEK293T cells that were transiently transfected with a *Gata6*-luciferase (*Gata6-Luc*) reporter plasmid and either a *Ctrl* or an *Hmga2* expression plasmid and *siCtrl* or *siATM* as indicated. Transfected cells were either untreated or treated with ATMin. Error bars, s.e.m. (n=3). Asterisks as in Fig. 12A. Bottom, *GATA6* expression was monitored by qRT-PCR in HEK293T cells that were transfected as in B. Error bars, s.e.m. (n=3). Asterisks as in Fig. 12A. (C) Nuclear protein extracts from HEK293T cells that were transfected/treated as in Fig. 29A were analyzed by WB using the indicated antibodies.

To determine the influence of the chromatin changes induced by *Hmga2*-GOF on *GATA6* expression, HEK293T cells were transiently transfected with *Hmga2* and a plasmid containing the luciferase reporter gene under the control of the *Gata6* promoter (Figure 30B, top). Forced expression of *Hmga2* increased more than fourfold the basal transcription of the *Gata6-Luc* reporter. In addition, expression of endogenous *GATA6* increased more than threefold after *Hmga2* transfection (bottom). Consistent with ChIP results, both approaches of ATM-LOF counteracted the enhanced expression of the *Gata6-Luc* reporter as well as endogenous *GATA6* after *Hmga2*-GOF thereby confirming the requirement of ATM for the effects caused by *Hmga2* on *GATA6* expression. WB analysis of protein extracts from HEK293T cells (Figure 30C) showed increased levels of GATA6 after *Hmga2*-GOF that were reduced after ATM inhibition.

4.3.2 ATM-mediated phosphorylation of H2AX is required for HMGA2-induced transcriptional activation of *Gata6*

H2AXS139ph is commonly used as a marker for DNA-DSB [101]. However, there is increasing evidence for additional functions of this histone modification [102-104, 137]. Following this line of ideas, the molecular mechanisms underlying HMGA2-induced chromatin modifications at the *Gata6* promoter was investigated in more detail using HEK293T cells that stably express a flag-tagged wild type H2AX ($H2AX^{wt}$) or a mutant H2AX ($H2AX^{S-A}$), in which the serine 139 was mutated to alanine (Figure 31A). $H2AX^{wt}$ and $H2AX^{S-A}$ were immunoprecipitated along with ATM in Co-IP analysis of protein extracts from both cell lines using HMGA2 specific antibody (lanes 2-3) showing that the interaction between HMGA2, H2AX and ATM was apparently not affected by the mutation. These results were confirmed by Co-IP using ATM specific antibody (Figure 31B). However, Co-IP using an antibody specific for phosphorylated ATM substrates (ATM subs; Figure 31C) showed that the S139A mutation abrogated the ATM-mediated phosphorylation of H2AX (lane 3) demonstrating the requirement of this amino acid residue for this specific post-translational modification. ChIP of chromatin from both cell lines (Figure 31D) showed accumulation of HMGA2, ATM and Pol II on the endogenous *GATA6* promoter after *Hmga2* transfection that was more prominent in the cells expressing $H2AX^{wt}$ (top). The presence of $H2AX^{S-A}$ (bottom) reduced the effects induced by *Hmga2*-GOF suggesting that ATM-mediated H2AXS139ph is required for the HMGA2-induced changes in the chromatin of the

GATA6 promoter. Moreover, expression analysis (Figure 31E) of a *Gata6-Luc* reporter (top) and the *GATA6* gene (bottom) demonstrated enhanced *GATA6* expression after *Hmga2*-GOF only in cells expressing H2AX^{wt}, correlating with ChIP results. WB analysis of protein extracts from both HEK293T cell lines (Figure 31F) showed increased levels of GATA6 after *Hmga2*-GOF only in an H2AX^{wt} background (lane 2) supporting gene expression analysis.

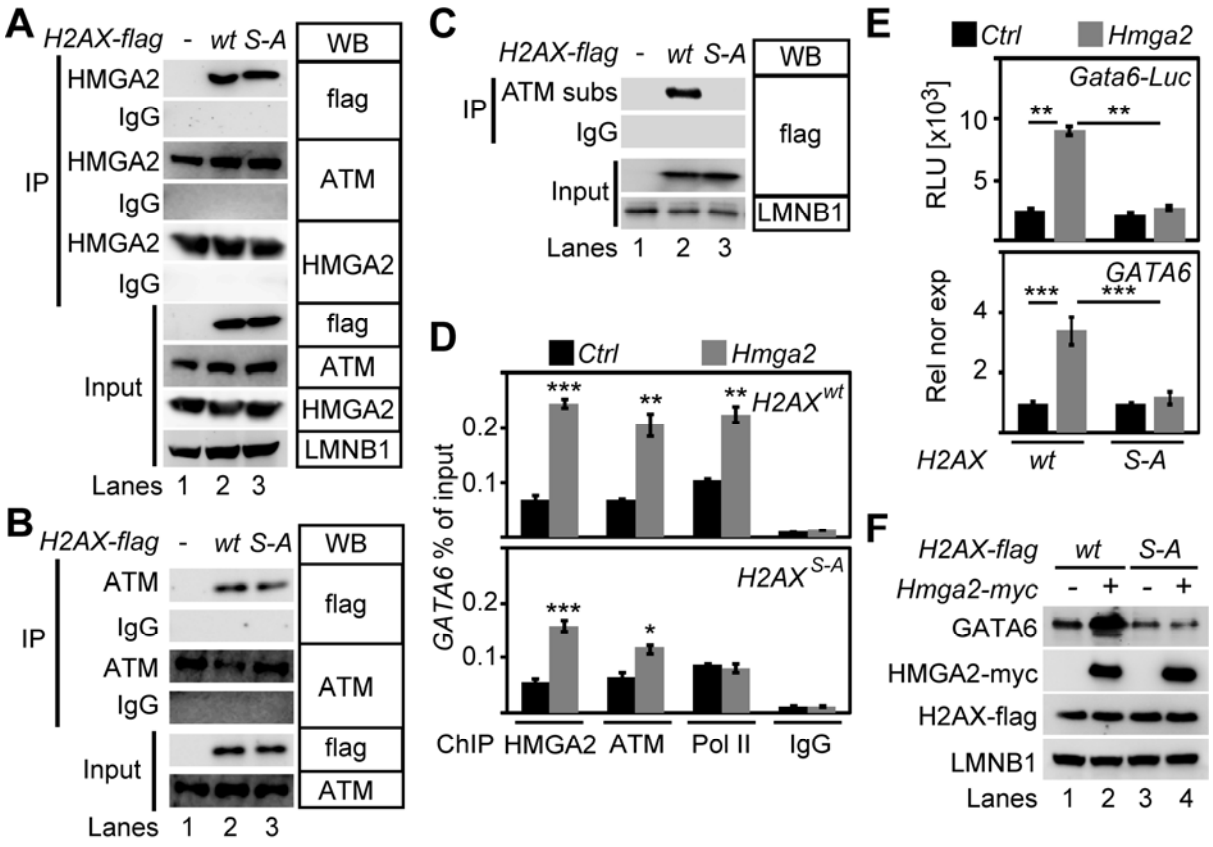

Figure 31. H2AX phosphorylation at Serine 139 is required for HMGA2-mediated transcriptional activation of *GATA6*. (A) Nuclear protein extracts from HEK293T cells stably expressing H2AX^{wt} or H2AX^{S-A} was analyzed by IP using an HMGA2-specific antibody or IgG control. Immunoprecipitated proteins were analyzed by WB using the indicated antibodies. (B) Nuclear protein extracts from HEK293T cells stably expressing H2AX^{wt} or H2AX^{S-A} was analyzed by IP using an ATM-specific antibody or IgG control. Immunoprecipitated proteins were analyzed by WB using the indicated antibodies. (C) Nuclear protein extracts from HEK293T cells stably expressing H2AX^{wt} or H2AX^{S-A} was analyzed by IP using an antibody specific for ATM subs or IgG control. (D) HEK293T cells stably expressing either H2AX^{wt} (top) or H2AX^{S-A} (bottom) were transiently transfected with either *Ctrl* or *Hmga2* expressing plasmid. Chromatin was isolated 48 hours after transfection and analyzed by ChIP using the indicated antibodies. Error bars, s.e.m. (n=3). Asterisks as in Fig. 12A. (E) Top, Luciferase reporter assays of HEK293T cells stably expressing either H2AX^{wt} or H2AX^{S-A} were transiently transfected with a *Gata6-Luc* reporter plasmid and control or *Hmga2* expression construct. Error bars, s.e.m. (n=3). Asterisks as in Fig. 12A. Bottom, *GATA6* expression was monitored by qRT-PCR in HEK293T cells that were transfected as in D. Error bars, s.e.m. (n=6). Asterisks as in Fig. 12A. (F) Nuclear protein extracts from HEK293T cells that were transfected as in E were analyzed by WB using the indicated antibodies.

4.3.4 ATM-mediated phosphorylation of H1 is required for HMGA2-induced transcriptional activation of *Gata6*

To investigate the molecular mechanism underlying the replacement of H1 by HMGA2, expression constructs for a myc-tagged wild type H1 ($H1^{wt}$) or a mutant H1 ($H1^{S-A}$), in which the serine 65 was mutated to alanine was used (Figure 32A). Co-IP analysis using HMGA2 specific antibody and protein extracts from HEK293T cells transfected with the empty vector (*Ctrl*) or these expression constructs revealed that both $H1^{wt}$ and $H1^{S-A}$ were immunoprecipitated along with ATM (lanes 2-3) supporting that the interaction between HMGA2, H1 and ATM was apparently not affected by the mutation. These results were confirmed by Co-IP using ATM specific antibody (Figure 32B). However, Co-IP using the ATM subs antibody (Figure 32C) showed that the S65A mutation abrogated the ATM-mediated phosphorylation of H1 (lane 3) demonstrating the requirement of this amino acid residue for this specific post-translational modification. ChIP of chromatin from HEK293T cells that were transfected with $H1^{wt}$ or $H1^{S-A}$ (Figure 32D) showed accumulation of HMGA2, ATM and Pol II on the endogenous *GATA6* promoter after *Hmga2*-GOF that was more prominent in the cells expressing $H1^{wt}$ (top). The presence of $H1^{S-A}$ (bottom) reduced the effects induced by *Hmga2*-GOF suggesting that ATM-mediated phosphorylation of H1 at S65 is required for the HMGA2-induced changes in the chromatin of the *GATA6* promoter. Moreover, expression analysis (Figure 32E) revealed twofold enhanced *GATA6* expression after *Hmga2*-GOF only in cells that were transfected with $H1^{wt}$ correlating with previous ChIP results. Western blot analysis of protein extracts from HEK293T cells (Figure 32F) showed increased levels of GATA6 after *Hmga2*-GOF only in an $H1^{wt}$ background supporting gene expression analysis.

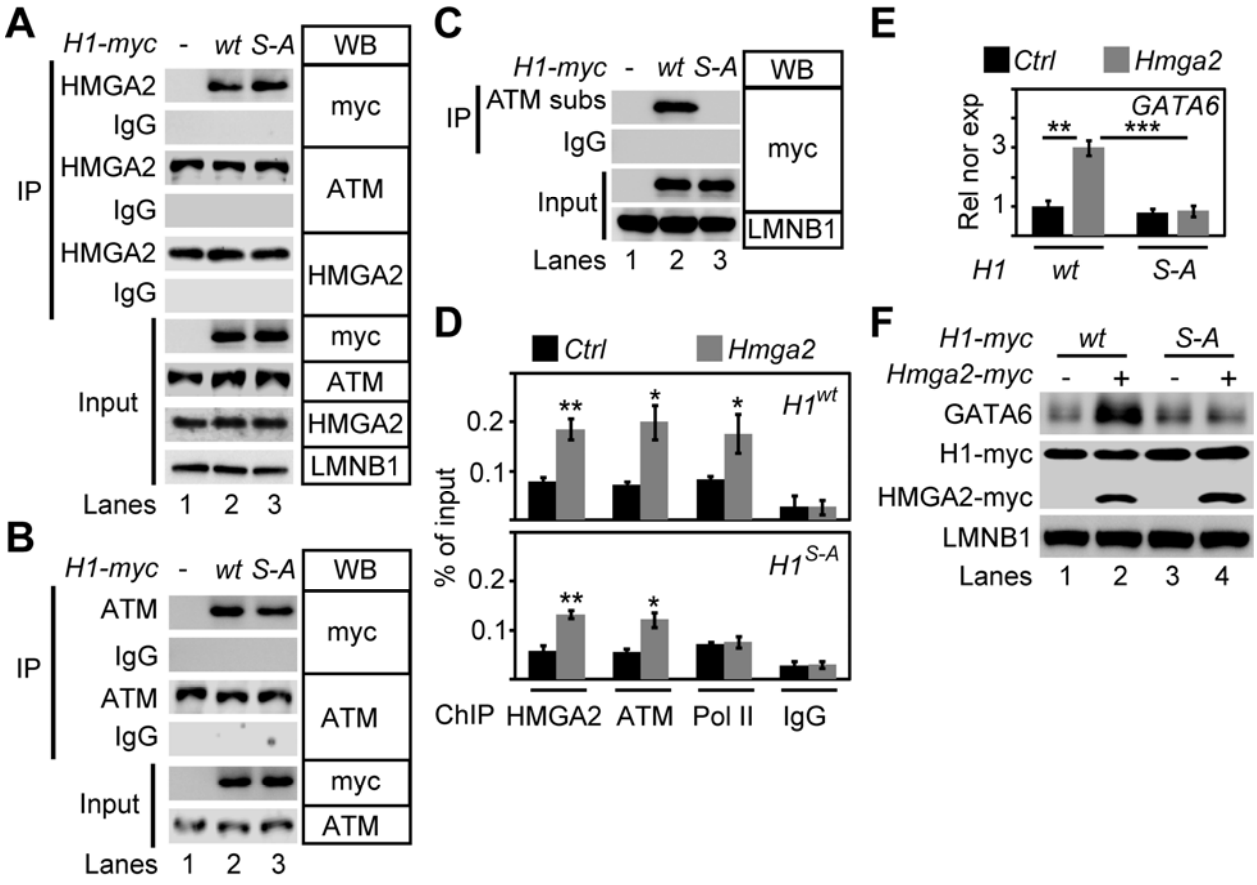

Figure 32. Histone H1 phosphorylation at Serine 65 is required for HMGA2-mediated transcriptional activation of *GATA6*. (A) Nuclear protein extracts from HEK293T cells transiently transfected with $H1^{wt}$ or $H1^{S-A}$ was analyzed by IP using an HMGA2-specific antibody or IgG control. Immunoprecipitated proteins were analyzed by WB using the indicated antibodies. (B) Nuclear protein extracts from HEK293T cells transiently transfected as in A were analyzed by IP using an ATM-specific antibody or IgG control. Immunoprecipitated proteins were analyzed by WB using the indicated antibodies. (C) Nuclear protein extracts from HEK293T cells transiently transfected as in A were analyzed by IP using an antibody specific for ATM subs or IgG control. (D) HEK293T cells transiently transfected with either $H1^{wt}$ (top) or $H1^{S-A}$ (bottom) and were co-transfected with *Ctrl* or *Hmga2* expression plasmid. Chromatin was isolated 48 hours after transfection and analyzed by ChIP using the indicated antibodies. Error bars, s.e.m. (n=3). Asterisks as in Fig. 12A. (E) *GATA6* expression was monitored by qRT-PCR in HEK293T cells that were transfected as in D. Error bars, s.e.m. (n=6). Asterisks as in Fig. 12A. (F) Nuclear protein extracts from HEK293T cells that were transfected as in E were analyzed by WB using the indicated antibodies.

4.3.5 HMGA2 activates *Gata6* expression via ATM-mediated phosphorylation of H2AX and H1

Two transgenic mouse lines *Hmga2*$^{-/-}$ [118] and *Hmga2* overexpression (GOF) [119] were used to confirm *in vitro* data. WB analysis of protein extracts from mouse embryos at E18.5 (Figure 33A) demonstrated the effect of both transgenic modifications on HMGA2 levels. *Hmga2*$^{-/-}$ abolished HMGA2 (Figure 33A, lanes 2-3) whereas transgenic *Hmga2*-GOF increased HMGA2 levels (Figure 33A, lanes 5-6). Interestingly, Co-IP using the ATM subs antibody (Figure 33B) showed that *Hmga2*$^{-/-}$ reduced H1- and H2AX-phosphorylation (Figure 33B, lane2) whereas transgenic *Hmga2*-GOF induced the opposite effect (Figure 33B, lane3). The total levels of H1 and H2AX were not affected in both mice lines thereby validating that the observed effects were indeed related to these post-translational modifications. In addition, WB of protein extracts of WT and both transgenic mice lines using H2AXS139ph antibody confirmed presented results (Figure 33A). ChIP using HMGA2- and ATM-specific antibodies and chromatin isolated from WT and both transgenic lines (Figure 33C) showed reduced association of HMGA2 and ATM to the *Gata6* promoter in *Hmga2*$^{-/-}$ whereas increased association of both proteins to the same promoter in transgenic *Hmga2*-GOF mice. Accordingly with the ATM ChIP results, decrease of H1- and H2AX-phosphorylation at the *Gata6* promoter in *Hmga2*$^{-/-}$ (Figure 33D, top; Figure 33E, left) was detected whereas the opposite resulted from the analysis of *Hmga2*-GOF chromatin by sequential ChIP (ChIP-reChIP) using ATM subs and subsequently H1 or H2AX antibodies. These results were confirmed by ChIP and after inverting the order of antibodies used for ChIP-reChIP (Figure 33D, bottom; Figure 33E, right) and using H2AXS139ph antibody (Figure 33F). Consistently with presented *in vitro* data, transgenic *Hmga2*-GOF increased the association of Pol II to the *Gata6* promoter when compared to WT mice (Figure 33C) whereas *Hmga2*$^{-/-}$ induced the reverse effect. Finally, *Gata6* expression analysis (Figure 33G) showed more than fivefold increase in *Hmga2*-GOF and 50% decrease in *Hmga2*$^{-/-}$ when compared to WT mice confirming presented *in vivo* ChIP results and validating presented *in vitro* data.

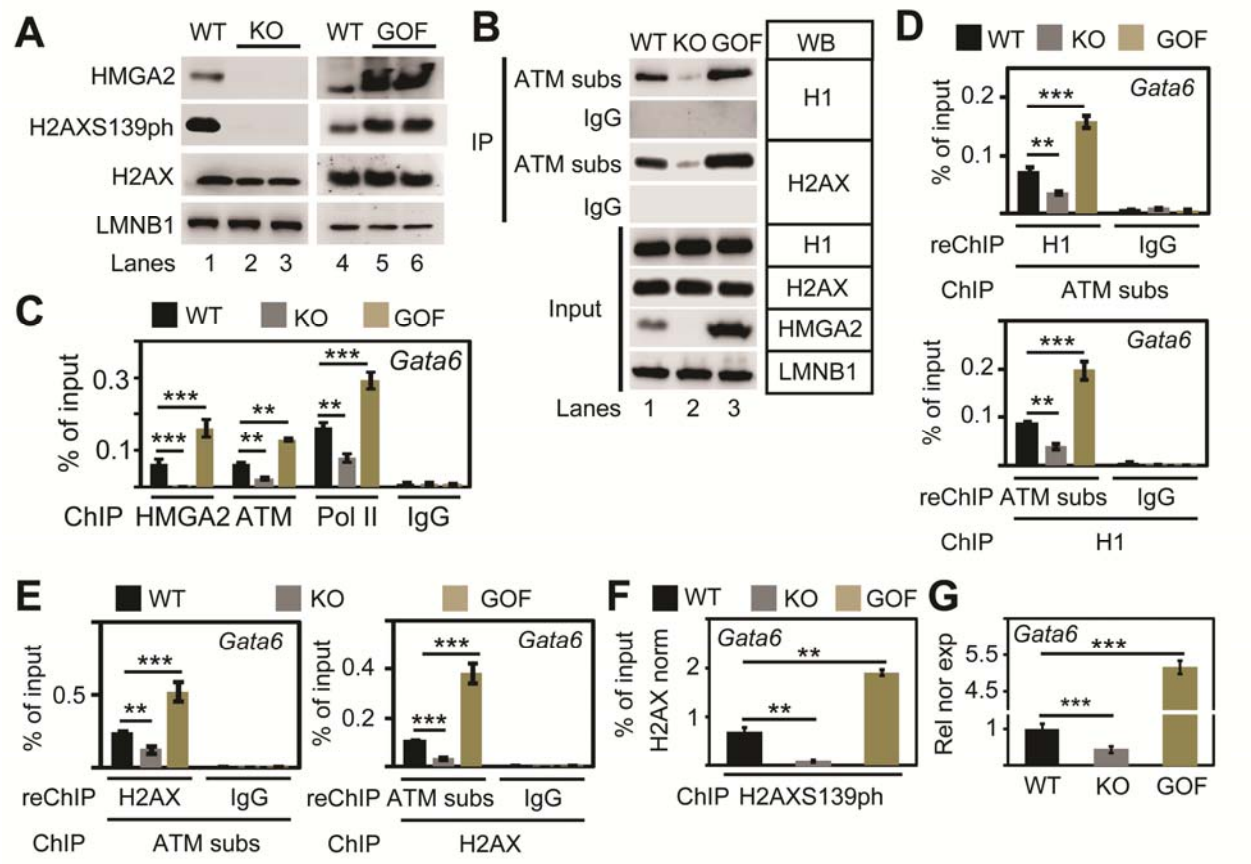

Figure 33. HMGA2 activates *Gata6* expression via ATM-mediated phosphorylation of H2AX and H1. (A) Lung protein extracts from WT, *Hmga2*-KO and *Hmga2*-GOF mice were analyzed by WB using the indicated antibodies. Two animals per transgenic mice line were analyzed. (B) Nuclear protein extracts from of WT, KO and GOF mice lung were analyzed by IP using an antibody specific for ATM subs or IgG, control. Immunoprecipitated proteins were analyzed by WB using the indicated antibodies. Input, 5% of material used for the IP. (C) Chromatin from WT, KO and GOF mice lung was analyzed by ChIP using the indicated antibodies. Error bars, s.e.m. (n=4). Asterisks as in Fig. 12A. (D) Chromatin from WT, KO and GOF mice lung was analyzed by sequential ChIP using first ATM subs (Top) or H1 (Bottom) antibody. The precipitated chromatin was further analyzed by a second ChIP (reChIP) using H1 (Left) or ATM subs (Right) antibody as indicated. Error bars, s.e.m. (n=4). Asterisks as in Fig. 12A. (E) Chromatin from WT, KO and GOF mice lung was analyzed by sequential ChIP using first ATM subs (Left) or H2AX (Right) antibody. The precipitated chromatin was further analyzed by reChIP using H2AX (Left) or ATM subs (Right) antibody as indicated. Error bars, s.e.m. (n=4). Asterisks as in Fig. 12A. (F) Chromatin from WT, KO and GOF mice lung was analyzed by ChIP using the indicated antibodies. Error bars, s.e.m. (n=4). Asterisks as in Fig. 12A. (G) *Gata6* expression was monitored by qRT-PCR in WT, KO and GOF mice lung. Error bars, s.e.m. (n=4). Asterisks as in Fig. 12A.

4.3.6 HMGA2-induced transcriptional activation of *Gata6* implicates promoter-specific nucleosome eviction

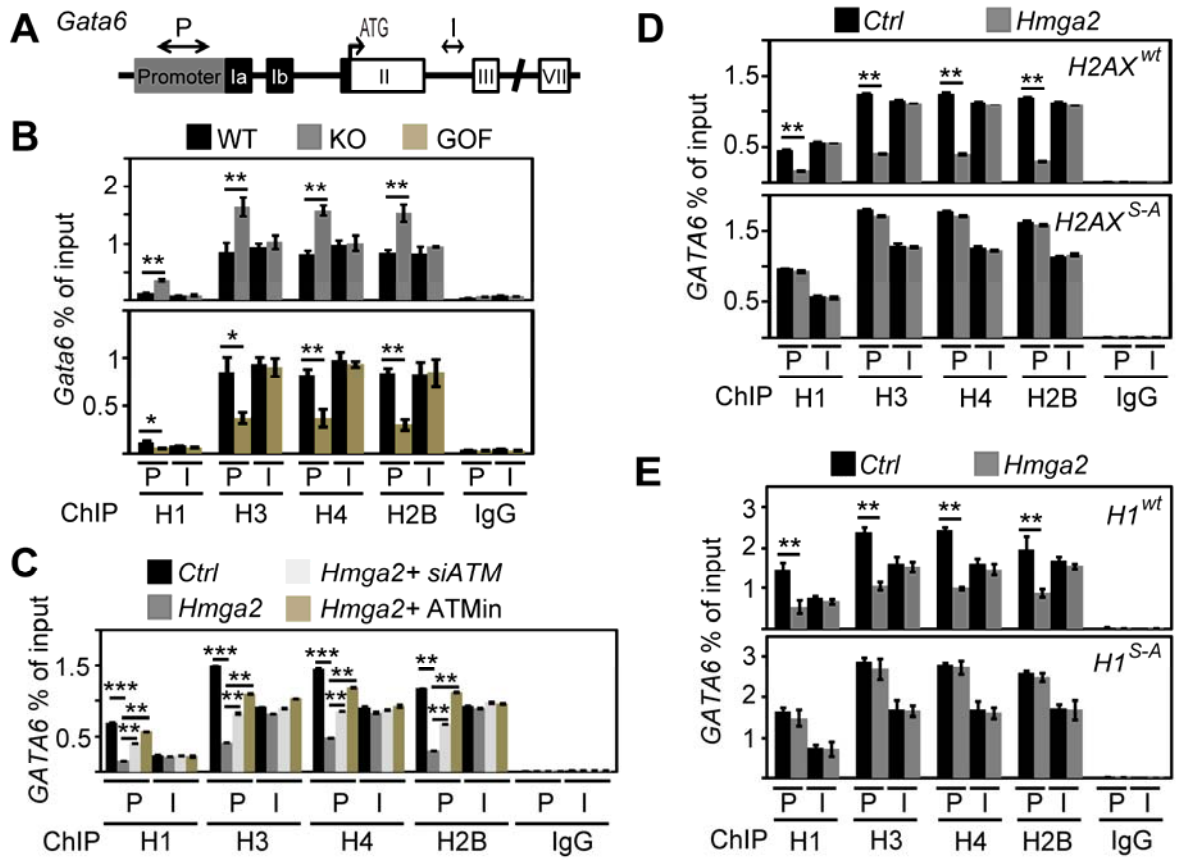

Figure 34. HMGA2-induced transcriptional activation of *Gata6* implicates promoter-specific nucleosome loss. (A) Schematic representation of the *Gata6* gene. The structure is conserved in human and mouse. The relative location of the primers used for ChIP in the promoter (P) and in the intragenic region (I) is shown. Exons are represented as black boxes (untranslated region) and white boxes (coding region). ATG, translation initiation start. (B) Chromatin from WT, KO and GOF mice lung was analyzed by ChIP using the indicated antibodies. P, promoter; I, intragenic region. Error bars, s.e.m. (n=3). Asterisks as in Fig. 12A. (C) Chromatin from HEK293T cells that were transfected/treated as in Fig. 30A was analyzed by ChIP using the indicated antibodies. Error bars, s.e.m. (n=3). Asterisks as in Fig. 12A. (D) Chromatin from HEK293T cells that were transfected as in Fig. 31D was analyzed by ChIP using the indicated antibodies. Error bars, s.e.m. (n=3). Asterisks as in Fig. 12A. (E) Chromatin from HEK293T cells that were transfected as in Fig. 32D was analyzed by ChIP using the indicated antibodies. Error bars, s.e.m. (n=3). Asterisks as in Fig. 12A.

A schematic representation of the *Gata6* gene is shown in Figure 34A. To investigate the effect of HMGA2 on the chromatin structure of the *Gata6* gene, the promoter (P) and an intragenic (I) region of *Gata6* was analyzed by ChIP using antibodies specific for different histones and chromatin from *Hmga2*$^{-/-}$, *Hmga2*-GOF and WT mice (Figure 34B). *Hmga2*$^{-/-}$ (top) increased the levels of linker histone H1 and core histones H3, H4 and H2B in the *Gata6* promoter without affecting the levels of histones in the intragenic region analyzed, suggesting that the effect was specific for the promoter. Interestingly, *Hmga2*-GOF (bottom) caused the contrary effect reducing the levels of all histones analyzed specifically in the *Gata6* promoter. Transfection of *Hmga2* into HEK293T cells (Figure 34C) also reduced the histone occupancy specifically in the *GATA6* promoter confirming presented *in vivo* data in *Hmga2*-GOF mice. Furthermore, the effect caused by *Hmga2*-GOF was antagonized after ATM-LOF by *siATM* or ATMin showing the requirement of ATM. Moreover, *H2AX*$^{S\text{-}A}$ (Figure 34D, bottom) and *H1*$^{S\text{-}A}$ (Figure 34E, bottom) blocked the histone eviction at the *Gata6* promoter induced by *Hmga2* thereby supporting that ATM-mediated phosphorylation of the mutated serines in their respective histones is required for the effects caused by *Hmga2*-GOF. Transient transfection of *Hmga2* induced release of linker histone H1 and core histones from the *GATA6* promoter (P) only in cells expressing H2AX^{wt} (Figure 34D, top) or H1^{wt} (Figure 34E, top). The levels of histones in the *Gata6* intragenic region analyzed remained unaltered upon *Hmga2* overexpression, confirming that the effect is specific to the promoter.

These data were further confirmed using an experimental system in which the *Gata6* promoter was *in vitro* reconstituted into chromatin using recombinant histones and nuclear protein extracts from HEK293T cells (Figure 35A-D). *Hmga2*-overexpression induced histones release (Figure 35C, lane 8) that was blocked by ATMin (Figure 35C, lane 10). Interestingly, ATM binds the *in vitro* reconstituted chromatin only after *Hmga2*-GOF (Figure 35C, lanes 5 and 7) supporting previously presented data (Figures 30A and 33C) and suggesting a role of HMGA2 as adaptor. However, ATMin blocked *Hmga2*-mediated ATM binding to the chromatin (Figure 35, lane 9) supporting the requirement of the kinase activity and suggesting an ATM activation by auto-phosphorylation. Furthermore, these results were confirmed by ChIP of the *Gata6* promoter *in vitro* reconstituted in chromatin (Figure 35D).

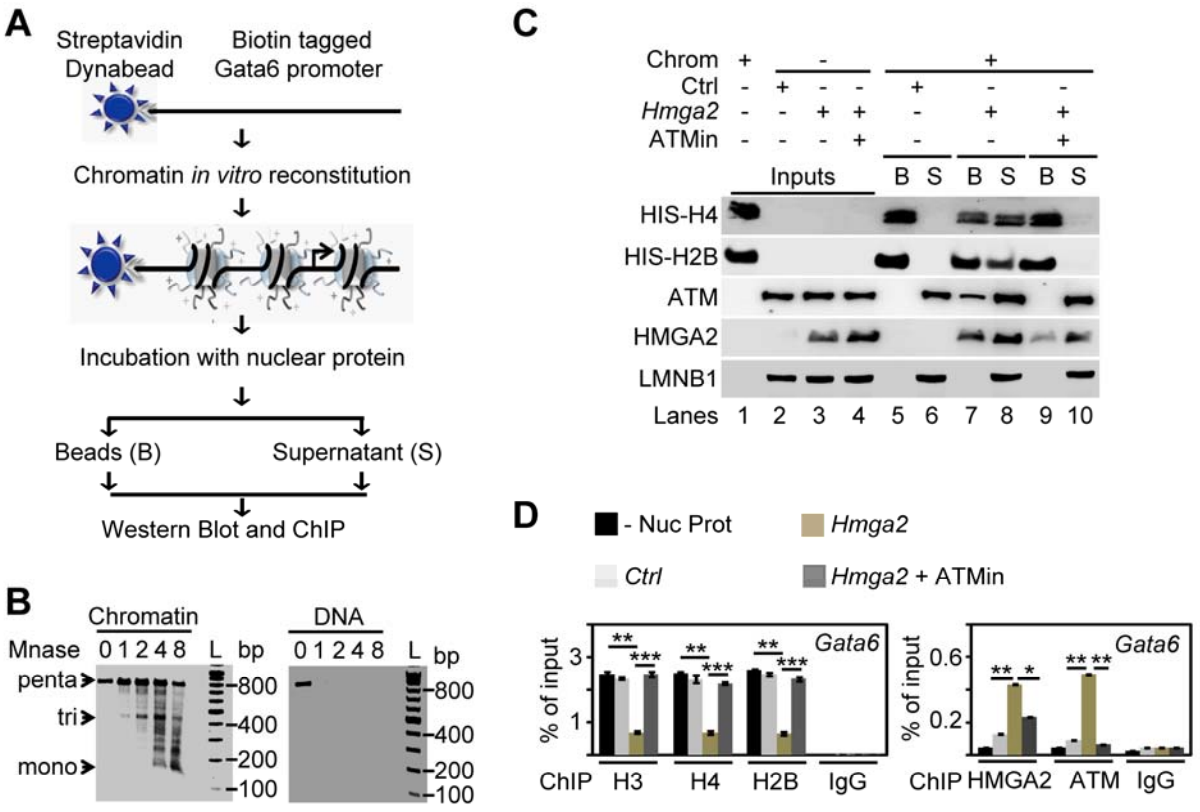

Figure 35. HMGA2-induced transcriptional activation of *Gata6* implicates promoter-specific nucleosome eviction. (A) Schematic diagram of analysis of *in vitro* reconstituted polynucleosomes by western blot and ChIP. An 850 bp fragment of the *Gata6* promoter was amplified by PCR using a biotinilated forward primer and coated to Streptavidin Dynabeads. The DNA loaded beads were used for *in vitro* reconstitution into chromatin by salt dialysis method using recombinant core histones. *In vitro* reconstituted polynucleosomes were incubated with nuclear extracts of HEK293T cells. After incubation, chromatin was separated using the magnetic beads and subjected to western blot and ChIP. (B) Quality of *in vitro* reconstituted polynucleosomes was analyzed by Mnase accessibility assay. Reconstitution of DNA into polynucleosomes (left) protects the naked DNA (right) from Mnase digestion. Min, minutes; L, 100bp DNA ladder. Arrowheads show the positions of mono-, tri- and pentanucleosomes. (C) WB analysis was performed using the indicated antibodies in the chromatin separated from beads (B) and supernatant (S) after incubation with nuclear extracts of HEK293T cells that were transiently transfected with a *Ctrl* or an *Hmga2-myc* expression plasmid. Transfected cells nuclear extracts were either untreated or treated with the ATMin as indicated. Representative blots were shown. (D) ChIP analysis was performed using the indicated antibodies in the chromatin that was separated from beads after incubation with nuclear extracts (Nuc Prot) of HEK293T cells that were transiently transfected with a *Ctrl* or an *Hmga2-myc* expression plasmid. Nuclear extracts were either untreated or treated with ATMin as indicated. Enrichment of the indicated proteins on the *Gata6* promoter after ChIP was monitored by qPCR. Error bars, s.e.m. (n=3). Asterisks as in Fig. 12A.

4.3.7 ATM-mediated H1S65ph precedes H2AXS139ph during HMGA2-induced *Gata6* transcriptional activation

To create proteins that mimic the biological activity of phosphorylated proteins, we substituted S65 and S139 in H1 and H2AX respectively by aspartic acid ($H1^{S\text{-}D}$ and $H2AX^{S\text{-}D}$). Transfection of HEK293T with $H1^{S\text{-}D}$ or/and $H2AX^{S\text{-}D}$ (Figure 36A, top) increased *GATA6* expression minimally. The increase of *GATA6* expression by these phosphomimetic mutants became more significant when *Hmga2* was co-transfected. Interestingly, the inhibiting effect of ATMin on *Hmga2*-enhanced *GATA6* expression (Figure 36A, bottom) was overcome by $H1^{S\text{-}D}$ and $H2AX^{S\text{-}D}$ single- or co-transfection supporting that ATM-catalyzed H1S65ph and H2AXS139ph mediate the enhancing effects of *Hmga2* on *GATA6* expression.

To determine the order of events of *GATA6* activation, HEK293T cells were transfected with the phosphomimetic mutants ($H1^{S\text{-}D}$ and $H2AX^{S\text{-}D}$) together with the $H1^{S\text{-}A}$ and $H2AX^{S\text{-}A}$ mutants in which ATM-mediated phosphorylation is prevented. Transfection of $H1^{S\text{-}D}$ alone or in combination with *Hmga2* increased *GATA6* expression only in the presence of $H2AX^{wt}$ (Figure 36B). $H2AX^{S\text{-}A}$ blocked the enhancing effect of $H1^{S\text{-}D}$ and *Hmga2* supporting that H2AXS139ph is required for *GATA6* activation and suggesting that is downstream of HMGA2 and H1S65ph. Consistent with this interpretation, $H2AX^{S\text{-}D}$ was not only able to increment *GATA6* expression alone or in combination with *Hmga2* (Figure 36C), but it was also able to overcome the blocking effect of $H1^{S\text{-}A}$ on *Hmga2*-enhanced *GATA6* expression supporting that H2AXS139ph is downstream of HMGA2 and H1S65ph. Furthermore, ChIP of the *GATA6* promoter revealed accumulation of H2AXS139ph after *Hmga2*-GOF (Figure 36D) that was blocked by $H1^{S\text{-}A}$ supporting the requirement of H1S65ph and suggesting that this post-translational modification precedes H2AXS139ph.

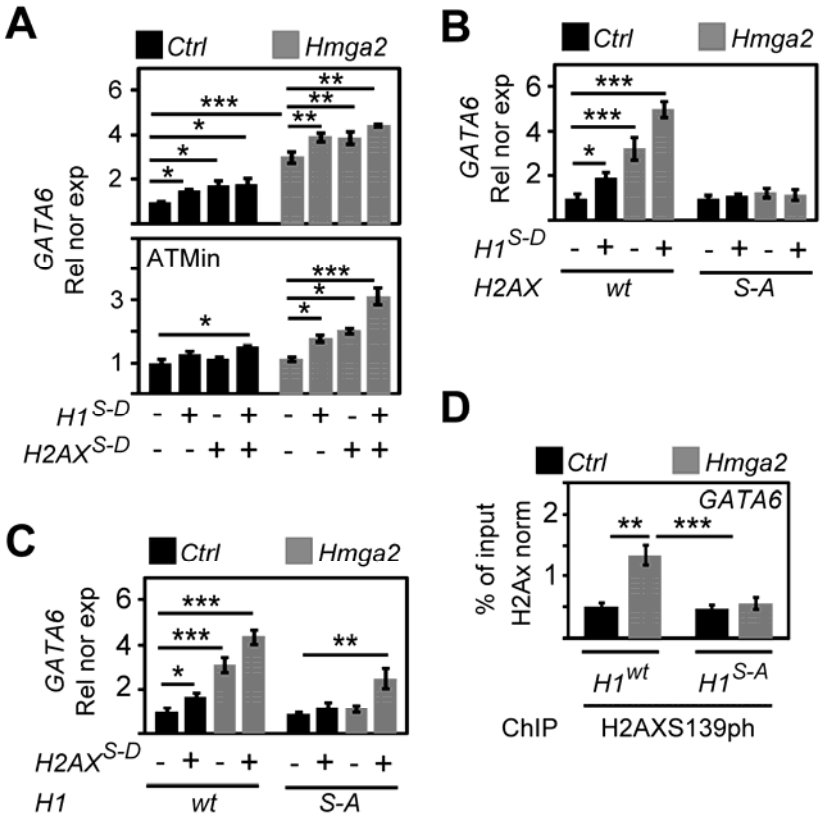

Figure 36. ATM-mediated H1S65ph precedes H2AXS139ph during HMGA2-induced transcriptional activation. (A) HEK293T cells that were treated with DMSO (solvent control, top) or ATMin (bottom) were transiently transfected with either *Ctrl* or *Hmga2* and/or $H1^{S\text{-}D}$ and/or $H2AX^{S\text{-}D}$ plasmid as indicated. *GATA6* expression was monitored by qRT-PCR. Error bars, s.e.m. (n=3). Asterisks as in Fig. 12A. (B) HEK293T cells stably expressing either $H2AX^{wt}$ or $H2AX^{S\text{-}A}$ was transiently transfected with Ctrl or *Hmga2* and/or $H1^{S\text{-}D}$ plasmid. *GATA6* expression was monitored by qRT-PCR. Error bars, s.e.m. (n=3). Asterisks as in Fig. 12A. (C) HEK293T cells transiently expressing $H1^{wt}$ or $H1^{S\text{-}A}$ was co-transfected with *Ctrl* or *Hmga2* and/or $H2AX^{S\text{-}D}$ as indicated. *GATA6* expression was monitored by qRT-PCR. Error bars, s.e.m. (n=3). Asterisks as in Fig. 12A. (D) Chromatin from HEK293T cells that were transfected as in Fig. 32D was analyzed by ChIP using H2AXS139ph and H2AX-specific antibodies. Error bars, s.e.m. (n=3). Asterisks as in Fig. 12A.

Chapter 5: DISCUSSION & CONCLUSION

HMG family member proteins are non-histone chromatin associated proteins having a key role in coupling signaling pathways to chromatin [32, 138, 139]. Several lines of evidence have underlined their role in development and disease [41, 47-50, 52-55, 65, 70, 71]. HMGA2, a member of HMGA family proteins having roles during lung development and homeostasis, have not been investigated before. Thus, the topic questioned in this thesis is of significant importance.

5.1 HMGA2 is required for proper distal epithelial cell differentiation during lung development and homeostasis

Hmga2 was originally identified in the genome wide *siRNA* based LOF screen, which was carried out to identify novel regulators of lung epithelial cell lineage during lung development. To validate this screen, *Hmga2* expression pattern was analyzed in mouse embryonic lung by three independent techniques, qRT-PCR, *RNA in situ* hybridization and immunofluorescence. *Hmga2* mRNA levels were high during early stages of lung development (Figure 11A, B); in which cells are undifferentiated, and decreased as lung development progressed, coincident with cell differentiation. Interestingly, a slight increase of *Hmga2* expression at E18.5 was detected (Figure 11A) that matches with the establishment of a bipotent progenitor cell population in the distal epithelium [140]. Later, *Hmga2* expression was reduced to a basal level in adult lung which correlate with previous reports in which HMGA2 was shown to be present at high levels in various undifferentiated tissues during embryonic development and its levels were strongly reduced in the corresponding adult tissues [40, 65, 110, 141, 142].

Sftpc is one of the most specific known markers of lung epithelial cell lineage in distal airways [11], hence in the LOF screening, a luciferase reporter gene under the control of the *Sftpc* promoter had been used. The co-localization of HMGA2 and SFTPC in same cells of the embryonic lung (Figure 13A) and reduced expression of *Sftpc* in the *Hmga2*$^{-/-}$ mice embryonic lung when compared to WT (Figure 12G, H) validated the screening. This finding was

interesting in the context of distal epithelial airways development hence further investigation was needed to understand the function of HMGA2 in this process.

Hmga2$^{-/-}$ mice embryos showed reduced body size compared to wild type embryos at E18.5 (Figure 12A) consistent with previous reports in which *Hmga2*$^{-/-}$ mice had a pygmy phenotype due to reduced expression of *Igf2bp2* [63, 65, 66]. Prior to this study, the lung of *Hmga2*$^{-/-}$ mice was not analyzed. *Hmga2*$^{-/-}$ mice embryonic lung showed an expansion of the mesenchyme at the expense of the epithelium (Figure 12E, F). To address this point, cell proliferation analysis was performed in epithelial and mesenchymal cells of *Hmga2*$^{-/-}$ mice embryonic lung (Figure 14A-D). This showed an increased cell proliferation in mesenchymal cells. Even though cell proliferation was more prominent in mesenchymal cells, increased epithelial cell proliferation was also observed (Figure 14 A-D). To understand this observation, cell proliferation was analyzed in distal epithelial differentiated cells and progenitor cells (Figure 15A, B). This showed an increased cell proliferation in epithelial progenitor cells and no significant change in distal epithelial differentiated cells. In addition, apoptosis analysis (Figure 16A, B) also showed increased epithelial cell apoptosis and no significant change in mesenchymal cell apoptosis confirming the expansion of the mesenchyme, hence supporting distal lung epithelial differentiation defect in *Hmga2*$^{-/-}$ mice.

Detailed analysis of *Hmga2*$^{-/-}$ mice adult lung also confirmed that *Hmga2* is required for proper distal epithelial cell differentiation not only during embryonic lung development but also in the adult lung homeostasis. In both cases, *Hmga2*$^{-/-}$ led to increased progenitor cells and defective epithelial cell differentiation (Figure 15A, B and Figure 17E-G). Increased numbers of progenitor cells (Figure 15B and Figure 17F, G) in the lung of *Hmga2*$^{-/-}$ mice generated an imbalance in cell differentiation that was reflected in a reduction of alveolar type II cells (Figure 15A, B and Figure 17E), thereby affecting both lung morphology as well as lung functionality (Figure 17B-D). These data correlate with previous reports where HMGA2 was shown to be required for adipogenesis, neurogenesis, spermatogenesis, cardiac and skeletal muscle development and their proper functions [47, 48, 65, 68-71].

5.2 HMGA2 modulates canonical WNT signaling during lung development and homeostasis

To identify potential molecular mechanism of HMGA2 for lung development and homeostasis, Affymetrix microarray-based expression analysis of *Hmga2*$^{-/-}$ and WT mice embryonic lung at E18.5 was performed (Figure 18A). This revealed an increased expression of either target or positive regulators of canonical WNT signaling pathway in the embryonic lung of *Hmga2*$^{-/-}$ mice. This was further confirmed by several independent techniques as qRT-PCR, WB and immunostaining as well as by using WNT reporter BAT-GAL mice (Figure 18 B-G). Taken together, this study showed that *Hmga2*$^{-/-}$ led to increased canonical WNT signaling resulting not only in defective epithelial differentiation but also in increased numbers of progenitor cells in the embryonic and adult lung.

Figure 37. Model: HMGA2 regulates canonical WNT signaling at different points of the pathway. Regulation of the secreted WNT glycoproteins (*Wnt2b*, *Wnt7b* and *Wnt11*) mediates the paracryne effect on the mesenchyme of the embryonic lung. In addition, HMGA2-mediated regulation of *Gata6* is a key process in fine-tuning the activity of canonical WNT signaling in developing airway epithelium. X, unknown transcription factors.

Hmga2$^{-/-}$ led to enhanced canonical WNT signaling due to an increase of secreted WNT glycoproteins as well as a reduction of the WNT signaling antagonizing proteins, GATA6 and FZD2, thereby supporting that HMGA2 regulates WNT signaling at different points of the pathway (Figure 37). The causal involvement of canonical WNT signaling in mediating the effect of *Hmga2*-LOF was demonstrated by the DKK1-induced rescue of *Hmga2*-LOF in embryonic lung explants (Figure 20A-E). In addition, it was also shown in adult lung that transgenic mice where WNT signaling is attenuated (*Ctnnb1*$^{+/-}$ mice; *CMV-Cre-,Ctnnb1*^{tm2Ke}) [120] or blocked by Doxycycline-inducible expression of *Dkk1* (Dox-ind *Dkk1* mice; *Rosa26rtTA, Tet (O) Dkk1*) [121] rescued the *Hmga2*-LOF effect (Figure 22C).

Directly regulation of *Gata6* by HMGA2 was shown by several independent techniques such as qRT-PCR, WB, immunostaining, luciferase assay and ChIP (Figure 24A-E). It was reported that GATA6 positively regulates *Fzd2* expression which results in blocking canonical WNT signaling in lung epithelial cells to control balance between progenitor expansion and lung epithelial differentiation [31]. HMGA2-mediated regulation of *Gata6* seems to be a key process in fine-tuning the activity of canonical WNT signaling in airway epithelium. The sequential order of events suggested in this study model (Figure 37) in which *Hmga2* acts upstream of *Gata6* was strongly supported by the fact that *Hmga2*$^{-/-}$ reduced expression of *Gata6* and its downstream target gene *Fzd2* (Figure 24B, C) as well as by the *Gata6*-mediated rescue experiments of *Hmga2*-LOF in MLE-12 cells (Figure 25B) and in adult lung (Figure 26B-D).

Hmga2$^{-/-}$ increased cell proliferation not only in the lung epithelium, where *Hmga2* is expressed, but also in the mesenchyme, suggesting a paracrine effect that could be explained by increased expression of the secreted components of WNT signaling. HMGA2 is known to activate transcription, the increased expression of *Wnt2b*, *Wnt7b* and *Wnt11* after *Hmga2*$^{-/-}$ suggest the participation of a transcription inhibitor that could block the expression of these secreted components of WNT signaling and whose expression could be regulated by HMGA2 (Figure 37). Interestingly, analysis of the *Wnt7b* promoter showed that deletion of the region between −1,005 bp and −829 bp relative to the second transcription start site increased significantly the basal transcription activity of a *Wnt7b*-luciferase reporter [23] suggesting that the binding element of a putative transcription inhibitor was deleted in this construct.

The phenotypes of *Hmga2*- and *Gata6*-LOF in embryonic lung explants are very similar (Figure 23A-B). However, the milder phenotype observed in the embryonic lung of *Hmga2*$^{-/-}$ mice when compared either with the *Gata6*$^{-/-}$ or the phenotype induced after *Hmga2*-KD in embryonic lung explants might be explained by redundancy in the function between *Hmga2* and *Hmga1*, other member of the HMGA protein family. *Hmga1* transcript was reduced after *Hmga2*-LOF (Figure 19C) but not affected in the *Hmga2*$^{-/-}$ mice (Figure 12C). *Hmga1* might compensate the *Hmga2*$^{-/-}$, thereby avoiding lethality at early embryonic stages, as it is the case after *Gata6*$^{-/-}$ [143, 144], or soon after birth due to defects in the lung, as it is the case after lung epithelium-specific ablation of *Gata6* [31]. To support this speculation, previous report have shown that *Hmga2/Hmga1* double knockout mice showed embryonic lethality [145] however individually *Hmga2*$^{-/-}$ mice or

Hmga1$^{-/-}$ mice did not show embryonic lethality [66, 146]. In addition, the expansion of the mesenchyme in the embryonic lung after *Hmga2*$^{-/-}$ and the apparent increase of epithelium in embryonic lung explants after *Hmga2*-KD might be explained by the differences of both LOF-systems. In the transgenic approach *Hmga2*-LOF takes place soon after fertilization and affects lung development from the initial stages of lung bud formation, whereas in the explant culture the LOF starts at E12.5 thereby reducing the rather indirect effect on the mesenchyme and making the effect on the epithelium more dominant.

Organ regeneration requires a proper balance between self-renewal and differentiation of tissue specific progenitor cells. This study suggests the possible role of *Hmga2* in the adult lung controlling the balance between BASCs expansion and differentiation (Figure 17E-G) by modulating the canonical WNT signaling (Figure 21A, B). BASCs represent one of several regional progenitor cell populations in the adult lung and are responsible for regeneration of bronchiolar and alveolar epithelium during homeostatic turnover and in response to injury [5, 6]. These data are consistent with previous studies, where it was shown that canonical WNT signaling is activated upon lung epithelial regeneration, and lung epithelium-specific ablation of *Gata6* enhanced canonical WNT activity which led to a premature and increased numbers of BASCs [31]. In addition, canonical WNT signaling has also been implicated in different regenerative processes including zebrafish tail regeneration, zebrafish cardiac regeneration and expansion of anterior heart field progenitors in mammals [147, 148].

HMGA2 regulates *Gata6* and *Fzd2* expression (Figure 24 B, C). FZD2 acts as a negative regulator of canonical WNT signaling in lung epithelium. Given the ability of these proteins to modulate canonical WNT signaling in the lung, it may be possible to use them as potential targets to activate this pathway to increase repair and regeneration after lung injury. However, due to the fact that HMGA2, WNT signaling and BASCs have been involved in lung cancer [6, 54, 149] one has to be careful before modulating the WNT pathway for this purpose.

5.3 HMGA2-induced transcription requires ATM-mediated histones phosphorylation and nucleosome eviction

This study deciphered the mechanism of transcriptional regulation mediated by the HMGA2. HMGA2 regulates the transcription of its target genes by modulating the chromatin structure and by recruiting other proteins to the transcription regulatory complex [40], However, precise molecular events are not well understood therefore the molecular mechanism of HMGA2-mediated transcriptional regulation of the *Gata6* promoter was investigated.

This study argues for a model (Figure 38) in which ATM-mediated phosphorylation of H1 and H2AX requires HMGA2 and increases after *Hmga2*-GOF. On the other hand, HMGA2-induced transcriptional activation of *Gata6* requires ATM-mediated phosphorylation of both histones. Furthermore, the evidence for the sequential order of events was presented in which H1S65ph precedes H2AXS139ph and both are a prerequisite for the subsequent disassembly of promoter-associated nulceosomes and transcriptional activation. The presented *in vitro* data were confirmed *in vivo* using two transgenic mice lines, one for *Hmga2*-LOF [118] and the other for *Hmga2*-GOF [119].

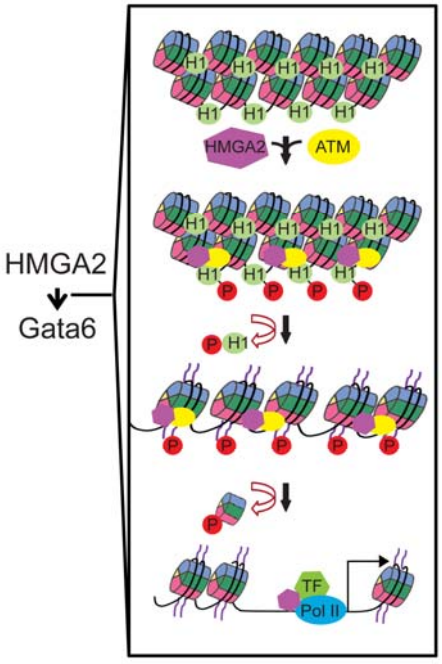

Figure 38. Model: HMGA2-induced transcriptional activation of *GATA6* requires ATM-mediated phosphorylation of histones and implicates nucleosome eviction. HMGA2 (purple hexagon) dependent ATM (yellow oval) mediated phosphorylation (red circle) of H1 induces the release of linker histone H1 (green oval) from the chromatin. Further HMGA2 dependent ATM mediated phosphorylation of H2AX induces release of promoter-associated nucleosomes to facilitate the accessibility of regulatory elements to transcription initiation factors. Transcription initiation factors (green hexagon and blue oval) bind to their regulatory elements and enhance transcription (black arrow) of target genes. Adatped [150].

HMGA proteins were shown to dynamically compete with H1 for binding to the linker DNA thereby loosening the chromatin [71, 91, 92]. In addition, displacement of H1 during the initial steps of gene activation has been reported [151]. However, presented data in this study provides new mechanistic insights linking these two events. This study demonstrated that ATM-mediated H1S65ph is required for HMGA2-induced *Gata6* activation (Figure 32D-F, Figure 33D, G and Figure 34E) which correlate with previous reports in which phosphorylation of H1 by CDK2 has been associated with hormone dependent transcriptional activation [151, 152].

H2AXS139ph is perhaps one of the most widely used biomarkers for DNA damage [101]. However, there is increasing evidence for additional functions of this histone modification. ATM-mediated H2AXS139ph plays a role during recombination of variable (V), diversity (D) and joining (J) segments which is the basis for antigen receptor diversity during lymphocyte differentiation [103]. H2AXS139ph is important during angiogenesis since hypoxia-driven neovascularization was significantly reduced in endothelial-specific H2AX-deficient mice and hypoxia induced H2AXS139ph in primary cultures of human endothelial cells [102]. Another study demonstrated that high basal levels of H2AXS139ph are required for stem cell self-renewal [104]. Findings of this study support a role of H2AXS139ph during *Hmga2*-induced gene activation that involves promoter specific nucleosome eviction to enhance transcription by Pol II (Figure 31D-F; Figure 33E-G and Figure 34D). Accordingly, it has been reported that promoters of active (or poised) genes are either nucleosome-free or marked with unstable nucleosomes that contain specific histone variants such as H3.3 and H2A.Z [153]. Although H2AX does not affect nucleosome conformation, it has a de-stabilizing effect that is enhanced by its phosphorylation and results in an impaired linker histone H1 binding [154], correlating with results presented in this study. Furthermore, the histone chaperone complex FACT catalyzes integration of H2AX into nucleosomes [155], induces disassembly of promoter-associated nucleosomes and enhances transcriptional activation. Interestingly, yeast FACT is a heterodimeric protein complex of Spt16 and Pob3 that interacts and functionally cooperates with the HMG1-like protein Nhp6 [156]. In addition, it has been reported that HMGA1 interacts with the multiprotein complex Mediator and the general transcription factor TFIID to form, together with Pol II, a functional pre-initiation complex on the core promoter during transcription initiation [45]. In summary, there are several lines of evidence that together with presented work in this thesis support a role of HMGA proteins and the chromatin modifications promoted by

them during transcription initiation by inducing promoter specific nucleosome disassembly and thereby facilitating the DNA access to the general transcription machinery.

HMGA2, ATM, H1 and H2AX have been related to biological events in which DNA-dependent processes as repair, replication, recombination and transcription are involved. Although packaging of the genome into chromatin constitutes a barrier for all these processes, the chromatin structure offers the possibility for a controlled implementation of all these processes. However, controlled chromatin disassembly might involve intermediates with single or even double strand breaks that might compromise the integrity of DNA. Thus, there must be mechanisms that ensure the integrity of the genome during opening of the chromatin. This perspective might explain the fact that proteins and histone modifications that were initially characterized during DNA repair also play a role during transcription, recombination and replication. In line with this hypothesis, a common characteristic between HMGA2- [66], ATM- [157-159] and H2AX- [160] transgenic mice is genomic instability. In addition, DNA repair linked histone modifications H3K56ac and H2Bub1 [161] have been related to transcription initiation [162].

5.4 Final Conclusion

This study demonstrated the role of the HMGA2, a member of HMGA family, as a key regulator of lung development and homeostasis by modulating the canonical WNT signaling by several lines of evidences.

This study also deciphered the molecular mechanism responsible for an HMGA2 mediated transcriptional activation of *Gata6*, in which HMGA2 acts as an adaptor to recruit ATM kinase on *Gata6* promoter for phosphorylation of the linker histone H1 at S65 (H1S65ph) and the core histone variant H2AX at S139 (H2AXS139ph). This induces a release of linker Histone H1 from the chromatin and subsequently of nucleosomes thereby facilitating the accessibility of regulatory elements to transcription initiation factors to enhance transcription of *Gata6*. Furthermore, the sequential order of events was demonstrated in which H1S65ph precedes H2AXS139ph and both are a prerequisite for the subsequent disassembly of promoter-associated nucleosomes and transcriptional activation. It also showed mutation of H2AX at serine 139 to alanine blocks the release of nucleosomes from the chromatin and recruitment of RNA Pol II. However, H2AXS139ph is commonly used as a marker for DNA double strand breaks [101] suggesting a novel role of this histone modification in transcriptional regulation.

In summary, this study propose HMGA2 mediated chromatin modulation at the *Gata6* promoter, as key processes for fine tuning the canonical WNT signaling during lung distal epithelial cell differentiation.

5.5 Outlook

In future, it would be interesting to analyze HMGA2 role in the lung injury model systems (bleomycin and/or Naphthalene) or in the pneumonectomy model to better understand HMGA2 role during lung regeneration.

This study suggests that HMGA2 is required as a regulator of canonical WNT signaling for proper lung epithelial cell differentiation. However, it is well known that HMGA2 is positively regulated by TGF-β1 signaling [57]. Therefore, *Hmga2* might play a crucial role in the interplay between these signaling pathways. Hence, it will be of interest to determine a potential opposing effect between these two signaling pathways in establishing the proximal-distal axis during branching morphogenesis and lung epithelium differentiation in the developing lung.

HMGA2 is known to activate transcription however, the increased expression of *Wnt2b*, *Wnt7b* and *Wnt11* after *Hmga2*$^{-/-}$ suggest participation of a transcription inhibitor that could block expression of these secreted components of WNT signaling and whose expression could be regulated by HMGA2 (Figure 37). Identification of this unknown mediator of HMGA2 will be the scope of future studies.

Milder phenotype observed in the embryonic lung of *Hmga2*$^{-/-}$ mice when compared with the *Gata6*$^{-/-}$ might be explained by redundancy in the function between *Hmga2* and *Hmga1*, other member of the HMGA protein family. Analysis of the lungs in inducible and conditional double transgenic mice (*Hmga2*$^{-/-}$:*Hmga1*$^{-/-}$) would further test the hypothesis.

This study established that HMGA2-induced transcriptional activation of *Gata6* requires ATM-mediated phosphorylation of histones and implicates nucleosome eviction. Further studies would be carried out to investigate whether the mechanism of *Gata6* regulation suggested here might be extended to other HMGA2 targets.

Chapter 6: REFERENCES

1. Rawlins, E.L. and B.L. Hogan, *Epithelial stem cells of the lung: privileged few or opportunities for many?* Development, 2006. **133**(13): p. 2455-65.
2. Kotton, D.N. and A. Fine, *Lung stem cells.* Cell Tissue Res, 2008. **331**(1): p. 145-56.
3. Kim, C.B., *Advancing the field of lung stem cell biology.* Front Biosci, 2007. **12**: p. 3117-24.
4. Daniel J. Weiss , M.A.B., Zea Borok , Dorothy B. Gail , Jay K. Kolls , Christopher Penland and Darwin J. Prockop, *Adult Stem Cells, Lung Biology, and Lung Disease. Report of a National Heart, Lung, and Blood Institute and Cystic Fibrosis Foundation Workshop.* Proceedings of the ATS, 2006. **3**: p. 15.
5. Giangreco, A., S.D. Reynolds, and B.R. Stripp, *Terminal bronchioles harbor a unique airway stem cell population that localizes to the bronchoalveolar duct junction.* American Journal of Pathology, 2002. **161**(1): p. 173-182.
6. Kim, C.F.B., et al., *Identification of bronchioalveolar stem cells in normal lung and lung cancer.* Cell, 2005. **121**(6): p. 823-835.
7. Eramo, A., T.L. Haas, and R. De Maria, *Lung cancer stem cells: tools and targets to fight lung cancer.* Oncogene, 2010. **29**(33): p. 4625-4635.
8. Barkauskas, C.E., et al., *Type 2 alveolar cells are stem cells in adult lung.* Journal of Clinical Investigation, 2013. **123**(7): p. 3025-3036.
9. Warburton, D., et al., *The molecular basis of lung morphogenesis.* Mech Dev, 2000. **92**(1): p. 55-81.
10. Costa, R.H., V.V. Kalinichenko, and L. Lim, *Transcription factors in mouse lung development and function.* Am J Physiol Lung Cell Mol Physiol, 2001. **280**(5): p. L823-38.
11. Cardoso, W.V. and J.N. Lu, *Regulation of early lung morphogenesis: questions, facts and controversies.* Development, 2006. **133**(9): p. 1611-1624.
12. Maeda, Y., V. Dave, and J.A. Whitsett, *Transcriptional control of lung morphogenesis.* Physiological Reviews, 2007. **87**(1): p. 219-44.
13. Weaver, M., et al., *Bmp signaling regulates proximal-distal differentiation of endoderm in mouse lung development.* Development, 1999. **126**(18): p. 4005-15.
14. Minoo, P. and C.G. Li, *Cross-talk between transforming growth factor-beta and Wingless/Int pathways in lung development and disease.* International Journal of Biochemistry & Cell Biology, 2010. **42**(6): p. 809-812.
15. Kimura, J. and G.H. Deutsch, *Key mechanisms of early lung development.* Pediatr Dev Pathol, 2007. **10**(5): p. 335-47.
16. Hogan, B.L.M., *Morphogenesis.* Cell, 1999. **96**(2): p. 225-233.
17. Rock, J.R. and B.L. Hogan, *Epithelial progenitor cells in lung development, maintenance, repair, and disease.* Annu Rev Cell Dev Biol, 2011. **27**: p. 493-512.
18. Wong, A.P. and J. Rossant, *Generation of Lung Epithelium from Pluripotent Stem Cells.* Curr Pathobiol Rep, 2013. **1**(2): p. 137-145.
19. Rao, T.P. and M. Kuhl, *An updated overview on Wnt signaling pathways: a prelude for more.* Circulation Research, 2010. **106**(12): p. 1798-806.
20. Reya, T. and H. Clevers, *Wnt signalling in stem cells and cancer.* Nature, 2005. **434**(7035): p. 843-850.
21. Tebar, M., et al., *Expression of Tcf/Lef and sFrp and localization of beta-catenin in the developing mouse lung.* Mech Dev, 2001. **109**(2): p. 437-40.
22. Shu, W., et al., *Wnt7b regulates mesenchymal proliferation and vascular development in the lung.* Development, 2002. **129**(20): p. 4831-42.
23. Weidenfeld, J., et al., *The WNT7b promoter is regulated by TTF-1, GATA6, and Foxa2 in lung epithelium.* Journal of Biological Chemistry, 2002. **277**(23): p. 21061-21070.
24. Wang, Z.S., et al., *Wnt7b activates canonical signaling in epithelial and vascular smooth muscle cells through interactions with Fzd1, Fzd10, and LRP5.* Mol Cell Biol, 2005. **25**(12): p. 5022-5030.
25. Mucenski, M.L., et al., *beta-catenin is required for specification of proximal/distal cell fate during lung morphogenesis.* Journal of Biological Chemistry, 2003. **278**(41): p. 40231-40238.
26. Shu, W., et al., *Wnt/beta-catenin signaling acts upstream of N-myc, BMP4, and FGF signaling to regulate proximal-distal patterning in the lung.* Dev Biol, 2005. **283**(1): p. 226-39.
27. Goss, A.M., et al., *Wnt2/2b and beta-catenin signaling are necessary and sufficient to specify lung progenitors in the foregut.* Dev Cell, 2009. **17**(2): p. 290-8.

28. Morrisey, E.E., et al., *GATA-6: A zinc finger transcription factor that is expressed in multiple cell lineages derived from lateral mesoderm.* Dev Biol, 1996. **177**(1): p. 309-322.
29. Keijzer, R., et al., *The transcription factor GATA6 is essential for branching morphogenesis and epithelial cell differentiation during fetal pulmonary development.* Development, 2001. **128**(4): p. 503-511.
30. Yang, H., et al., *GATA6 regulates differentiation of distal lung epithelium.* Development, 2002. **129**(9): p. 2233-46.
31. Zhang, Y., et al., *A Gata6-Wnt pathway required for epithelial stem cell development and airway regeneration.* Nature Genetics, 2008. **40**(7): p. 862-870.
32. Ozturk N, S.I., Mehta A, Braun T, Barreto G, *HMGA proteins as modulators of chromatin structure during transcriptional activation.* Front. Cell Dev. Bio., 2014.
33. Bustin, M., *Revised nomenclature for high mobility group (HMG) chromosomal proteins.* Trends in Biochemical Sciences, 2001. **26**(3): p. 152-153.
34. Catez, F. and R. Hock, *Binding and interplay of HMG proteins on chromatin: lessons from live cell imaging.* Biochim Biophys Acta, 2010. **1799**(1-2): p. 15-27.
35. Reeves, R., *Nuclear functions of the HMG proteins.* Biochim Biophys Acta, 2010. **1799**(1-2): p. 3-14.
36. Reeves, R., *Molecular biology of HMGA proteins: hubs of nuclear function.* Gene, 2001. **277**(1-2): p. 63-81.
37. Sgarra, R., et al., *HMGA molecular network: From transcriptional regulation to chromatin remodeling.* Biochim Biophys Acta, 2010. **1799**(1-2): p. 37-47.
38. Sgarra, R., et al., *Nuclear phosphoproteins HMGA and their relationship with chromatin structure and cancer.* FEBS Lett, 2004. **574**(1-3): p. 1-8.
39. Hammond, S.M. and N.E. Sharpless, *HMGA2, MicroRNAs, and Stem Cell Aging.* Cell, 2008. **135**(6): p. 1013-1016.
40. Pfannkuche, K., et al., *The high mobility group protein HMGA2: a co-regulator of chromatin structure and pluripotency in stem cells?* Stem Cell Rev, 2009. **5**(3): p. 224-30.
41. Fusco, A. and M. Fedele, *Roles of HMGA proteins in cancer.* Nature Reviews Cancer, 2007. **7**(12): p. 899-910.
42. Cui, T. and F. Leng, *Specific recognition of AT-rich DNA sequences by the mammalian high mobility group protein AT-hook 2: a SELEX study.* Biochemistry, 2007. **46**(45): p. 13059-66.
43. Winter, N., et al., *Chromatin immunoprecipitation to analyze DNA binding sites of HMGA2.* PLoS One, 2011. **6**(4): p. e18837.
44. Li, O., et al., *High-level expression of DNA architectural factor HMGA2 and its association with nucleosomes in human embryonic stem cells.* Genesis, 2006. **44**(11): p. 523-9.
45. Xu, M., et al., *Core promoter-selective function of HMGA1 and Mediator in Initiator-dependent transcription.* Genes Dev, 2011. **25**(23): p. 2513-24.
46. Cattaruzzi, G., et al., *The second AT-hook of the architectural transcription factor HMGA2 is determinant for nuclear localization and function.* Nucleic Acids Res, 2007. **35**(6): p. 1751-1760.
47. Chieffi, P., et al., *HMGA1 and HMGA2 protein expression in mouse spermatogenesis.* Oncogene, 2002. **21**(22): p. 3644-3650.
48. Caron, L., et al., *A new role for the oncogenic high-mobility group A2 transcription factor in myogenesis of embryonic stem cells.* Oncogene, 2005. **24**(41): p. 6281-6291.
49. Anand, A. and K. Chada, *In vivo modulation of Hmgic reduces obesity.* Nature Genetics, 2000. **24**(4): p. 377-380.
50. Sun, M., et al., *HMGA2/TET1/HOXA9 signaling pathway regulates breast cancer growth and metastasis.* Proc Natl Acad Sci U S A, 2013. **110**(24): p. 9920-5.
51. Kumar, M.S., et al., *HMGA2 functions as a competing endogenous RNA to promote lung cancer progression.* Nature, 2014. **505**(7482): p. 212-+.
52. Hock, R., et al., *HMG chromosomal proteins in development and disease.* Trends in Cell Biology, 2007. **17**(2): p. 72-79.
53. Di Cello, F., et al., *HMGA2 participates in transformation in human lung cancer.* Molecular Cancer Research, 2008. **6**(5): p. 743-750.
54. Winslow, M.M., et al., *Suppression of lung adenocarcinoma progression by Nkx2-1.* Nature, 2011. **473**(7345): p. 101-U120.
55. Morishita, A., et al., *HMGA2 Is a Driver of Tumor Metastasis.* Cancer Research, 2013. **73**(14): p. 4289-4299.

56. Zentner, M.D., et al., *Requirement for high mobility group protein HMGI-C interaction with STAT3 inhibitor PIAS3 in repression of alpha-subunit of epithelial Na+ channel (alpha-ENaC) transcription by Ras activation in salivary epithelial cells.* J Biol Chem, 2001. **276**(32): p. 29805-14.
57. Thuault, S., et al., *Transforming growth factor-beta employs HMGA2 to elicit epithelial-mesenchymal transition.* J Cell Biol, 2006. **174**(2): p. 175-83.
58. Watanabe, S., et al., *HMGA2 maintains oncogenic RAS-induced epithelial-mesenchymal transition in human pancreatic cancer cells.* Am J Pathol, 2009. **174**(3): p. 854-68.
59. Lee, Y.S. and A. Dutta, *The tumor suppressor microRNA let-7 represses the HMGA2 oncogene.* Genes Dev, 2007. **21**(9): p. 1025-30.
60. Mayr, C., M.T. Hemann, and D.P. Bartel, *Disrupting the pairing between let-7 and Hmga2 enhances oncogenic transformation.* Science, 2007. **315**(5818): p. 1576-1579.
61. Rice, S.J., et al., *MicroRNA-33a mediates the regulation of high mobility group AT-hook 2 gene (HMGA2) by thyroid transcription factor 1 (TTF-1/NKX2-1).* J Biol Chem, 2013. **288**(23): p. 16348-60.
62. Zhu, S., et al., *MicroRNA-10A* and MicroRNA-21 modulate endothelial progenitor cell senescence via suppressing high-mobility group A2.* Circulation Research, 2013. **112**(1): p. 152-64.
63. Brants, J.R., et al., *Differential regulation of the insulin-like growth factor II mRNA-binding protein genes by architectural transcription factor HMGA2.* FEBS Lett, 2004. **569**(1-3): p. 277-83.
64. Cleynen, I., et al., *HMGA2 regulates transcription of the Imp2 gene via an intronic regulatory element in cooperation with nuclear factor-kappaB.* Mol Cancer Res, 2007. **5**(4): p. 363-72.
65. Li, Z., et al., *An HMGA2-IGF2BP2 axis regulates myoblast proliferation and myogenesis.* Dev Cell, 2012. **23**(6): p. 1176-88.
66. Zhou, X., et al., *Mutation responsible for the mouse pygmy phenotype in the developmentally regulated factor HMGI-C.* Nature, 1995. **376**(6543): p. 771-4.
67. Copley, M.R., et al., *The Lin28b-let-7-Hmga2 axis determines the higher self-renewal potential of fetal haematopoietic stem cells.* Nat Cell Biol, 2013. **15**(8): p. 916-25.
68. Baldassarre, G., et al., *Onset of natural killer cell lymphomas in transgenic mice carrying a truncated HMGI-C gene by the chronic stimulation of the IL-2 and IL-15 pathway.* Proc Natl Acad Sci U S A, 2001. **98**(14): p. 7970-5.
69. Fedele, M., et al., *Role of the high mobility group A proteins in human lipomas.* Carcinogenesis, 2001. **22**(10): p. 1583-91.
70. Monzen, K., et al., *A crucial role of a high mobility group protein HMGA2 in cardiogenesis.* Nat Cell Biol, 2008. **10**(5): p. 567-74.
71. Kishi, Y., et al., *HMGA regulates the global chromatin state and neurogenic potential in neocortical precursor cells.* Nat Neurosci, 2012. **15**(8): p. 1127-33.
72. Antequera, F., *Structure, function and evolution of CpG island promoters.* Cellular and Molecular Life Sciences, 2003. **60**(8): p. 1647-1658.
73. Ramirez-Carrozzi, V.R., et al., *A unifying model for the selective regulation of inducible transcription by CpG islands and nucleosome remodeling.* Cell, 2009. **138**(1): p. 114-28.
74. Deaton, A.M. and A. Bird, *CpG islands and the regulation of transcription.* Genes Dev, 2011. **25**(10): p. 1010-22.
75. Butler, J.E. and J.T. Kadonaga, *The RNA polymerase II core promoter: a key component in the regulation of gene expression.* Genes Dev, 2002. **16**(20): p. 2583-92.
76. Juven-Gershon, T. and J.T. Kadonaga, *Regulation of gene expression via the core promoter and the basal transcriptional machinery.* Dev Biol, 2010. **339**(2): p. 225-9.
77. Levine, M. and R. Tjian, *Transcription regulation and animal diversity.* Nature, 2003. **424**(6945): p. 147-51.
78. Munshi, N., et al., *Coordination of a transcriptional switch by HMGI(Y) acetylation.* Science, 2001. **293**(5532): p. 1133-6.
79. Yie, J., et al., *The role of HMG I(Y) in the assembly and function of the IFN-beta enhanceosome.* EMBO J, 1999. **18**(11): p. 3074-89.
80. Panne, D., *The enhanceosome.* Current Opinion in Structural Biology, 2008. **18**(2): p. 236-242.
81. Panne, D., T. Maniatis, and S.C. Harrison, *An atomic model of the interferon-beta enhanceosome.* Cell, 2007. **129**(6): p. 1111-23.
82. Bouallaga, I., et al., *An enhanceosome containing the Jun B/Fra-2 heterodimer and the HMG-I(Y) architectural protein controls HPV 18 transcription.* EMBO Rep, 2000. **1**(5): p. 422-7.

83. Bouallaga, I., et al., *HMG-I(Y) and the CBP/p300 coactivator are essential for human papillomavirus type 18 enhanceosome transcriptional activity.* Mol Cell Biol, 2003. **23**(7): p. 2329-40.
84. Chen, B., J. Young, and F.F. Leng, *DNA Bending by the Mammalian High-Mobility Group Protein AT Hook 2.* Biochemistry, 2010. **49**(8): p. 1590-1595.
85. Pentimalli, F., et al., *HMGA1 protein is a novel target of the ATM kinase.* European Journal of Cancer, 2008. **44**(17): p. 2668-2679.
86. Palmieri, D., et al., *HMGA proteins promote ATM expression and enhance cancer cell resistance to genotoxic agents.* Oncogene, 2011. **30**(27): p. 3024-35.
87. Natarajan, S., et al., *HMGA2 Inhibits Apoptosis through Interaction with ATR-CHK1 Signaling Complex in Human Cancer Cells.* Neoplasia, 2013. **15**(3): p. 263-+.
88. Landolin, J.M., et al., *Sequence features that drive human promoter function and tissue specificity.* Genome Research, 2010. **20**(7): p. 890-898.
89. French, S.W., M.C. Schmidt, and J.C. Glorioso, *Involvement of a high-mobility-group protein in the transcriptional activity of herpes simplex virus latency-active promoter 2.* Mol Cell Biol, 1996. **16**(10): p. 5393-9.
90. Foti, D., et al., *A nucleoprotein complex containing Sp1, C/EBP beta, and HMGI-Y controls human insulin receptor gene transcription.* Mol Cell Biol, 2003. **23**(8): p. 2720-32.
91. Zhao, K., et al., *Sar-Dependent Mobilization of Histone H1 by Hmg-I/Y in-Vitro - Hmg-I/Y Is Enriched in H1-Depleted Chromatin.* Embo Journal, 1993. **12**(8): p. 3237-3247.
92. Catez, F., et al., *Network of dynamic interactions between histone H1 and high-mobility-group proteins in chromatin.* Molecular and Cellular Biology, 2004. **24**(10): p. 4321-4328.
93. Snijders, A.P., et al., *Characterization of post-translational modifications of the linker histones H1 and H5 from chicken erythrocytes using mass spectrometry.* J Proteome Res, 2008. **7**(10): p. 4326-35.
94. Ju, B.G., et al., *A topoisomerase IIbeta-mediated dsDNA break required for regulated transcription.* Science, 2006. **312**(5781): p. 1798-802.
95. Contreras, A., et al., *The dynamic mobility of histone H1 is regulated by cyclin/CDK phosphorylation.* Molecular and Cellular Biology, 2003. **23**(23): p. 8626-8636.
96. Belotserkovskaya, R., et al., *FACT facilitates transcription-dependent nucleosome alteration.* Science, 2003. **301**(5636): p. 1090-3.
97. Schwabish, M.A. and K. Struhl, *Asf1 mediates histone eviction and deposition during elongation by RNA polymerase II.* Mol Cell, 2006. **22**(3): p. 415-22.
98. Malini, E., et al., *HMGA Interactome: new insights from phage display technology.* Biochemistry, 2011. **50**(17): p. 3462-8.
99. Lavin, M.F., *Ataxia-telangiectasia: from a rare disorder to a paradigm for cell signalling and cancer.* Nat Rev Mol Cell Biol, 2008. **9**(10): p. 759-69.
100. Rogakou, E.P., et al., *DNA double-stranded breaks induce histone H2AX phosphorylation on serine 139.* J Biol Chem, 1998. **273**(10): p. 5858-68.
101. Redon, C.E., et al., *Recent developments in the use of gamma-H2AX as a quantitative DNA double-strand break biomarker.* Aging-Us, 2011. **3**(2): p. 168-174.
102. Economopoulou, M., et al., *Histone H2AX is integral to hypoxia-driven neovascularization.* Nature Medicine, 2009. **15**(5): p. 553-558.
103. Steinel, N.C., et al., *The ataxia telangiectasia mutated kinase controls Igkappa allelic exclusion by inhibiting secondary Vkappa-to-Jkappa rearrangements.* J Exp Med, 2013. **210**(2): p. 233-9.
104. Turinetto, V., et al., *High basal gammaH2AX levels sustain self-renewal of mouse embryonic and induced pluripotent stem cells.* Stem Cells, 2012. **30**(7): p. 1414-23.
105. McManus, K.J. and M.J. Hendzel, *ATM-dependent DNA damage-independent mitotic phosphorylation of H2AX in normally growing mammalian cells.* Molecular Biology of the Cell, 2005. **16**(10): p. 5013-5025.
106. Mukhametshina, R.T., et al., *Quantitative proteome analysis of alveolar type-II cells reveals a connection of integrin receptor subunits beta 2/6 and WNT signaling.* J Proteome Res, 2013. **12**(12): p. 5598-608.
107. Huang, D.W., B.T. Sherman, and R.A. Lempicki, *Systematic and integrative analysis of large gene lists using DAVID bioinformatics resources.* Nature Protocols, 2009. **4**(1): p. 44-57.
108. Edgar, R., M. Domrachev, and A.E. Lash, *Gene Expression Omnibus: NCBI gene expression and hybridization array data repository.* Nucleic Acids Res, 2002. **30**(1): p. 207-10.
109. Bellusci, S., et al., *Evidence from normal expression and targeted misexpression that bone morphogenetic protein-4 (Bmp-4) plays a role in mouse embryonic lung morphogenesis.* Development, 1996. **122**(6): p. 1693-1702.

110. Hirning-Folz, U., et al., *The expression pattern of the Hmgic gene during development.* Genes Chromosomes Cancer, 1998. **23**(4): p. 350-7.
111. Konduri, S.D., et al., *Promoter methylation and silencing of the tissue factor pathway inhibitor-2 (TFPI-2), a gene encoding an inhibitor of matrix metalloproteinases in human glioma cells.* Oncogene, 2003. **22**(29): p. 4509-16.
112. Metivier, R., et al., *Estrogen receptor-alpha directs ordered, cyclical, and combinatorial recruitment of cofactors on a natural target promoter.* Cell, 2003. **115**(6): p. 751-63.
113. Barreto, G., et al., *Gadd45a promotes epigenetic gene activation by repair-mediated DNA demethylation.* Nature, 2007. **445**(7128): p. 671-5.
114. Lee, H.S., et al., *A cooperative activation loop among SWI/SNF, gamma-H2AX and H3 acetylation for DNA double-strand break repair.* Embo Journal, 2010. **29**(8): p. 1434-1445.
115. Maretto, S., et al., *Mapping Wnt/beta-catenin signaling during mouse development and in colorectal tumors.* Proc Natl Acad Sci U S A, 2003. **100**(6): p. 3299-304.
116. Del Moral, P.M. and D. Warburton, *Explant culture of mouse embryonic whole lung, isolated epithelium, or mesenchyme under chemically defined conditions as a system to evaluate the molecular mechanism of branching morphogenesis and cellular differentiation.* Methods Mol Biol, 2010. **633**: p. 71-9.
117. Esquibies, A.E., et al., *VEGF attenuates hyperoxic injury through decreased apoptosis in explanted rat embryonic lung.* Pediatric Research, 2008. **63**(1): p. 20-25.
118. Xiang, X., K.F. Benson, and K. Chada, *Mini-mouse: disruption of the pygmy locus in a transgenic insertional mutant.* Science, 1990. **247**(4945): p. 967-9.
119. Ikeda, K., P.J. Mason, and M. Bessler, *3 ' UTR-truncated Hmga2 cDNA causes MPN-like hematopoiesis by conferring a clonal growth advantage at the level of HSC in mice.* Blood, 2011. **117**(22): p. 5860-5869.
120. Brault, V., et al., *Inactivation of the beta-catenin gene by Wnt1-Cre-mediated deletion results in dramatic brain malformation and failure of craniofacial development.* Development, 2001. **128**(8): p. 1253-1264.
121. Volckaert, T., et al., *Parabronchial smooth muscle constitutes an airway epithelial stem cell niche in the mouse lung after injury.* J Clin Invest, 2011. **121**(11): p. 4409-19.
122. Moffat, J., et al., *A lentiviral RNAi library for human and mouse genes applied to an arrayed viral high-content screen.* Cell, 2006. **124**(6): p. 1283-98.
123. Konigshoff, M., et al., *WNT1-inducible signaling protein-1 mediates pulmonary fibrosis in mice and is upregulated in humans with idiopathic pulmonary fibrosis.* Journal of Clinical Investigation, 2009. **119**(4): p. 772-787.
124. Ertel, F., et al., *In vitro reconstitution of PHO5 promoter chromatin remodeling points to a role for activator-nucleosome competition in vivo.* Mol Cell Biol, 2010. **30**(16): p. 4060-76.
125. Sharma, N., D.I. Lopez, and J.K. Nyborg, *DNA binding and phosphorylation induce conformational alterations in the kinase-inducible domain of CREB. Implications for the mechanism of transcription function.* J Biol Chem, 2007. **282**(27): p. 19872-83.
126. Shevchenko, A., et al., *Linking genome and proteome by mass spectrometry: large-scale identification of yeast proteins from two dimensional gels.* Proc Natl Acad Sci U S A, 1996. **93**(25): p. 14440-5.
127. Cox, J. and M. Mann, *MaxQuant enables high peptide identification rates, individualized p.p.b.-range mass accuracies and proteome-wide protein quantification.* Nat Biotechnol, 2008. **26**(12): p. 1367-72.
128. Del Riccio, V., M. van Tuyl, and M. Post, *Apoptosis in lung development and neonatal lung injury.* Pediatr Res, 2004. **55**(2): p. 183-9.
129. Zeng, X., et al., *A dual-kinase mechanism for Wnt co-receptor phosphorylation and activation.* Nature, 2005. **438**(7069): p. 873-7.
130. Mao, B.Y., et al., *LDL-receptor-related protein 6 is a receptor for Dickkopf proteins.* Nature, 2001. **411**(6835): p. 321-325.
131. Bilic, J., et al., *Wnt induces LRP6 signalosomes and promotes dishevelled-dependent LRP6 phosphorylation.* Science, 2007. **316**(5831): p. 1619-22.
132. Kazanskaya, O., A. Glinka, and C. Niehrs, *The role of Xenopus dickkopf1 in prechordal plate specification and neural patterning.* Development, 2000. **127**(22): p. 4981-92.
133. De Langhe, S.P., et al., *Dickkopf-1 (DKK1) reveals that fibronectin is a major target of Wnt signaling in branching morphogenesis of the mouse embryonic lung.* Developmental Biology, 2005. **277**(2): p. 316-331.
134. Ishitani, T., et al., *The TAK1-NLK mitogen-activated protein kinase cascade functions in the Wnt-5a/Ca(2+) pathway to antagonize Wnt/beta-catenin signaling.* Mol Cell Biol, 2003. **23**(1): p. 131-9.
135. Bakkenist, C.J. and M.B. Kastan, *DNA damage activates ATM through intermolecular autophosphorylation and dimer dissociation.* Nature, 2003. **421**(6922): p. 499-506.

136. Kozlov, S.V., et al., *Autophosphorylation and ATM activation: additional sites add to the complexity.* J Biol Chem, 2011. **286**(11): p. 9107-19.
137. Chaumeil, J., et al., *Higher-order looping and nuclear organization of Tcra facilitate targeted rag cleavage and regulated rearrangement in recombination centers.* Cell Rep, 2013. **3**(2): p. 359-70.
138. Semple, R.K., *From bending DNA to diabetes: the curious case of HMGA1.* J Biol, 2009. **8**(7): p. 64.
139. Pogna, E.A., A.L. Clayton, and L.C. Mahadevan, *Signalling to chromatin through post-translational modifications of HMGN.* Biochimica Et Biophysica Acta-Gene Regulatory Mechanisms, 2010. **1799**(1-2): p. 93-100.
140. Desai, T.J., D.G. Brownfield, and M.A. Krasnow, *Alveolar progenitor and stem cells in lung development, renewal and cancer.* Nature, 2014. **507**(7491): p. 190-4.
141. Ashar, H.R., et al., *In vivo modulation of HMGA2 expression.* Biochim Biophys Acta, 2010. **1799**(1-2): p. 55-61.
142. Nishino, J., et al., *Hmga2 Promotes Neural Stem Cell Self-Renewal in Young but Not Old Mice by Reducing p16(Ink4a) and p19(Arf) Expression.* Cell, 2008. **135**(2): p. 227-239.
143. Koutsourakis, M., et al., *The transcription factor GATA6 is essential for early extraembryonic development (vol 126, pg 723-732, 1999).* Development, 1999. **126**(9).
144. Morrisey, E.E., et al., *GATA6 regulates HNF4 and is required for differentiation of visceral endoderm in the mouse embryo.* Genes & Development, 1998. **12**(22): p. 3579-3590.
145. Federico, A., et al., *Hmga1/Hmga2 double knock-out mice display a "superpygmy" phenotype.* Biol Open, 2014.
146. Fedele, M., et al., *Haploinsufficiency of the Hmga1 gene causes cardiac hypertrophy and myelo-lymphoproliferative disorders in mice.* Cancer Res, 2006. **66**(5): p. 2536-43.
147. Stoick-Cooper, C.L., et al., *Distinct Wnt signaling pathways have opposing roles in appendage regeneration.* Development, 2007. **134**(3): p. 479-489.
148. Cohen, E.D., et al., *Wnt/beta-catenin signaling promotes expansion of Isl-1 - positive cardiac progenitor cells through regulation of FGF signaling.* Journal of Clinical Investigation, 2007. **117**(7): p. 1794-1804.
149. Mucenski, M.L., et al., *Beta-catenin regulates differentiation of respiratory epithelial cells in vivo.* Am J Physiol Lung Cell Mol Physiol, 2005. **289**(6): p. L971-9.
150. Singh I, Ö.N., Mehta A, Hasan D, Cosentino C, Sebastian C, Krüger M, Carraro G, Mostoslavsky R, Bellusci S, Braun T and Barreto G, *HMGA2-induced transcriptional activation requires ATM-mediated phosphorylation of histones and implicates histone eviction.* Cell Res, 2014. **under revision**.
151. Vicent, G.P., et al., *Four enzymes cooperate to displace histone H1 during the first minute of hormonal gene activation.* Genes Dev, 2011. **25**(8): p. 845-62.
152. Bhattacharjee, R.N., et al., *Histone H1 phosphorylation by cdk2 selectively modulates mouse mammary tumor virus transcription through chromatin remodeling.* Molecular and Cellular Biology, 2001. **21**(16): p. 5417-5425.
153. Jin, C.Y., et al., *H3.3/H2A.Z double variant-containing nucleosomes mark 'nucleosome-free regions' of active promoters and other regulatory regions.* Nature Genetics, 2009. **41**(8): p. 941-U112.
154. Li, A., et al., *Phosphorylation of histone H2A.X by DNA-dependent protein kinase is not affected by core histone acetylation, but it alters nucleosome stability and histone H1 binding.* J Biol Chem, 2010. **285**(23): p. 17778-88.
155. Heo, K., et al., *FACT-mediated exchange of histone variant H2AX regulated by phosphorylation of H2AX and ADP-ribosylation of Spt16.* Mol Cell, 2008. **30**(1): p. 86-97.
156. Formosa, T., et al., *Spt16-Pob3 and the HMG protein Nhp6 combine to form the nucleosome-binding factor SPN.* EMBO J, 2001. **20**(13): p. 3506-17.
157. Barlow, C., et al., *Atm-deficient mice: a paradigm of ataxia telangiectasia.* Cell, 1996. **86**(1): p. 159-71.
158. Elson, A., et al., *Pleiotropic defects in ataxia-telangiectasia protein-deficient mice.* Proc Natl Acad Sci U S A, 1996. **93**(23): p. 13084-9.
159. Xu, Y., et al., *Targeted disruption of ATM leads to growth retardation, chromosomal fragmentation during meiosis, immune defects, and thymic lymphoma.* Genes Dev, 1996. **10**(19): p. 2411-22.
160. Celeste, A., et al., *Genomic instability in mice lacking histone H2AX.* Science, 2002. **296**(5569): p. 922-7.
161. Kari, V., et al., *The H2B ubiquitin ligase RNF40 cooperates with SUPT16H to induce dynamic changes in chromatin structure during DNA double-strand break repair.* Cell Cycle, 2011. **10**(20): p. 3495-504.
162. Minsky, N., et al., *Monoubiquitinated H2B is associated with the transcribed region of highly expressed genes in human cells.* Nature Cell Biology, 2008. **10**(4): p. 483-490.

Chapter 7: APPENDIX

Table 1: List of Primers. Oligonucleotide sequences used for qRT-PCR, ChIP and cloning.

Gene	Primer sequence	
mGata6	Forward	5'ATGGCGTAGAAATGCTGAGGG
	Reverse	5'TGAGGTGGTCGCTTGTGTAG
mSftpc	Forward	5'CGTGGTTGTGGTGGTGGTC
	Reverse	5'GGATGCTCTCTGGAGCCATC
mFzd2	Forward	5'CCGCTCTTCGTATACCTGTTC
	Reverse	5'CGGATGCGGAAGAGTGACA
mGapdh	Forward	5'TGAGTATGTCGTGGAGTCTAC
	Reverse	5'TGGACTGTGGTCATGAGCC
mTub1a1	Forward	5'CCGCGAAGCAGCAACCAT
	Reverse	5'CCAGGTCTACGAACACTGCC
Axin2	Forward	5'GAGTAGCGCCGTGTTAGTGACT
	Reverse	5'CCAGGAAAGTCCGGAAGAGGTATG
Fgfr2	Forward	5'GCTTCTCAGTGAGTTTTAATAACAGC
	Reverse	5'GAATGATGCTGGGCTTTTGC
Mycn	Forward	5'TGTGTTGACATTAAGAATGTTGGTTTAC
	Reverse	5'TTTCCAAGGTCATGGCAGAAC
Bmp4	Forward	5'CCCTTTCCACTGGCTGATCA
	Reverse	5'GGGACACAACAGGCCTTAGG
Wnt 2b	Forward	5'TGTGTCAACGCTACCCAGAC
	Reverse	5'TAGCATAGACGAACGCTGCC
Wnt 11	Forward	5'GCTGCGTCTGGAAGAAGCTAT
	Reverse	5'AGTGGATAGGGAGAGTGCGG
Wnt7b	Forward	5' GCATCCAAGGTCAACGCAAT
	Reverse	5'CTCAGAGTCTCATGGTCCCTTTG
Hmga1	Forward	5'CCAGTGAAGTGCCAACTCCGA

	Reverse	5’CGGCACTGCGAGTGGTGATC
Scgb1a1	Forward	5’CTGAAGAGACTGGTGGATACC
	Reverse	5’GTTTATTGCAAGAGGAAGGA
hGATA6	Forward 1	5’CTCGGCTTCTCTCCGCGCCTG
	Reverse 1	5’AGCTGAGGCGTCCCGCAGTTG
	Forward 2	5’GCGGTTTCGTTTTCGGGGAC
	Reverse 2	5’AAGGGATGCGAAGCGTAGGA
hGAPDH	Forward	5’GCAAATTCCATGGCACCGT
	Reverse	5’TCGCCCCACTTGATTTTGG
hTUB1A1	Forward	5’GAGAGGAGGAGGCACCGAAAA
	Reverse	5’AGGCATTGCCAATCTGGACAC
mGata6 (ChIP)	Forward 1	5’CCCACGACCTGAGCATCCCG
	Reverse 1	5’GAGGGACTCGCCCCCTCCTG
	Forward 2	5’CCAGCTCCTTCCGAGCCAAGT
	Reverse 2	5’GGGGCGCCCAGCTAAAGGAC
	Forward 3	5’CCGGGGTGGACTCGCTCCTA
	Reverse 3	5’GCCAGGCTGTGGGTCGGAAC
	Forward 4	5’ACTCCGGACCAGCCTCCACC
	Reverse 4	5’GCCTCCACCGGGCTGCTTTT
	Forward 5	5’GGACGTGGTTGGACGTGAGG
	Reverse 5	5’CCCGAAAACGAAACCGCCGC
	Forward 6	5’ACGTGCGGAACTCTCTTCACCG
	Reverse 6	5’AGGGTGCCCTCCTCCGTCAC
	Forward 7	5’CCAGCAACTGCAGGACGCCG
	Reverse 7	5’CCCGGCTGGACCACAACAGC
	Forward 8	5’GTGGCTTTCATTGCGCTTCA
	Reverse 8	5’CAGCCCGTTACTGCATGGTA
	Forward 1	5’ATTCCTTGCCCCCTCCCCCG
	Reverse 1	5’TGGGGTGGAGAGGTGCCTTGT
	Forward 2	5’ACCACCACGACCTGAGCCGT

hGATA6 (ChIP)	Reverse 2	5'TTGGCAGTGCACAGTCCCGC
	Forward 3	5'TTCCCTCCTTCCCTCCGGGC
	Reverse 3	5'TAACTACCGGCTCCCGCCCC
	Forward 4	5'ACGGTCCGGCGTTTCTGCTG
	Reverse 4	5'GGGGCAGCAGTCTGGGTCCT
	Forward 5	5'AGGTGGGGCACTTTCATGTT
	Reverse 5	5'AGAATACCCGGGAGCAGTCA
Hmga2 KO mice genotyping	Forward T	5'ATTCTGGAGACGCAGGAAGA
	Reverse T	5'TGCTCCTGGGAGTAGATTGG
	Forward C	5'CAAATGTTGCTTGTCTGGTG
	Reverse C	5'GTCAGTCGAGTGCACAGTTT
Hmga2 overexpression mice genotyping	Forward	5'GAGCCAACCTGTGAGCCCT
	Reverse	5'CCTTCCATTCAAAATGTAGGTACTCTGTTC
mGata6 promoter cloning into TOPO TA cloning vector	Forward	5'CCCACGACCTGAGCATCCCG
	Reverse	5'GCCAGGCTGTGGGTCGGAAC
mHmga2 subcloning into pCDNA3.1 (A)-Myc/His vector	Forward	5'CACGAATTCAGGAGGTATGAGCGCACGCGG
	Reverse	5'GTGCTCGAGATCCTCCTCTGCGGACTC
H2AX (S139→D) point mutation	Forward	5'GCCACCCAGGCCGACCAGGAGTACTAATCT
	Reverse	5'AGATTAGTACTCCTGGTCGGCCTGGGTGGC
H1(S65→A) point mutation	Forward	5'GGTGAGAACGCCGACGCCCAGATCAAGTTG TCC
	Reverse	5'GGACAACTTGATCTGGGCGTCGGCGTTCTCA CC
H1(S65→D) point mutation	Forward	5'GGTGAGAACGCCGACGACCAGATCAAGTTG TCC
	Reverse	5'GGACAACTTGATCTGGTCGTCGGCGTTCTCA CC

Table 2: List of Antibodies

Antibodies	Cat. No.	Company	WB	IF/FACS	IP	ChIP
HMGA2	59170AP	Biocheck	+	+		
HMGA2	sc-30223x	Santa Cruz		+	+	+
TUBA1A	T5168	Sigma	+			
GATA6	AF1700	R&D system	+	+		
FZD2	ab52565	Abcam	+	+		
ABC	05-665	Millipore	+	+		
CTNNB1	ab6302	Abcam		+		
LRP6	3395	Cell signaling	+			
pLRP6	2568	Cell signaling	+			
AXIN2	ab32197	Abcam	+			
BMP4	4680	Millipore	+			
MYCN	sc-791	Santa Cruz	+			
LMNB1	sc-6216	Santa Cruz	+	+		
His-tag	ab9108	Abcam	+			
Myc-tag	ab9132	Abcam	+			
Flag-tag	F1804	Sigma	+	+		
H1	sc-8030	Santa Cruz	+			+
ATM	sc-23922	Santa Cruz	+		+	+
ATMS1981ph	sc-47739	Santa Cruz	+			
phospho-(Ser/Thr) ATM substrate	2851S	Cell Signaling			+	+
H2AX	07-627	Millipore	+			+
H2AXS139ph	05-636	Millipore	+	+		+
SCGB1A1	sc-9772	Santa Cruz		+		
CDH1	ab11512	Abcam		+		
VIM-Cy3	C9080	Sigma		+		
PCNA	sc7907	Santa Cruz		+		
MKi67	ab15580	Abcam		+		

pan-cytokeratin	C5992	Sigma		+		
Pro-SFTPC	AB3786	Millipore		+		
SFTPC	sc-7706	Santa cruz		+		
SOX9	sc-17341	Santa Cruz		+		
ACTA2-Cy3	C6198	Sigma		+		
clCASP3	9664S	Cell signaling		+		
Pol II	ab5408	Abcam				+
H2B	07-371	Millipore				+
H3	ab1791	Abcam				+
H4	05-858	Millipore				+
rIgG	sc-2027	Santa Cruz			+	+
mIgG	sc-2025	Santa Cruz			+	+
gIgG	sc-2028	Santa Cruz				+
rIgG-HRP	sc-2305	Santa Cruz	+			
mIgG-HRP	715-035-150	Jackson Lab	+			
gIgG-HRP	sc-2020	Santa Cruz	+			
gαrAl488	A11008	Invitrogen		+		
gαmAl555	A21422	Invitrogen		+		
dαgAl647	A21447	Invitrogen		+		
dαratCF633A	20137	Biotium		+		
dαrCF488A	20015	Biotium		+		
dαmCF568A	20105	Biotium		+		
Note: Antibody used for specific experiment indicated by '+' sign.						

Table 3: List of Abbreviations

Abbreviations	Term
+/+	Wild type
+/-	Heterozygous Knockout
-/-	Homozygous Knockout
°C	Degrees centigrade
aa	Amino acids
AGE	Agarose gel electrophoresis
ATMS1981ph	Phosphorylated ataxia talengiectasia mutated at serine 1981
ATP	Adenosine triphosphate
AT II	Alveolar type II
BADJ	Bronchioalveolar duct junctions
BASCs	Bronchioalveolar stem cells
BLAST	Basic Local Alignment Search Tool
bp	Base pairs
BRE	TFIIB recognition element
BSA	Bovine serum albumin
cDNA	DNA complementary to mRNA
ChIP	Chromatin Immuno-precipitation
CTRL	Control
DAPI	4',6-diamidino-2-phenylindole
DEPC	Diethylpyrocarbonate
dH2O	Distilled water

DMEM	Dulbecco's Modified Eagle Medium
DMSO	Dimethyl sulfoxide
DNA	Deoxyribonucleic acid
dNTP	Deoxyribonucleotide triphosphate
DPE	Downstream promoter elements
DSB	DNA double strand breaks
DTT	Dithiothreitol
E	embryonic day
ECL	Enhanced chemiluminiscence
E.coli	*Escherichia coli*
EDTA	Ethylenediaminetetraacetic acid
EGTA	Ethylene glycol tetraacetic acid
EMT	Epithelial-Mesenchymal Transformation
EtBr	Ethidium bromide
FCS	Fetal calf serum
GEO	Gene expression omnibus
GFP	Green fluorescence protein
GO	Gene ontology
GOF	Gain of function
h	Hour
H1S65ph	Phosphorylated Histone H1 at serine 65
H2AXS139ph	Phosphorylated Histone H2AX at serine 139
HEK	Human embryonic kidney cell line

HMG	High mobility group
HMGA	High mobility group AT-hook protein
INR	Initiator sequences
IP	Immuno-precipitation
ISH	In situ hybridization
KO	Homozygous Knockout
kb	Kilo base pairs
kDa	Kilo Dalton
KEGG	Kyoto Encyclopedia of Genes and Genomes
l	Liter
LC-MS/MS	Liquid chromatography-mass spectrometry/mass spectrometry
LOF	Loss of function
Luc	Luciferase
mg	Milligram
min	Minute
ml	Milliliter
MLE-12	Murine lung epithelial type II cell line-12
mM	Millimol
mRNA	Messenger RNA
MW	Molecular weight
NCBI	National Center of Biotechnology Information
nm	Nanometer
P	Postnatal day

PAGE	Polyacrylamide gel electrophoresis
PBS	Phosphate buffered saline
PCR	Polymerase chain reaction
PEEP	Positive end-expiratory pressure
PEI	Polyethylenimine
PFA	Paraformaldehyde
pH	Negative logarithm of hydrogen ions concentration
PMSF	Phenylmethanesulfonyl fluoride
Pol II	RNA polymerase II
qPCR	Quantitative Polymerase Chain Reaction
RNA	Ribonucleic acid
Rnase	Ribonuclease
rpm	Revolutions per minute
RT	Room temperature
RT-PCR	Reverse Transcriptase Polymerase Chain Reaction
SDS	Sodium dodecyl sulphate
sec	Second
siRNA	Short interfering RNA
SQ	Serine-Glutamine amino acid residues
TAE	Tris-acetate-EDTA
TBE	Tris-borate-EDTA
TE	Tris-EDTA buffer
TF	Transcription factor

TGFβ	Transforming Growth Factor β
Tris	Tris-(hydroxymethyl)-aminomethan
TSS	Transcription start site
U	Unit
µg	Microgram
µm	Micrometer
µl	Microlitre
UTR	Untranslated region
UV	Ultraviolet
V	Volt
v/v	Volume/volume
W	Watt
WB	Western blot
w/v	Weight/volume
X-gal	5-bromo-4-chloro-3-indolyl-D-galactopyranoside

Table 4: Gene and Protein Nomenclature

Human Gene	Mouse Gene	Protein Name
HMGA2	*Hmga2*	HMGA2
GATA6	*Gata6*	GATA6
FZD2	*Fzd2*	FZD2
LMNB1	*Lmnb1*	LMNB1
SFTPC	*Sftpc*	SFTPC
GAPDH	*Gapdh*	GAPDH
TUB1A1	*Tub1a1*	TUB1A1
AXIN2	*Axin2*	AXIN2
FGFR2	*Fgfr2*	FGFR2
MYCN	*Mycn*	MYCN
BMP4	*Bmp4*	BMP4
HMGA1	*Hmga1*	HMGA1
SCGB1A1	*Scgb1a1*	SCGb1A1
WNT2B	*Wnt2b*	WNT2B
WNT11	*Wnt11*	WNT11
WNT7B	*Wnt7b*	WNT7B
ATM	*Atm*	ATM
H2AX	*H2ax*	H2AX

ACKNOWLEDGEMENT

A thesis is never solely the work of the author. Support and encouragement comes from different sources in different ways. It is a pleasant part that I have now the opportunity to express my gratitude to all of them.

I would like to show my gratitude to Prof. Dr. Dr. Thomas Braun and Dr. Guillermo Barreto for giving me the opportunity to perform my thesis work at the Max Planck Institute for Heart Lung Research in Dr. Barreto's Laboratory.

I would like to express my gratitude to Prof. Dr. Dr. Thomas Braun and Prof. Werner Seeger for their creative suggestions and constructive criticism for this thesis.

My warm thanks go to my immediate supervisor Dr. Guillermo Barreto for his strong motivation and kind guidance during my Ph.D. research. I would like to thank him for providing constant guidance, contribution, encouragement, and critical reading and helpful suggestions for this thesis, manuscripts and scientific personality development. It is difficult for me to find proper and enough words for all his support and for making this journey of mine a pleasurable and unforgettable one.

It is my pleasure to take the honor to thank Prof. Dr. Rainer Renkawitz, Institute for Genetics, Justus-Liebig-Universität Giessen, Giessen, for acting as my university supervisor enabling my thesis at the MPI as well as for his creative suggestions and constructive criticism.

I would like to express my gratitude to Prof. Ralf Schermuly, Institute for Pulmonary Pharmacotherapy, Justus-Liebig-Universität Giessen, and to PD Dr. Thomas Böttger, MPI-HLR, Bad Nauheim, for acting as my Ph.D. defense examiners for Dr. rer. nat. degree.

I want to show my gratitude to Prof. Saverio Bellusci, Dr. Gianni Carraro and Aditi Mehta for constructive discussion and support in lung development study; Nihan Öztürk for constructive discussion and support in ChIP and point mutation analysis; Dr. Marcus Krüger for Mass spectrometry based proteome analysis; PD Dr. Thomas Böttger and Adriana Contreras for Affymetrix based expression analysis; Dr. Matthew Wheeler for BAT-GAL transgenic mice; Dr. Robert Voswinckel, Dr. Vandana Nikam, Dr. Swati Dabral and Nefertiti Elnikhely for helpful discussions; Dr. Chao Ming Chao for lung stereology; Prof. R. Mostoslavsky, Prof. S. Liebner, Prof. P. Grouse, Prof. P.R. Strauss and Prof. J. Kwon for reagents; Anja Schmall for thesis abstract translation into German; Savai's and Dobreva's lab members for their kind help.

I would like also to thank my colleagues in Dr. Barreto's laboratory for their help and for creating a good atmosphere in the group. In addition, I would like to thank to MPI employees for their kind cooperation and help throughout my thesis period.

Finally, I am grateful to the International Max Planck Research School for Heart and Lung Research (IMPRS) as well as the University of Giessen and Marburg Lung Center (UGMLC) for supporting this project.

Last but not least, I dedicate this thesis to the ones who are always there for me. You kept the light for me when it was really dark. I love you from the bottom of my heart, my dear family: my father Anilkumar, my mother Indumati, my brother Indresh and my wife Anshu!

This work was supported by a grant from ''LOEWE-Initiative der Landesförderung" (Wiesbaden Germany) (III L 4 – 518/15.004 2009) and the ''Deutsche Forschungsgemeinschaft" (DFG, Bonn, Germany) (BA 4036/1-1).

EIDESSTATTLICHE ERKLÄRUNG

„Ich erkläre: Ich habe die vorgelegte Dissertation selbständig und ohne unerlaubte fremde Hilfe und nur mit den Hilfen angefertigt, die ich in der Dissertation angegeben habe. Alle Textstellen, die wörtlich oder sinngemäß aus veröffentlichten Schriften entnommen sind, und alle Angaben, die auf mündlichen Auskünften beruhen, sind als solche kenntlich gemacht. Bei den von mir durchgeführten und in der Dissertation erwähnten Untersuchungen habe ich die Grundsätze guter wissenschaftlicher Praxis, wie sie in der „Satzung der Justus-Liebig-Universität Gießen zur Sicherung guter wissenschaftlicher Praxis“ niedergelegt sind, eingehalten.“

CV removed.